Mathematical analysis, coupling and control design for models of synthetic biological oscillators

Eleni Firippi

UNIVERSITÉ CÔTE D'AZUR

ÉCOLE DOCTORALE
SCIENCES ET TECHNOLOGIES DE L'INFORMATION ET DE LA COMMUNICATION

THÈSE DE DOCTORAT

Analyse mathématique, couplage et contrôle pour modèles d'oscillateurs biologiques synthétiques

Eleni FIRIPPI

Inria Sophia Antipolis-Méditerranée

Présentée en vue de l'obtention du grade de docteur en *Automatique traitement du signal et des images* d'*Université Côte d'Azur*

Dirigée par : Madalena Chaves

Soutenue le : 16 Décembre 2020

Devant le jury, composé de :

Élisabeth Remy, Institut de Mathématiques de Marseille, France

Steffen Waldherr, Katholieke Universiteit Leuven, Belgique

Jean-Paul Comet, Université Côte d'Azur I3S, France

Franck Delaunay, Institut de Biologie Valrose (iBV), Nice, France

Luca Scardovi, University of Toronto, Canada

Jacques-Alexandre Sepulchre, Institut de Physique de Nice, France

Ioannis Stratis, National and Kapodistrian University of Athens, Greece

AGENCE NATIONALE DE LA RECHERCHE ANR

UNIVERSITÉ CÔTE D'AZUR

ÉCOLE DOCTORALE
SCIENCES ET TECHNOLOGIES DE L'INFORMATION ET DE LA COMMUNICATION

Inria

Thèse

Présentée en vue de l'obtention du grade de docteur en
Automatique traitement du signal et des images
D'Université Côte d'Azur

par

Eleni FIRIPPI

Analyse mathématique, couplage et contrôle pour modèles d'oscillateurs de biologiques synthétiques

Soutenue le 16 décembre 2020, devant le jury, composé de :

Directrice de thèse	Madalena Chaves, Directrice de recherche, Inria Sophia Antipolis, France
Rapporteurs	Élisabeth Remy, Chargée de recherche, Institut de Mathématiques de Marseille, France Steffen Waldherr, Associate Professor, Katholieke Universiteit Leuven, Belgium
Examinateurs	Jean-Paul Comet, Professeur, Université Côte d'Azur I3S, France Franck Delaunay, Professeur, Institut de Biologie Valrose (iBV), France Luca Scardovi, Associate Professor, University of Toronto, Canada Jacques-Alexandre Sepulchre, Maître de Conferences, Institut de Physique de Nice Université Côte d'Azur, France Ioannis Stratis, Professor, National and Kapodistrian University of Athens, Greece

UNIVERSITÉ CÔTE D'AZUR

ÉCOLE DOCTORALE
SCIENCES ET TECHNOLOGIES DE L'INFORMATION ET DE LA COMMUNICATION

Inria

Thesis

Submitted in fulfillment of the requirements for the degree of Doctor in the
Université Côte d'Azur

Specialized in: Automation, Signal and Image Processing

by

Eleni FIRIPPI

Mathematical analysis, control design and coupling for models of synthetic biological oscillators

Defended on the 16th of December 2020 in front of the Jury composed by:

Supervisor	Madalena Chaves, Research director, Inria Sophia Antipolis, France
Reviewers	Élisabeth Remy, Chargée de recherche, Institut de Mathématiques de Marseille, France Steffen Waldherr, Associate Professor, Katholieke Universiteit Leuven, Belgium
Examiners	Jean-Paul Comet, Professeur, Université Côte d'Azur I3S, France Franck Delaunay, Professeur, Institut de Biologie Valrose (iBV), France Luca Scardovi, Associate Professor, University of Toronto, Canada Jacques-Alexandre Sepulche, Maître de Conferences, Institut de Physique de Nice, Université Côte d'Azur, France Ioannis Stratis, Professor, National and Kapodistrian University of Athens, Greece

Abstract

Biological oscillators are present in most living organisms and play major roles in their development and regulation. Synthetic biology is a rising multidisciplinary field that aims to create new circuits from biomolecular elements, with the goal to better understand the dynamics underlying complex biological systems. Mathematical models play a crucial role in the study and improvement of synthetic design, to ensure the desired functionality of the new genetic circuits, as well as to provide predictions on the efficient and robust performance of the implementation. To contribute to the design and analysis of synthetic oscillators, in a first step, we analytically study a two-gene synthetic oscillator, applying both bifurcation analysis and the piecewise affine (PWA) framework, and propose a variant of the model to enhance its oscillatory capacity. In a second step, inspired by circadian rhythms, we study a network of N two-gene synthetic PWA oscillators, and compare the effect of three different coupling topologies on the dynamics and synchronization properties of the network. In a third step, motivated by the interconnection of the cell cycle and circadian clock, we analyze the coupling of the two-gene oscillator with two other synthetic oscillators: the repressilator and a reduced cell cycle model. Two main bidirectional coupling schemes are considered and we perform a "controler-follower" analysis to characterize the capacity of each system to determine or control the period of the coupled system. Based on this analysis, we can identify the coupling schemes admitting a wider range of dynamical responses, as well as suggest strategies for period-control of two coupled oscillators and tunability of a system through the coupling with another system.

Keywords: piecewise affine systems; synthetic biology; biological oscillators; bifurcation analysis; coupled oscillators.

Résumé

Les oscillateurs biologiques jouent un rôle majeur dans le développement et la régulation de la plupart des organismes vivants. La biologie synthétique est un domaine multidisciplinaire qui vise à construire de nouveaux circuits à partir d'éléments biomoléculaires, pour recréer et mieux comprendre la dynamique de ces systèmes biologiques complexes. Dans ce contexte, les modèles mathématiques sont indispensables pour étudier et prédire le comportement des nouveaux circuits génétiques, ainsi que pour fournir des prévisions sur la performance efficace et robuste de l'implémentation. Dans un premier temps, nous étudions analytiquement un oscillateur synthétique à deux gènes, par des techniques d'analyse de bifurcation et en utilisant les modèles affines par morceaux (PWA). Nous proposons une variante du modèle qui augmente la région de paramètres admettant des oscillations périodiques. Dans un second temps, par analogie avec les rythmes circadiens, nous étudions un réseau de N oscillateurs synthétiques à deux gènes et comparons la dynamique et les propriétés de synchronisation du réseau pour trois topologies de couplage différentes. Par la suite, pour décrire l'interconnexion du cycle cellulaire et de l'horloge circadienne, nous analysons le couplage de l'oscillateur à deux gènes avec deux autres oscillateurs synthétiques : le répressilateur et un modèle réduit du cycle cellulaire. Par une analyse du type « contrôleur-suiveur » nous avons caractérisé la capacité de chaque système à contrôler la période du système couplé. Sur la base de cette analyse, nous suggérons des techniques et des schémas d'interconnexion pour affiner et contrôler la période d'un système de deux oscillateurs couplés.

Mots-clés : systèmes affines par morceaux, biologie synthétique, oscillateurs biologiques, analyse de bifurcation, oscillateurs couplés.

Acknowledgements

First of all, I would like to thank my advisor Madalena Chaves, for giving me the opportunity to work on this thesis and learn so many new things from her, and for her continuous support, guidance and courage. It was a great pleasure meeting her, *Merci pour tout Madalena !*

I also thank Franck Delaunay for his guidelines and for the nice experience to exchange with a biologist. Many thanks to Luca Scardovi for his advice and the interesting discussions during the first year of my PhD.

I would like to thank all Biocore team members for welcoming me from the beginning, *Merci à tous, c'était un grand plaisir de vous rencontrer et travailler avec vous ces trois années*.

I also thank the people from McTao and Factas teams, as well as Marie-Line, who has been very helpful during these three years. I would like also to thank the PhD Seminars Organizing Committee for the nice experience, along with all students that I met at Inria center. Many thanks to Juliette Leblond, for her advice, support and the nice conversations. I also thank my friend Dorella for her important help, support and all pleasant moments.

I would like to thank my parents for always encouraging me and for helping me with the new steps in my life, and my sister, for her love, and for always being supportive and inspiring. Lastly, I would like to thank Christos, for the continuous support and patience during these years, for always motivating me and for helping me to overcome difficulties, *thank you for everything*.

Contents

List of Figures

List of Tables

Glossary: Some Basic Definitions in Dynamical Systems Theory

Phase space Considering a dynamical system $\dot{x}_i = f_i(x_1, x_2, \ldots, x_n)$, the *phase space* is the n-dimensional space with coordinates the components $x_i, i = 1, 2, \ldots, n$ of a state vector of the system. A *fixed point* of a dynamical system is given by $\dot{x}_i = 0$, for all i.

Trajectory The curve that corresponds to the change of position in the phase space of a state of a dynamical system at a given time frame.

Stability An orbit (a trajectory) is characterized Lyapunov *stable* if the course in time of any point stays in a small neighborhood: for a trajectory $X(t)$ with initial condition X_0 for any $\varepsilon > 0$ there exists $\delta(\varepsilon) > 0$ such that for all $\tilde{X}(t)$ it holds $\|X(t) - \tilde{X}(t)\| < \varepsilon$ for any $\tilde{X}(t)$ with $\|X_0 - \tilde{X}_0\| < \delta(\varepsilon)$.

Bifurcation In a dynamical system, a *bifurcation* can occur with variations in the parameter values that cause a qualitative change in the system's behavior.

Hopf Bifurcation A *Hopf bifurcation* is a critical point where a change in a system's stability occurs and a periodic solution emerges. Criterion derived from the linerization around a fixed point of a system: a pair of complex conjugate eigenvalues crosses the complex plane imaginary axis.

Poincaré map A first return map or *Poincaré map* of a continuous dynamical system, is a map that represents the transversal intersection of a periodic orbit in the phase space, with a subspace of dimension smaller by one than the phase space dimension (Poincaré section). Considering a periodic orbit initiated within a section of the space, which exits that section after a period of time, one can fix the point at which this orbit first returns to this section, and create a map (first return map) to link the first point to the second.

Phase lock Phase lock or synchronization occurs when two or more periodic systems oscillate with a constant pattern of relative phase angles.

Network synchronization A network of coupled dynamical systems with periodic behavior is considered to achieve synchronization when all the nodes of the network (all systems) start to evolve in time at the same frequency (synchronization in frequency). Additionally, if all the systems (with the same frequency) have also identical phase angles (phase synchronization), then the coupled oscillators in the network are considered to be synchronized in frequency and phase.

Chapter 1

Introduction

1.1 Introducing the thesis topic and motivation

The goal of this thesis is to study models of biological genetic oscillators and their coupling for applications in synthetic biology. A topic that lies at the interdisciplinary crossing between mathematical and computational analysis, systems and synthetic biology, hence three main perspectives need to be discussed in order to introduce the thesis main idea and motivation:

From a mathematical perspective: mathematical modeling provides predictions of how a synthetic circuit will operate when it is implemented in living cell conditions; and what will be the impact of certain modifications on the system. Desired functionalities of synthetic circuits often include oscillatory behavior. For the successful and effective implementation of synthetic oscillators, mathematical modeling and analysis are required for the improvement of the circuit design, with main goal of enhancing the performance of the system by increasing robustness of the periodic solutions with respect to parameter variations. Thus, for a given model of an oscillator, it is important to establish the existence and uniqueness of periodic solutions, as well as characterize the regions of parameters where periodic solutions exist.

Recent approaches in synthetic gene circuits design, are directed at the study of combined or coupled modules, to model more complex natural pathways and comprehend experimental observations. Studying mathematically the coupling of two or more dynamical systems with oscillatory behavior raises several important questions that will be addressed in this thesis: what type of dynamic behavior characterizes the coupled system; in which way the coupling scheme affects the system response; do the dynamical features of the systems as individuals have an impact on the coupled system response; how to characterize the potential of the coupled system for period control or tunability; can one of the systems control the other's period and amplitude, through suitable coupling schemes.

From a synthetic biology perspective: research in the rapid developing field of synthetic biology and molecular engineering seeks to study, design and construct new biological circuits. In this context, synthetic models that represent the core function of complex biological processes have been developed with the objective to be implemented in a living cell environment. The systems studied in this thesis follow the principles of synthetic biology, in terms of design, dynamical features and capacities. Employing both mathematical analysis and numerical simulations, we wish to provide predictions and suitable conditions, with the potential to be utilized as directions for synthetic circuit design and improvement.

From a biological perspective: the thesis is motivated by studies of complex biological mechanisms with rhythmicity, such as the cell cycle and the circadian clock. These biological processes have been modelled and studied to a great extent, not only as individual biological oscillators, but more recently, also as interconnected mechanisms. Breakthroughs in molecular biology suggest bidirectional links between the two oscillators. The deeper comprehension of this interconnection aims to contribute to the development and improvement of medical treatments for several diseases, including cancer.

In the next sections of this chapter, we present principles of mathematical modeling of molecular processes based on the literature; we describe the synthetic biology concepts in which we aim to contribute with this thesis, and present the basic definitions and characteristics of the biological oscillators that motivate our work.

1.2 Synthetic biology approaches

Synthetic biology is a rapidly growing field, which coupled with computational systems biology, seeks to design and create new biological circuits in order to understand the complex pathways in living organisms and open new horizons in the approach to biology. Production of "green" biofuels, clinical diagnostics, medical treatments and construction of artificial micro-organisms and genetic devices are some of the numerous synthetic biology applications (Weber and Fussenegger, 2011).

This relatively new area requires engineering concepts for the synthetic circuit design, improvement and efficient performance. The conceptual basis and objectives of the synthetic biology approaches rely mainly on new findings in molecular biology. Theoretical knowledge extracted from experimental studies sets the principles to follow and the hypotheses to investigate about molecular networks and interactions. Current experimental observations have major contributions to synthetic circuit design and modeling. Hence the latest developments in the field of synthetic bioengineering include systems composed of pathways designed to tackle challenges in modeling, such as the complexity and the means of regulation in the natural biological networks (Cheng and Lu, 2012,Brophy and Voigt, 2014,Hsiao, Swaminathan, and Murray, 2018).

The construction of synthetic gene circuits in a living cell environment (*in vivo*) attempt to clone biological pathways, with the main purpose to studying and comprehending their features and behavior, gaining insight into the complex way of their functioning. At the same time, numerical simulations and computations (implementation *in silico*), combined with theoretical knowledge, contribute to experimental synthetic biology set-up and design by providing guidelines, validation and prediction (He, Murabito, and Westerhoff, 2016,Del Vecchio, Dy, and Qian, 2016,Hsiao, Swaminathan, and Murray, 2018).

After the engineering part of the circuit design, the scientists face the challenge of the suitable choice, configuration and supervision of the components for the implementation. In this context, control theory techniques are employed to complement the joint effort of biologists and bio-engineers for efficient design and enhanced performance. The objective is to deploy control theoretical tools that will contribute to the intended activity of the circuits and would potentially be part of the synthetic implementation. Feedback control is of a great interest to the field of bio-engineering,

since it appears to follow observations of natural regulation, and it provides promising results in terms of robustness of the synthetic circuits performance under diverse conditions (Del Vecchio, Dy, and Qian, 2016,Hsiao, Swaminathan, and Murray, 2018). Furthermore, synthetic biologists use enhancers that can be considered as external inputs or control tools, such as drugs or inducers, to regulate molecular activities and interactions, in order to promote their robustness and performance (Hsiao, Swaminathan, and Murray, 2018).

A plethora of research in synthetic biology patterns, tools, techniques and frameworks has been published since 2000, showing intriguing results, with main focus on gene regulation and molecular interactions (Hsiao, Swaminathan, and Murray, 2018). In particular, on biological mechanisms and interactions that act as switches and oscillators regulating the cellular activity (Tyson et al., 2008).

The implementation of new synthetic circuits in a cell, uses basic molecular components such as pieces of DNA, and relies in gene expression and its regulatory mechanisms. The next section very briefly refers to basic definitions and descriptions of biological processes, at the basis of gene regulatory networks.

1.3 Gene Regulatory Networks

1.3.1 Gene expression

In all organisms, a *gene* is a chain of organic molecules that contains all the necessary information for the *gene expression*, i.e. the synthesis of a functional product. A gene product can be transformed into *messenger RNA* through the biochemical process of *transcription*. The messenger RNA is used to synthesize the corresponding protein, through the process of *translation* (for a reference used throughout this section see, for instance, Bruce Alberts and Walter, 2002). The gene expression is initiated with the enzyme *RNA polymerase*, which creates the gene product using the DNA pattern. This enzyme must bind to a specific site of the gene, the *promoter*, see Fig.1.1. A promoter is a sequence of DNA and it is an essential module of the gene expression, along with other elements of the gene structure, due to its location near the gene binding sites for the *transcription factors*. The transcription factors are proteins that regulate the gene expression, determining whether a gene is active or not ("on" or "off"). The transcription factors that bind to the gene in order to enhance the transcription rate or its synthesis, are called *activators*; conversely, the proteins that block the transcription rate are called *repressors*.

In Fig. 1.1 we present an abstract illustration of the transcription-translation process. When an activator binds to the gene, (additionally to the binding of RNA polymerase to the promoter), it enhances the gene expression. Whereas if a repressor binds to the gene, it blocks the transcription process, preventing mRNA synthesis.

A *gene regulatory network* (GRN) is defined as a group of molecular components or *regulators*, that are linked to each other and with other cellular structures to control the gene expression and its products, i.e. proteins and functional RNA.

Mathematical modeling is employed for the analysis, study and comprehension of the core functions and gene regulations that underlie complex biological mechanisms. The next section recalls basic steps for the representation of gene expression processes by mathematical models.

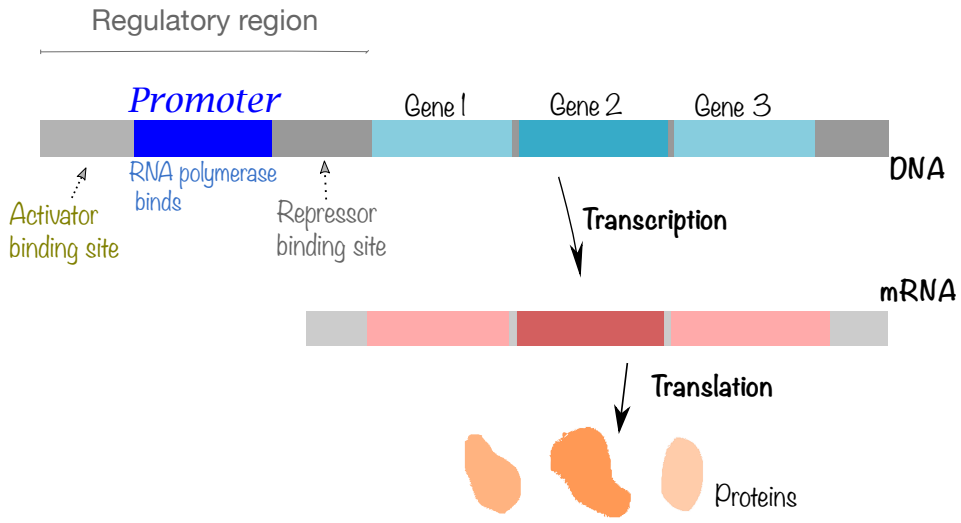

FIGURE 1.1: A simplified scheme illustrating gene expression in bacteria.

1.3.2 Modeling gene regulatory networks

Basic definitions In mathematical models of gene regulatory networks, the molecular links between the components of the network can be expressed through a system of ordinary differential equations (ODEs): $\dot{x}_i = f_i(x_1,\ldots,x_n)$, where $x_i, \in [0,+\infty)$, $i = 1,\ldots,n$, represents the the concentration of molecular species j (such as mRNA or proteins) and the $f_i : \mathbb{R}^n_{\geq 0} \to \mathbb{R}_{\geq 0}$ depend on the nodes x_j that have an effect on species x_i.

Throughout this thesis, we will focus on some of the most common forms of interactions between the molecular elements of a regulatory network: inhibition or activation of gene transcription and synthesis or degradation of gene products. These interactions can commonly be expressed by mathematical formulations based on *mass-action* laws, *saturation* or *Hill functions* (Jong, 2002). Analytically, an increasing Hill function is defined as:

$$h^+(x_j,\theta_j,m_j) = \frac{x_j^{m_j}}{\theta_j^{m_j} + x_j^{m_j}} \tag{1.1}$$

with $x_j \in [0,+\infty)$, $m_j \in \mathbb{R}_{>0}$, and is well suited to represent the activation or *synthesis rate* of a given gene as a function of a transcription factor x_j. The activity threshold $\theta_j > 0$ characterizes the concentration of species x_j which is needed to effectively activate transcription. The Hill exponent m_j represents a cooperative effect.

Respectively, in the case of repression of the given gene by a species x_j, the inhibition function can be represented as decreasing Hill function:

$$h^-(x_j,\theta_j,m_j) = \frac{\theta_j^{m_j}}{\theta_j^{m_j} + x_j^{m_j}} = 1 - h^+(x_j,\theta_j,m_j) \tag{1.2}$$

also with $x_j \in [0,+\infty)$, $m_j \in \mathbb{R}_{>0}$ and $\theta_j > 0$. The synthesis rate of a species x_i is represented by a function $g : \mathbb{R}^n_+ \to \mathbb{R}_+$, $g_i(x) > 0$. In general, functions g_i can be written as sums of products of Hill functions. The natural decay or *degradation rate*

of a species x_i is frequently described by a linear function $d : \mathbb{R}_+ \to \mathbb{R}_+$, $d_i(x) = \gamma_i x$, where the parameter $\gamma_i \geq 0$ represents the velocity of degradation of species x_i. Finally, the concentration of species x_i is governed by the equation:

$$\dot{x_i} = g_i(x) - d_i(x). \tag{1.3}$$

Example: negative feedback loop Indicatively, we give an example of a *negative feedback loop*, that is a common motif in genetic networks; it consists of two antagonistic components, the proteins A and B, with concentrations x_1, x_2: A promotes the synthesis of the protein B (activation) and B inhibits A (repression): A$\to$ B, B $\dashv$ A. This interaction can be mathematically modeled through the ODE system:

$$\begin{aligned} \dot{x_1} &= \kappa_{10} + \kappa_{11} \frac{\theta_2^{m_2}}{\theta_2^{m_2} + x_2^{m_2}} - \gamma_1 x_1 \\ \dot{x_2} &= \kappa_{20} + \kappa_{21} \frac{x_1^{m_1}}{\theta_1^{m_1} + x_1^{m_1}} - \gamma_2 x_2 \end{aligned} \tag{1.4}$$

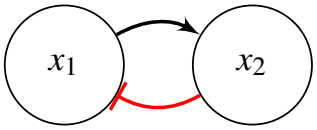

FIGURE 1.2: A negative feedback loop of two genes, an activator (x_1) and a repressor (x_2).

The parameters κ_{i1} denote maximal synthesis rates and κ_{i0} denote basal activity. To study the dynamical behavior of this system, a qualitative analysis is shown in Fig. 1.3, which depicts the phase space with the two nullclines intersecting at the single steady state, the direction of the vector field in each region, and one trajectory.

Under the following parameter conditions: $\gamma_1 < (k_{10} + k_{11})$, $\theta_2 < (\kappa_{20} + \kappa_{21})/\gamma_2$ and m_i, $i = \{1,2\}$ large, there is one single steady state x^* for system 1.4, which is stable.

Piecewise affine systems To facilitate the analysis and further study of continuous models for gene regulatory networks with higher order of complexity, the piecewise affine framework introduced by Glass and Kauffman, 1973 is very useful (see also Casey, Jong, and Gouzé, 2006). In this framework, Hill functions are approximated by *step functions*. To *qualitatively* relate this approximation with species concentrations, consider large values of the Hill exponent ($m_i \to \infty$), then it follows that for x_i above the threshold θ_i (respectively, below the threshold θ_i), the Hill function converges to 1 (respectively to 0).

We recall the Hill functions and notation of §1.3.2. Define $\mathcal{N}$ the set of species $i = 1,\ldots,n$ composing a gene regulatory network. The function (1.1), that expresses activity of some species j, is now approximated by the increasing step function $s^+ : \mathbb{R}_+ \times \mathbb{R}_+ \to \{0,1\}$:

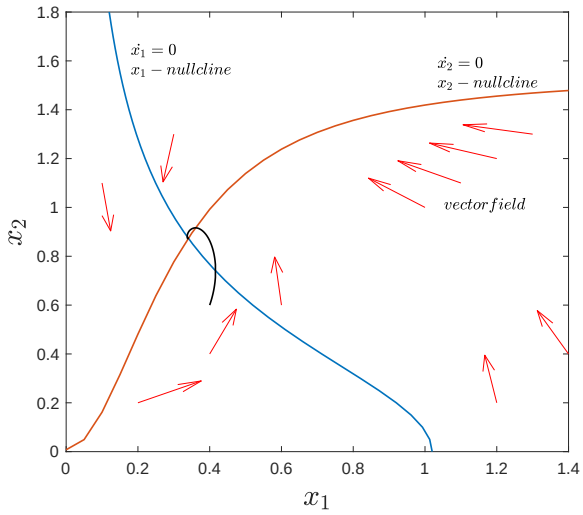

FIGURE 1.3: The phase portrait of system 1.4 is divided by the nullclines into four regions. One trajectory converging to the steady state is shown in black. The red arrows represent the direction and sign of the vector field in each of the four regions of the phase portrait. Parameters used: $\kappa_{10} = 0.02$, $\kappa_{11} = 1$, $\theta_1 = 0.3$, $\gamma_1 = 1$, $\kappa_{20} = 0.05$, $\kappa_{21} = 2$, $\theta_2 = 0.6$, $\gamma_2 = 1.3$, $m_1 = m_2 = 2$.

$$s^+(x_j,\theta_j) = \begin{cases} 1, & \text{if } x_j > \theta_j \\ 0, & \text{if } x_j < \theta_j. \end{cases} \tag{1.5}$$

Respectively, the step function representing inhibition is given by $s^- : \mathbb{R}_+ \times \mathbb{R}_+ \to \{0,1\}$, $s^-(x_j,\theta_j) = 1 - s^+(x_j,\theta_j)$.

The synthesis rate of species x_i, which is regulated by species x_j, $j \in \mathscr{J}$, $\mathscr{J} \subset \mathscr{N}$ and is represented by the function $g_i : \mathbb{R}_+ \to \mathbb{R}_+$, can now be written as:

$$g_i(x) = \sum_{j \in J} \kappa_{ij} \delta_{ij}(x), \tag{1.6}$$

where $\kappa_{ij} > 0$ are synthesis parameters, and $\delta_{ij} : \mathbb{R}_+ \to \{0,1\}$, is a combination of step functions expressing the effect of species j on species i. It takes values $\{0,1\}$ as the regulations are expressed by combinations of step functions.

For the example 1.3.2 of the negative feedback loop, the piecewise affine system associated with (1.4), is therefore defined as:

$$\begin{aligned} \dot{x_1} &= \kappa_{10} + \kappa_{11} s^-(x_2,\theta_2) - \gamma_1 x_1 \\ \dot{x_2} &= \kappa_{20} + \kappa_{21} s^+(x_1,\theta_1) - \gamma_2 x_2 \end{aligned} \tag{1.7}$$

The phase space of the system is now partitioned into the following *regular domains* (Casey, Jong, and Gouzé, 2006):

- $D_{10} = \{(x_1,x_2) \in \mathbb{R}^2_+ : x_1 \in [0,\theta_1], x_2 \in [0,\theta_2)\}$

- $D_{11} = \{(x_1,x_2) \in \mathbb{R}^2_+ : x_1 \in [\theta_1,+\infty), x_2 \in [0,\theta_2)\}$
- $D_{01} = \{(x_1,x_2) \in \mathbb{R}^2_+ : x_1 \in [\theta_1,+\infty), x_2 \in [\theta_2,(\kappa_{20}+\kappa_{21})/\gamma_2)\}$
- $D_{00} = \{(x_1,x_2) \in \mathbb{R}^2_+ : x_1 \in [0,\theta_1], [\theta_2,(\kappa_{20}+\kappa_{21})/\gamma_2)\}$

Here, each regular domain is labeled by the corresponding value of the step functions: for instance, in D_{10}, since both x_1 and x_2 are below their thresholds, it follows that synthesis of x_1 is turned on, $s^-(x_2,\theta_2) = 1$, while synthesis of x_2 is turned off, $s^+(x_1,\theta_1) = 0$. In each of the four domains the system is affine and the solution can be explicitly computed in terms of the *focal points*, which are given in Table 1.1. In D_{10} the solution of the system has the form:

$$\begin{aligned} x_1(t) &= \phi^1_{10} + (x_1(t_0) - \phi^1_{10})\exp(-\gamma_1(t-t_0)) \\ x_2(t) &= \phi^2_{10} + (x_2(t_0) - \phi^2_{10})\exp(-\gamma_2(t-t_0)), \end{aligned} \tag{1.8}$$

and similarly for the other domains. The global solution is given by a concatenation of the solutions in each region, in the appropriate sequence.

TABLE 1.1: Focal points for system 1.7.

$\phi_{10} = ((\kappa_{10}+\kappa_{11})/\gamma_1, \kappa_{20}/\gamma_2)$
$\phi_{11} = ((\kappa_{10}+\kappa_{11})/\gamma_1, (\kappa_{20}+\kappa_{21})/\gamma_2)$
$\phi_{01} = (\kappa_{10}/\gamma_1, (\kappa_{20}+\kappa_{21})/\gamma_2)$
$\phi_{00} = (\kappa_{10}/\gamma_1, \kappa_{20}/\gamma_2)$

More complex dynamics, such as multistability or periodic behavior, can be identified depending on the interaction between the system components. For instance, positive or negative feedback loops are two of the most common motifs in biological systems, and they combine in various ways to produce different regulatory network topologies and different dynamical behavior (Tsai et al., 2008). Both of these motifs have been implemented in synthetic biology, leading to fresh interpretations of molecular regulations and natural pathways.

In this thesis we study classic and novel synthetic models characterized by oscillatory dynamics. The next section is dedicated to giving a brief description of well studied synthetic oscillators that contributed to bringing insight into molecular interactions and dynamics.

1.4 Synthetic genetic oscillators

Two paradigms of synthetic genetic circuits appeared in 2000, in the same issue of the journal *Nature*: the repressilator by Elowitz and Leibler, which is a circuit exhibiting oscillatory behavior (see §1.4.1 below), and the toggle switch designed by Gardner, Cantor, and Collins, 2000. The toggle switch is a gene regulatory network synthetically constructed in bacteria *E. coli*. It consists of two genes that mutually inhibit each other, forming a positive feedback loop as illustrated in Fig. 1.4. The

dynamics exhibits two stable steady states, allowing the system to switch from one stable steady state to another, following a suitable external stimulus.

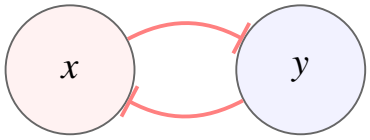

FIGURE 1.4: Toggle switch network.

Biological oscillators govern crucial physiological pathways and mechanisms, such as the cell cycle, the circadian rhythms, the neuronal system, the heart rate and many others (Goldbeter, 2008). Here we discuss oscillatory circuits that came from research developments in synthetic biology and appear frequently in the literature. We consider two generic categories of circuits: the first consists of repressilator models and the second of two-gene circuits with additional auto-regulation of the components.

1.4.1 Repressilators

A repressilator generally consists of a group of genes, organized in a cyclic topology, where each gene represses transcription of the next (Fig. 1.5).

Goodwin oscillator The first synthetic circuit, the *Goodwin oscillator* (Goodwin, 1963), consists of one gene that represses itself leading to oscillatory behavior under certain conditions, with robust period according to simulations. However, the in vivo implementation showed non-robust oscillations (Stricker et al., 2008, Purcell et al., 2010).

Repressilator A successor of the Goodwin oscillator is a well known synthetic circuit, the *repressilator*, implemented by Elowitz and Leibler, 2000. It was first introduced as a synthetic regulatory network of three genes each of which inhibits the next gene of the network, successfully formulating a negative feedback loop. Mathematical analysis of the model indicates oscillatory behavior with suitable parameters, generated by a Hopf bifurcation (Müller et al., 2006). The system represents networks with cyclic topology, Fig. 1.5 and it has applications to genetic networks, neuroscience and engineering.

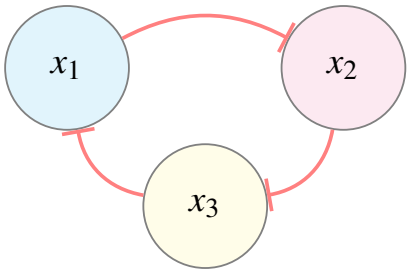

FIGURE 1.5: Repressilator network.

Following the analysis of Müller et al., 2006, the term "repressilator" covers a wider range of models; in particular, as repressilators can be considered the networks of one or more genes (an odd number of genes) that formulate a cycle or *ring* of genes, in which each gene represses its successor in the network. The three-gene repressilator has been implemented numerically in different frameworks (ODEs, stochastic modeling), showing oscillatory capacity, as well as tunable amplitude and period by increasing the time delay in the system (Wang, Jing, and Chen, 2005, Purcell et al., 2010).

The in vivo implementation of the circuit was performed using proteins of different type bacteria and it was embedded in E.coli. Several questions arise from the in vivo implementation of synthetic circuits, for instance how the synthetic network is integrated in the whole organism. In the repressilator network, the results indicated a correlation between the repressilator activity and the global cell growth regulation. However, the overall view showed noisy oscillatory behavior (Elowitz and Leibler, 2000). In 2016, the repressilator was newly implemented, using several modifications in the biological system, which lead to more regular and robust oscillations (Potvin-Trottier et al., 2016).

Recently, studies on the improvement of the repressilator design in terms of dynamical behavior and robust oscillatory behavior provide new results (Tyler, Shiu, and Walton, 2019). Moreover, the repressilator was initially designed to act as biological clock (Elowitz and Leibler, 2000), and it has shown to capture features of the *circadian clock*, in terms of oscillations and core molecular interactions (Pett et al., 2016).

1.4.2 Two-gene oscillators with auto-regulation

Amplified feedback oscillators This category of two-gene oscillators comprises synthetic circuits composed of a gene that activates the transcription of the second gene, while the latter inhibits the first gene. There is an additional positive loop acting on the gene activator, promoting its own transcription (auto-regulation) (Fig. 1.6).

Mathematical analysis of models with such topology (Atkinson et al., 2003, Guantes and Poyatos, 2006,Conrad et al., 2008), suggest that oscillations occur from saddle-node bifurcation on an invariant circle or a subcritical Hopf bifurcation as a result of great difference between the activator and repressor dynamics. Numerical simulations also reveal oscillations with large period due to conservation of the components high concentration levels for an extended time (Guantes and Poyatos, 2006). For realistic parameter values, numerical simulations of the model studied by Atkinson et al., 2003, showed dumped oscillations and in vivo implementation of the model follows these observations.

Various amplified synthetic oscillators with different hypotheses for the components interactions, including intermediate links with detailed molecular pathways, have been studied and implemented. In general, although the mathematical analysis, the simulations of the models, and the hypotheses tested imply capacity for oscillatory behavior, no robust or sustained oscillations were observed when implemented in vivo (Purcell et al., 2010). However, the topology in Fig. 1.6 is of great interest to the synthetic biologists that intend to design models with sustained oscillatory

dynamics. In the next paragraphs we present the synthetic circuits that supported oscillatory behavior when implemented in a living cell environment.

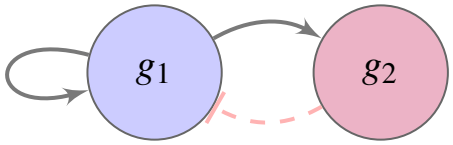

FIGURE 1.6: The two-gene oscillator by Tigges et al., 2009: g_1 represents the first gene whom the sense copy is translated into protein, g_2 represents the second gene that acts as a repressor through activation of the antisense of gene 1, which represses the translation of gene 1.

Two-gene oscillator with positive auto-regulation

The successful in vivo implementation of a synthetic two-gene oscillator in eukaryotic cells was an innovative achievement in synthetic biology, made by Tigges et al., 2009. The two-gene oscillator is designed as a synthetic mammalian circadian clock, i.e. as a synthetic oscillator with dynamical features that imitate core functions of a complex biological mechanism. The circuit is formed by a pair of genes of type *sense-antisense* (DNA sequences that are reverse copies of each other). The sense copy or transcript of the first gene (activator) is translated into a protein that promotes its own transcription (auto-regulation) and that of the other gene. The second gene activates the antisense copy of the first gene, while the antisense copy represses the transcription of the first gene through *hybridization* during the step of translation. The process of hybridization is the combination of the two sense-antisense molecules to form a single molecule. The circuit can be schematically represented as illustrated in Fig. 1.6.

The model was calibrated from in vivo experimental data and it includes time-delay. Numerical simulations indicate that the system is characterized by tunabable period. Oscillations are robust to variations of degradation rates, yet affected by the *gene dosage* (amount of gene copies). The gene dosage was also shown to influence the amplitude of the limit cycle and the period. In addition, control by repression of the sense-gene activation leads the oscillations to start or shut down. In vivo implementation is in accordance with the discussed predicted dynamical characteristics and showed sustained oscillations with a period of 170 ± 71 (mean $\pm$ s.d.) min (Tigges et al., 2009, Purcell et al., 2010).

In the study of Tigges et al., 2010, an alternative configuration of the initial model was implemented as an attempt to obtain an oscillator with large period (approximately 26h). The system showed sustained oscillations, though it lost the period tunability. On top of that, only a minor percentage of the cells underwent oscillations. Overall, simulations and in vivo implementation of the two-gene oscillators introduced by Tigges et al., highlight results on molecular interactions (sense-antisense), dynamical behaviors (gene dosage and period tunability) and capacities (sustained oscillations).

Two-gene oscillator with positive and negative auto-regulation

Consistency and robustness of the desired oscillatory behavior is crucial for in vivo implementation of synthetic networks. A synopsis on extensively studied and implemented synthetic oscillators suggests that the two-gene oscillator introduced by Smolen, Baxter, and Byrne, 1998, has shown reliability and robust performance when compared to other implemented circuits. Its topology is described as a two-gene oscillator composed of a transcriptional factor (activator) that activates the transcription of itself and of the other gene; the latter represses the transcription of the activator, while it also represses its own activity.

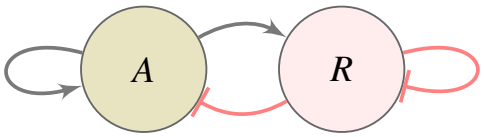

FIGURE 1.7: Smolen oscillator network.

Mathematical analysis of the system in different types of models have shown capacity for diverse dynamical behaviors (Smolen, Baxter, and Byrne, 1998,Purcell et al., 2010). In the model of Hasty et al., 2002 oscillations occur with supercritical or subcritical Hopf bifurcation due to faster degradation rate of the activator. For a comprehensive model based on experiments using an inducer for the activation, coexistence of two periodic orbits -with longer and shorter period respectively appears for higher inducer levels. Whereas lower inducer levels result in one periodic orbit and one stable equilibrium point leading to damped oscillations (Stricker et al., 2008).

Numerical simulations suggested a period of approximately 40 min for the ODE models of Smolen oscillator (Smolen, Baxter, and Byrne, 1998, Stricker et al., 2008). Regarding the form of the limit cycle and the oscillations characteristics, a feature that has been observed is the much higher concentration of the activator. By adding time delay in the models with larger period, the oscillations of the system were replaced by new periodic orbits induced by the delay, hence with the same period as the delay (Smolen, Baxter, and Byrne, 1999). Furthermore, in the version of the model based on experimental data (Stricker et al., 2008), increasing the time delay, the parameter region in which oscillations occur also increased. On top of that, this detailed system has shown to have the capacity for tunable period. In particular, higher levels of the inducers for repression and activation, are in favor of period increase, decrease or stabilization accordingly. In addition, with the use of parameters to express the temperature, it was observed that the period decreases as the temperature becomes higher (Stricker et al., 2008, Purcell et al., 2010).

The circuit was implemented using the araC and lacI genes for the activator and the repressor respectively. Surprisingly, more than 99% of cells yielded oscillations, the period of which was the same as predicted in simulations, approximately 40 min. Moreover, the tunability of the period and its correlation with the temperature, were also observed in the experimental results (Stricker et al., 2008). Ultimately, robust oscillatory behavior is of great significance for in vivo implementation of synthetic oscillators, and indeed Smolen oscillator has shown to possess this capacity.

1.5 Circadian rhythms and intercellular connections

Among the natural biological oscillators, throughout this thesis we will be especially motivated by circadian rhythms and its interactions with other cellular oscillators, in particular, the cell cycle. This is partly in the context of interdisciplinary project *ICycle*, whose goal is to study and understand the interconnections between cell cycle and circadian clock, using both mathematical and computational analysis and synthetic biology approaches.

Circadian rhythms Internal rhythms that govern biological activities, they are ubiquitous in nature: endogenous rhythmicities have been observed in plants, insects, animals, humans. The word *circadian* comes from the latin "circa" and "diēm", which means "around a day", pointing to the fact that the rhythmicity is related to the day-night cycle (24h). Circadian rhythmicities are endogenous and autonomous mechanisms that can be adjusted by external or internal factors, like (sun) light, temperature, or hormones (Harmer, Panda, and Kay, 2001,Herzog, 2007).

In mammalian tissues, circadian rhythms are driven by a central mechanism, the *circadian clock*, which is a biochemical complex mechanism with oscillatory properties. The circadian system in mammals is organized hierarchically: the central circadian clock receives signals from external stimuli, for example light, it translates the information making suitable adaptations and transmits this information to the peripheral clocks of individual cells and organs. In humans, the central clock is situated in the brain, in a group neurons called the suprachiasmatic nuclei (SCN) (Ralph et al., 1990,Reppert and Weaver, 2002). The SCN maintains the rhythmicity in physiological activities through the regulation of a large amount of genes.

The interactions of the circadian clock molecular components lead to rhythmicity of 24h (Czeisler et al., 1999). The oscillations are driven by a core negative feedback loop, that involves transcriptional factors for repression (Per/Cry) and activation (Bmal1/Clock) (Gekakis et al., 1998). There are also secondary feedback loops related to the core loop: the complex of proteins Bmal1/Clock promotes the transcription of Rev-erbα and RORα genes (Preitner et al., 2002,Sato et al., 2004), while the produced REV-ERB protein acts as repressor of Bmal1, and ROR proteins as activator.

Disruptions of circadian rhythms are linked to several problems and diseases. For instance, the jet lag is a common experience for people travelling across time zones. More importantly, desychrony of circadian rhythms is linked to more serious conditions, like tumorigenesis and cancer.

Cell cycle and circadian clock The most important events during the life of a cell (*cell cycle*) are the DNA synthesis, growth and preparation for cell division (mitosis) and finally the cell division into two daughter cells. These events are driven by a network of proteins that form large complexes, the cyclin-dependent kinases (CDKs). It has been observed that genes playing major role in cell division and proliferation, are regulated by the circadian clock (indicatively, for references see the reviews of Hunt and Sassone-Corsi, 2007, Gaucher, Montellier, and Sassone-Corsi, 2018). Experimental observations indicate that the molecular links between the circadian clock and the cell cycle are formed -among others- by the transcriptional factor Bmal1 that

promotes the expression of the kinase inhibitor Wee1 (Matsuo et al., 2003), crucial component of mitotic phase. More recently, new experimental evidence shows that there exist bidirectional interactions between the cell cycle and the clock (Feillet et al., 2014,Bieler et al., 2014). For the molecular links characterizing the cell cycle effect on the circadian clock, there are indications of interaction from the cyclin-dependent kinase CDK1 to the protein REV-ERBα, through phosphorylation (Zhao et al., 2016). However, the molecular interactions and means of bidirectional connection of the the cell cycle and circadian clock are not yet fully understood (Feillet et al., 2015). Model-based studies explore the mutual coupling of the two biological oscillators indicating robust synchronization under strong bidirectional interconnection (Gérard and Goldbeter, 2012,Yan and Goldbeter, 2019).

Circadian clock and chronotherapy As a result of the circadian rhythms crucial role as a controller of individual cells normal activities, several diseases and drug effects can also be regulated by the circadian system. *Chronotherapy* refers to therapies based on timing drug-taking relative to the phases of the circadian cycle, with the main purpose to improve treatments and patient response. Hence the study and comprehension of the molecular interconnections of the circadian clock and cell cycle can contribute to developments in chronotherapeutics.

1.6 Coupling of biological oscillators

Coupled oscillators are connected oscillators in a fashion that their individual activity is diffused between them. Coupled oscillators are subject of study and application in many fields: mathematics, physics, mechanics and biology. The dynamics of coupled oscillators has been extensively studied and analyzed, yet questions on the mechanisms establishing their interaction remain open. Synchronization in frequency, synchronization in phase, chaotic behavior or stabilization are phenomena observed in a coupled system of oscillators. The synchronization was first described by Christian Huygens in 1665, with two pendulum clocks of identical frequency that operate close enough on the same wall, and in this way they synchronize.

Coupled circadian clocks The coupling of biological oscillators appears in several physiological mechanisms. An outstanding example is the circadian system in mammals, (as we mention in previous paragraph) with the central clock SCN to consist of approximately 20,000 neural cells organized in a fashion that allows their communication and synchronization (Herzog, 2007,Brancaccio et al., 2014), while it is also connected to peripheral clocks across the organism (Mohawk, Green, and Takahashi, 2012). The circadian rhythm is responsible for the synchronization and collective activity of brain cells (Hastings, Maywood, and Brancaccio, 2018). Experimental studies of the coupled network of neurons in the mammalian SCN (Aton et al., 2005,Welsh, Takahashi, and Kay, 2010), and model-based investigations on the schematic way of interaction between the oscillators, (Kunz and Achermann, 2003, Bernard et al., 2007, Hafner, Koeppl, and Gonze, 2012), seek to comprehend its complex underlying mechanisms generating sustained oscillations and synchronization.

Also, several models for a coupled network of circadian oscillators investigate conditions and individual dynamics under which synchronization of oscillators is achieved (Gonze et al., 2005, To et al., 2007, Komin et al., 2011).

The network of coupled circadian oscillators has inspired several theoretical studies in the literature for synchronization and network dynamics of coupled identical oscillators (Mirollo and Strogatz, 1990,Matthews, Mirollo, and Strogatz, 1991, Ashwin, 1992,Glass, 2001). Recent works on networks of identical oscillators, provide a classification of clusters of synchronized elements to the same state (Sorrentino et al., 2016, Chen, Engelbrecht, and Mirollo, 2017).

The circadian clock constitutes by itself a coupled network of neurons and peripheral clocks. In parallel, major events in the life of the cell are controlled by circadian rhythms (Khapre, Samsa, and Kondratov, 2010,Panda, 2016), thus raising the question of the synchronization of the two mechanisms. Apart from experimental studies pointing towards this bidirectional interaction (recall §1.5), this relation has also attracted much attention motivating many mathematical modeling and computational/simulation studies. Remarkably, studies based on realistic models for the cell cycle regulation of the circadian clock, have shown entrainement for the cell cycle (Zámborszky, Hong, and Csikász Nagy, 2007, Gérard and Goldbeter, 2012, El Cheikh, Bernard, and El Khatib, 2014). On the other hand, numerical simulations of detailed bidirectionally coupled models including the indicated molecular interactions, have partly reproduced experimental observations (Traynard et al., 2016, Almeida, Chaves, and Delaunay, 2020). Moreover, model-based investigations for the dynamics of the coupled system cell cycle-circadian clock, have shown capacity for robust synchronization under suitable conditions on the bidirectional coupling (Yan and Goldbeter, 2019).

Coupled synthetic circuits Recent research in synthetic biology is set to explore the next stage in the construction of synthetic circuits, which is directed at coupling two (or more) known circuits. This will allow the (re)construction of systems with more complex dynamics, aimed at capturing physiological regulations or improvement and control purposes.

Computational studies of designs for combined synthetic modules (Teng et al., 2014) or coupled synthetic circuits (Perez-Carrasco et al., 2018) yield complex dynamical behaviors. Moreover, the repressillator is designed to model a biological clock, hence networks of repressilator representing the circadian clock coupled with other components, have been applied highlighting specific gene regulations (Pett et al., 2018). Furthermore, the coupling of synthetic systems can also serve for synthetic design enhancement, for instance for period modulation through a coupled element (Tomazou et al., 2018).

1.7 Thesis structure

Having described the thesis motivation and thematic background, we now present the organization of the main manuscript, consisting of the following chapters:

- **Chapter 2**

Based on bifurcation analysis, we first study different configurations of the Smolen oscillator, and then propose a variant with an extended parameter region for oscillations. We study the system with piecewise affine approximation and we prove existence and uniqueness of the periodic orbit under suitable analytical conditions on the parameters of the system. This chapter is partly based on the paper:

Firippi and Chaves, 2020. "Topology-induced dynamics in a network of synthetic oscillators with piecewise affine approximation". In: *Chaos: An Interdisciplinary Journal of Nonlinear Science* 30.11, p. 113128.

- **Chapter 3**

  Using the variant of the Smolen oscillator developed in Chapter 2, we present a network of N identical two-gene oscillators with piecewise affine approximation, with coupling schemes based on three different topologies. Our study provides analytical results for the coupled network dynamics, showing that new behavior may emerge due to the coupling, depending on parameter conditions. Numerical simulations for large N, illustrate and complement the theoretical part of our study. This chapter is also part of the paper:

  Firippi and Chaves, 2020, "Topology-induced dynamics in a network of synthetic oscillators with piecewise affine approximation". In: *Chaos: An Interdisciplinary Journal of Nonlinear Science* 30.11, p. 113128.

- **Chapter 4**

  Motivated by breakthroughs in molecular biology pointing towards the bidirectional connection between the cell cycle and the circadian clock through specific components, we study the coupling of the proposed variant of Smolen oscillator to act as a biological clock, and a reduced model of the mammalian cell cycle, calibrated from experimental data. We analyze different coupling schemes seeking to understand the role of the involved components on the coupled system response. Also, we relate the coupled system response with individual system dynamics. Moreover, we provide results for the coupled system period response based on a "controller-follower" analysis. This chapter is based on the paper:

  Firippi, Eleni and Madalena Chaves (Oct. 2019). "Period -control in a coupled systemof two genetic oscillators for synthetic biology". In: *IFAC-PapersOnLine* 52, pp. 70-75.

- **Chapter 5**

  Using numerical simulations, we explore the coupling of the proposed variant of Smolen oscillator and a well-studied synthetic oscillator, the three-gene repressilator. We apply one of the coupling schemes studied in chapter 4, for purposes of comparison and supplementation. The study of the coupled system under different coupling conditions, highlights the case of strong coupling between two robust oscillators. In this case, our analysis indicates that the coupled system has a period larger than each of the individual systems, thereby suggesting ways of tuning the period of one system by suitable coupling with the other system.

We close the manuscript with a conclusion on the results and contribution of our study, and a discussion on the perspectives, potential applications and possible extensions of our work.

Some of the perspectives are related to preliminary work that we incorporate in the manuscript as last sections. Notably, we present preliminary work on experimental data coming from the collaboration with Franck Delaunay, whose chronobiology laboratory is a partner in the interdisciplinary project ICycle (`https://project.inria.fr/icycle/`. Diffusion not authorized/ Diffusion non autorisée.

Finally, we also include a preliminary work on the coupling of N two-gene oscillators considering the continuous proposed model, and applying topological coupling schemes analogous to those studied in Chapter 3.

Chapter 2

Analysis and Improvement of Synthetic Circuit Design

From synthetic biology perspective we are interested in developing strategies for the improvement of circuits design. To improve the performance and robustness of the oscillatory dynamics in a living cellular environment, we consider the problem of augmenting the parameter region admitting periodic solutions.

We study the dynamics of a two-gene synthetic oscillator which has been implemented in living cellular conditions, the Smolen oscillator (Smolen, Baxter, and Byrne, 1998). This circuit has already shown capacity for robust oscillatory behavior when implemented in vivo, as we discuss in Introduction §1.4.2. Having as main objective to enhance its potential for effective implementation, we focus on the enlargement of the parameter intervals for sustained oscillations.

In a first step, to characterize the region of parameters which admits sustained oscillations for the two-gene oscillator, we first compute numerically the limit cycle solutions of the system as a function of its parameters, and then propose one way to increase the region of oscillations, based on bifurcation analysis.

As a second step, we analyze the proposed variant of Smolen oscillator in the piecewise affine framework. We study the piecewise affine system proving existence and uniqueness of the periodic solution. Furthermore, we analytically characterize the appropriate parameter conditions for the periodic solution.

2.1 The Smolen Oscillator

The two dimensional model introduced by Smolen, Baxter, and Byrne, 1998 is composed of two transcription factors *TF-A* and *TF-R* and models a negative feedback circuit of a form that appears for instance in the mechanism of the circadian clock: TF-A is a transcriptional activator that can bind to responsive elements DNA sequences (REs) and TF-R is a protein that represses transcription by competing with TF-A for binding to REs. Besides the core negative feedback loop there are also additional negative and positive autoregulations to the activator and the repressor. For simplicity, *TF-A* and *TF-R* are denoted *A* and *R* respectively. Considering that *A* activates both components and R represses both components in a similar way the

model of the oscillator becomes:

$$\begin{aligned} \frac{dA}{dt} &= V_A \frac{A^2}{A^2 + \theta_0(1 + R/\theta_2)} - \gamma_A A + r_{bas} \\ \frac{dR}{dt} &= V_R \frac{A^2}{A^2 + \theta_1(1 + R/\theta_2)} - \gamma_R R \end{aligned} \tag{2.1}$$

The parameters V_A, $V_R > 0$ express the synthesis rate of the two transcriptional factors and are measured in min^{-1}. The degradation rate parameters γ_A, $\gamma_R > 0$ are also measured in min^{-1}. The term r_{bas} denotes basal activity. The concentration and activity thresholds θ_0, θ_1, $\theta_2 > 0$ are considered to be dimensionless. For the parameter set given by Smolen, Baxter, and Byrne, 1998 (we call it p_S) the model has a periodic solution.

System (2.1) is a good candidate for implementation in synthetic biology, due to its reduced dimension. However, in a neighbourhood of p_S, the region of parameters where oscillations are observed is rather small. In this study, our first goal is to better understand the effect of each parameter in generating oscillations, and propose a more efficient design.

2.1.1 An improved Smolen Oscillator

Three alternative cases for the model have been explored with the objective of improving the design of system (2.1), such that periodic solutions are observed for a larger region of the parameter set: (a) eliminating the autoregulation of the activator (positive self-loop on A), (b) eliminating both self-loops and (c) eliminating the autoregulation of the repressor (negative self-loop on R). From our analysis and simulations only the third case (c) appeared to admit periodic solutions.

c.Removing self-inhibition If the self-inhibition loop on R is removed the system (2.1) becomes:

$$\begin{aligned} \frac{dA}{dt} &= V_A \frac{A^2}{A^2 + \theta_0(1 + R/\theta_2)} - \gamma_A A + r_{bas} \\ \frac{dR}{dt} &= V_R \frac{A^2}{A^2 + \theta_1} - \gamma_R R \end{aligned} \tag{2.2}$$

The time solution and the phase portrait for system 2.2 are depicted in Fig. 2.2.

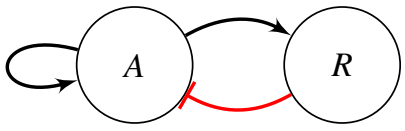

FIGURE 2.1: Smolen oscillator without repressor autoregulation.

In the next paragraphs, we will compare the dynamics of the original system (2.1) with the alternative (2.2).

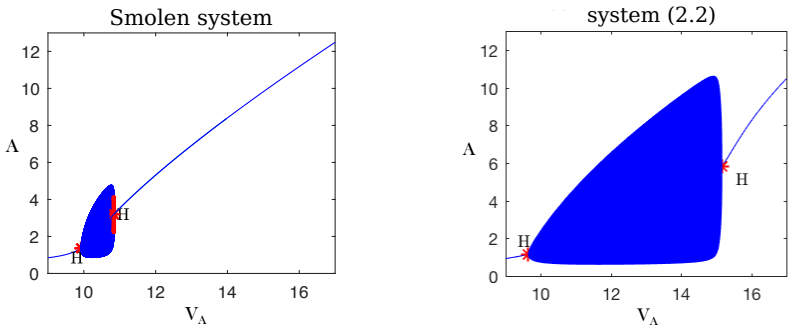

FIGURE 2.3: Bifurcation analysis for the V_A parameter (synthesis rate of A) and the the amplitude of the limit cycle, for the two systems, the Smolen model and case (2.2). The red stars indicate critical Hopf bifurcation.

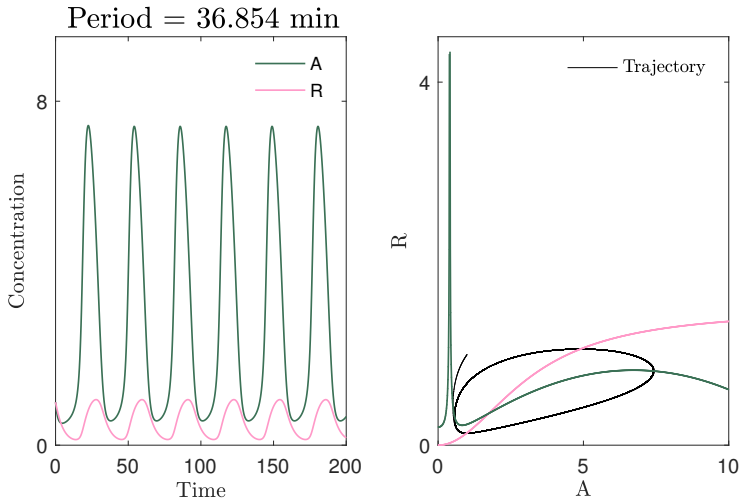

FIGURE 2.2: Activity of the Smolen oscillator eliminating the autoregulation of the repressor, model (2.2). The parameter values are: $V_A = 13.5\ min^{-1}$, $V_R = 0.3\ min^{-1}$, $\gamma_A = 1\ min^{-1}$, $\gamma_R = 0.2\ min^{-1}$, $r_{bas} = 0.4\ min^{-1}$, $\theta_0 = 10, \theta_1 = 10, \theta_2 = 0.2$.

2.1.2 Bifurcation analysis

Using the numerical toolbox MatCont for MATLAB, developed by Govaerts, Kuznetsov, and Dhooge, 2005, we perform bifurcation analysis for the model parameters given by Smolen, Baxter, and Byrne, 1998. First, we performed bifurcation analysis for the activator synthesis rate parameter V_A, for the original model (2.1) and case (2.2), shown in Fig. 2.3. Comparing the results we observe that the interval in which periodic solutions exist for the system, increased significantly for the case (2.2): the length of the interval increased by a factor 6. A second observation is that the amplitude of the limit cycle increased -approximately doubled- for (2.2).

We also perform two parameter bifurcation analysis for the repressor parameters of (2.1) and (2.2). The results are in an agreement with the one parameter analysis

regarding the increase of the oscillations interval. From the comparison we conclude that removing the autoregulation of the repressor increases the parameter region where oscillations exist, by approximately doubling the range allowed for each parameter.

We next further analyse the system (2.2) in the context of the piecewise affine formalism (PWA), introduced by Glass and Kauffman, 1973. The general idea of this formalism is to approximate the Hill functions expressing activation and inhibition by step functions: the state space is partitioned into rectangular domains, in which the vector field is affine. From our analysis, we will establish suitable parameter configurations and compute the first return map of the PWA system and prove that there exists a unique stable periodic orbit for certain parameter conditions.

2.2 Piecewise affine formalism

The piecewise affine (PWA) systems studied first by Glass and Kauffman, 1973 facilitate the system further study and analysis. This formalism is based on the approximation of the Hill functions that express the activation and inhibition (or repression), by increasing and decreasing step functions.

A synopsis of the PWA formalism based on the study by Casey, Jong, and Gouzé, 2006 is recalled in this section: if x_i is the concentration of the gene i and θ_i^j the concentration threshold that characterises the effect of x_i on x_j, the increasing step function $s^+ : \mathbb{R}_+ \times \mathbb{R}_+ \to \{0,1\}$ is defined:

$$s^+(x_i, \theta_i^j) = \begin{cases} 1, & \text{if } x_i > \theta_i^j \\ 0, & \text{if } x_i < \theta_i^j \end{cases} \tag{2.3}$$

Accordingly, the step function to express inhibition (or repression) will be: $s^- : \mathbb{R}_+ \times \mathbb{R}_+ \to \{0,1\}$, $s^-(x_i, \theta_i^j) = 1 - s^+(x_i, \theta_i^j)$. The superscript j indicates the interaction of species i on species j of the network.

The production rate of variables $x_i \in [0, +\infty)$, $i = 1, \ldots, n$ is given by the function $f_i : \mathbb{R}_+^n \to \mathbb{R}_+$:

$$f_i(x) = \sum_{1 \le l \le m} \kappa_{il} D_{il}(x) \tag{2.4}$$

where $\kappa_{il} > 0$ are the synthesis rate parameters and $D_{il} : \mathbb{R}_+^n \to \{0,1\}$ are *Boolean*-valued functions that express the regulation of variable x_i by other variables ($m \le n$). The functions $D_{il}(x)$ may be products of increasing or decreasing step functions $s^{+/-}(x_i, \theta_i^j)$.

A general form of the system will be:

$$\dot{x_i} = \kappa_{i0} + f_i(x) - \gamma_i x_i \tag{2.5}$$

where κ_{i0} is a basal term, $x = (x_1, \ldots, x_n)^t > 0$ contains the species concentrations and $\gamma_i x_i > 0$ expresses the degradation rate of species x_i.

The thresholds θ_i^j define hyperplanes and divide the phase space into *regular domains*. The regions such that $x_i = \theta_i^j$ for some i and j are called *switching domains*

and form the boundaries of the regular domains. In each regular domain B, the vector field is uniquely defined, the synthesis rate is constant ($\kappa_{i0} + \kappa_{iB}$):

$$\dot{x_i} = \kappa_{i0} + \kappa_{iB} - \gamma_i x_i$$

where κ_{iB} is the value of $f_i(x)$ in B and the computation of the system solution, while $x \in B$, is straightforward, with trajectories moving towards the corresponding *focal point* $\phi_{iB} = (\kappa_{i0} + \kappa_{iB})/\gamma_i$. As the trajectory reaches the boundary of B, the vector field changes and the solution must be computed in the new domain.

In PWA systems, a general property is that a focal point belonging to its own domain (i.e., $\phi_{iB} \in B$) is a locally stable steady state. The connection between continuous and piecewise affine models has been closely studied by Casey, Jong, and Gouzé, 2006. In the general approach the continuous activation and inhibition functions given by Hill functions are approximated by step functions and lead to a partition of the state space into rectangular domains. In contrast, for the two-gene oscillator (2.2), this approximation leads to a partition defined by a quadratic curve.

2.3 Piecewise Affine system approximates a Two-gene Synthetic Oscillator

In system (2.2), the function expressing synthesis of the repressor $h_R : \mathbb{R}_+ \to \mathbb{R}_+$ is simply:

$$h_R(A;\theta_1) = \frac{A^2}{A^2 + \theta_1}, \tag{2.6}$$

while the function expressing synthesis of the activator is given by a composition of two Hill functions $h_A : \mathbb{R}_+^2 \to \mathbb{R}_+$:

$$h_A((A,R);(\theta_0,\theta_2)) = \frac{A^2}{A^2 + \theta_0(1 + R/\theta_2)}. \tag{2.7}$$

Synthesis of the repressor (2.6) can be straightforwardly approximated by $s_R^+ : \mathbb{R}_+ \to \{0,1\}$:

$$s_R^+(A;\theta_1) = \begin{cases} 1, & \text{if } A^2 > \theta_1 \\ \\ 0, & \text{if } A^2 < \theta_1 \end{cases} \tag{2.8}$$

The case of (2.7) is more complex to deal with. A multiplicative approximation of the form $s^+(A;\theta_1)s^-(R;\theta_2)$ does not faithfully represent the dynamics of the continuous system. So, we chose to approximate the activation part by an increasing step function with a switching value that depends on R, as follows $s_A^+ : \mathbb{R}_+^2 \to \{0,1\}$:

$$s_A^+((A,R);(\theta_0,\theta_2)) = \begin{cases} 1, & \text{if } A^2 > \theta_0(1 + R/\theta_2) \\ \\ 0, & \text{if } A^2 < \theta_0(1 + R/\theta_2). \end{cases} \tag{2.9}$$

This is a step function with a coordinate-dependent switching value. This induces a partition of the state space with non-rectangular regular domains, as analyzed in the next section. Applying these approximations, the PWA associated with (2.2) becomes:

$$\begin{aligned} \frac{dA}{dt} &= V_A s_A^+((A,R);(\theta_0,\theta_2)) - \gamma_A A + r_{bas} \\ \frac{dR}{dt} &= V_R s_R^+(A;\theta_1) - \gamma_R R. \end{aligned} \tag{2.10}$$

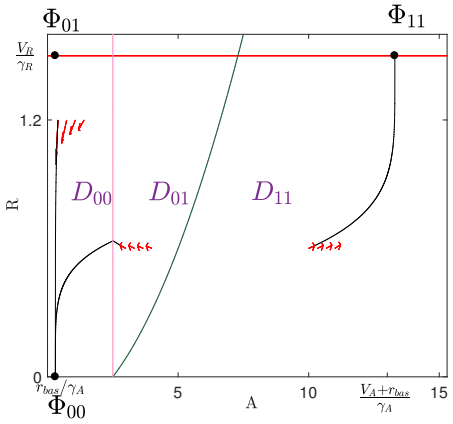

FIGURE 2.4: An initial PWA system with activity thresholds θ_0 and θ_1 equal.

2.3.1 Regular domains and the role of the activity thresholds in generating oscillations

The phase space of the PWA system (2.10) will be divided in domains by the two threshold hyperplanes $A^2 = \theta_1$ and $A^2 = \theta_0(1+R/\theta_2)$, $R \in [0, V_R/\gamma_R]$. However, these domains are no longer rectangles, but instead are defined by a quadratic curve:

$$\mu(A) = \theta_2(A^2 - \theta_0)/\theta_0. \tag{2.11}$$

According to the original parameter set by Smolen, Baxter, and Byrne, 1998 it holds that $\sqrt{\theta_1} = \sqrt{\theta_0}$, and with this condition the phase space is partitioned into three domains:

- $\tilde{D}_{00} = \{(A,R) \in \mathbb{R}_+^2 : A \in [0, \sqrt{\theta_1}], R \in [0, +\infty)\}$
- $\tilde{D}_{10} = \{(A,R) \in \mathbb{R}_+^2 : A \in [\sqrt{\theta_1}, \sqrt{\theta_0(1+(V_R/\gamma_R)/\theta_2)}], R > \mu(A)\}$
- $\tilde{D}_{11} = \{(A,R) \in \mathbb{R}_+^2 : A \in [\sqrt{\theta_1}, +\infty), R \in [0, \mu(A))\}$

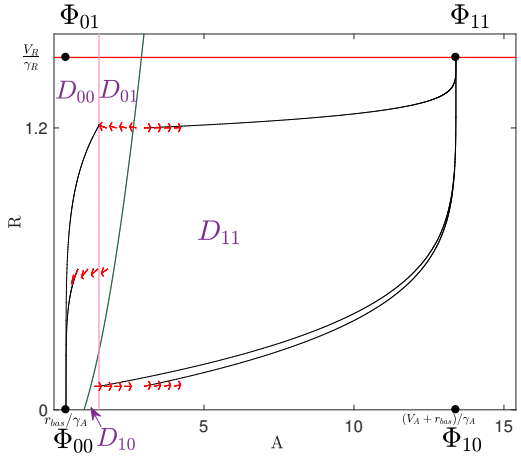

FIGURE 2.5: PWA system of the Smolen model with $\theta_1 > \theta_0$, other parameter values as in Fig. 2.2.

It is not difficult to compute the focal points in each of these three domains and check that, for a large range of parameters, $\phi_{00}, \phi_{01} \in \tilde{D}_{00}$ and $\phi_{11} \in \tilde{D}_{11}$ (see also Fig. 2.4). Therefore, trajectories in the domain $\tilde{D}_{00}$ converge to the locally stable fixed point $\phi_{00} = (\phi_{00}^A, \phi_{00}^R) = (r_{bas}/\gamma_A, 0)$. Similarly, trajectories in $\tilde{D}_{01}$ are attracted by the focal point $\phi_{01} = (\phi_{01}^A, \phi_{01}^R) = (r_{bas}/\gamma_A, V_R/\gamma_R)$ and trajectories in $\tilde{D}_{11}$ converge to the locally stable fixed point $\phi_{11} = (\phi_{11}^A, \phi_{11}^R) = ((V_A + r_{bas})/\gamma_A, V_R/\gamma_R)$, see Fig. 2.4. It is not difficult to see that this state space conformation prevents the existence of periodic oscillations.

A closer look shows that requiring $\sqrt{\theta_1} > \sqrt{\theta_0}$ will shift the line $A = \sqrt{\theta_1}$ to the right of the plane and introduce a fourth region in the state space. Four domains D_{ij}, $i, j \in \{0, 1\}$ will be formed under the condition $\sqrt{\theta_1} > \sqrt{\theta_0}$:

- $D_{10} = \{(A,R) \in \mathbb{R}^2_+ : A \in [0, \sqrt{\theta_1}], R \in [0, \mu(A))\}$
- $D_{11} = \{(A,R) \in \mathbb{R}^2_+ : A \in [\sqrt{\theta_1}, +\infty), R \in [0, \mu(A))\}$
- $D_{01} = \{(A,R) \in \mathbb{R}^2_+ : A \in [\sqrt{\theta_1}, +\infty), R > \mu(A)\}$
- $D_{00} = \{(A,R) \in \mathbb{R}^2_+ : A \in [0, \sqrt{\theta_1}], R > \mu(A)\}$

The focal points in each of the four domains are given in Table 2.1 where, for an appropriate but still very large range of parameters, it is possible to place each focal point outside its domain.

Indeed, if the focal point ϕ_{00} in domain D_{00} is shifted to the domain D_{10} and similarly ϕ_{ij} to the following domain in anti-clockwise sense, then the trajectories will be attracted to the corresponding focal point in the neighbor domain. In this way, trajectories are expected to cross the threshold hyperplanes and, since the vector field is uniquely defined in each domain, an oscillatory behavior will eventually be formed by the four trajectory parts.

TABLE 2.1: Focal points, and their location under conditions (a)-(c).

$\phi_{10} = (\phi_{10}^A, \phi_{10}^R) = ((V_A + r_{bas})/\gamma_A, 0)$	D_{11}
$\phi_{11} = (\phi_{11}^A, \phi_{11}^R) = ((V_A + r_{bas})/\gamma_A, V_R/\gamma_R)$	D_{01}
$\phi_{01} = (\phi_{01}^A, \phi_{01}^R) = (r_{bas}/\gamma_A, V_R/\gamma_R)$	D_{00}
$\phi_{00} = (\phi_{00}^A, \phi_{00}^R) = (r_{bas}/\gamma_A, 0)$	D_{10}

2.4 Analysis of the Piecewise Affine Two-gene system

We now choose suitable parameter conditions so that the focal points will be shifted as: ϕ_{00} is in the domain D_{10}, $\phi_{10} \in D_{01}$, $\phi_{11} \in D_{01}$ and $\phi_{01} \in D_{00}$, see Fig. 2.6 and Table 2.1. For this conformation of the focal points, we will next show that system (2.10) does admit sustained periodic oscillations.

To prove the existence of a limit cycle we will compute the *Poincaré map* of system (2.10) and show that it has a unique fixed point. In each of the four domains D_{ij} there is a map G_{ij} that establishes a correspondence between an entry point at one boundary of D_{ij} and a corresponding exit point after the solution crosses D_{ij}. The Poincaré map is given by the composition of these four maps.

2.4.1 Parameter Conditions

The configuration listed in Table 2.1 is obtained from the conditions on the parameters (a) to (f), stated below and assumed to hold throughout the remainder of this chapter. For simplicity, let γ denote γ_R/γ_A and let $\delta > 0$ be small. Condition (a) guarantees the existence of four regions (compare Figs. 2.4 and 2.6), while (b) and (c) guarantee, respectively, that $\phi_{11} \in D_{01}$ and $\phi_{00} \in D_{10}$:

(a) $\sqrt{\theta_0} < \sqrt{\theta_1}$ and $\gamma_R < \gamma_A$,

(b) $\sqrt{\theta_0} + \delta < \dfrac{r_{bas}}{\gamma_A} < \sqrt{\theta_1} - \delta$

(c) $\sqrt{\theta_1} + \delta < \dfrac{V_A + r_{bas}}{\gamma_A} < \sqrt{\theta_0\left(1 + \dfrac{V_R/\gamma_R}{\theta_2}\right)} - \delta$

The inequalities (d)-(f) will be applied below in Lemma 3 to determine the signs of the first and second derivatives of the crossing maps G_{ij}, which will help to establish the existence of periodic orbits. Condition (d) guarantees that the map G_{11} has a negative first derivative:

(d) $\left| -\gamma \dfrac{\mu(\sqrt{\theta_1}) - \phi_{11}^R}{\sqrt{\theta_1} - \phi_{11}^A} \right| > 2\phi_{11}^A \dfrac{\theta_2}{\theta_0}.$

Conditions (e) establish the size of the first derivatives of the maps G_{ij} at the point $x = \sqrt{\theta_1}$:

(e) i. $\left| -\gamma \dfrac{\mu(\sqrt{\theta_1}) - \phi_{ij}^R}{\sqrt{\theta_1} - \phi_{ij}^A} + 2\sqrt{\theta_1}\dfrac{\theta_2}{\theta_0} \right| > 1, ij \in \{10, 01\}$

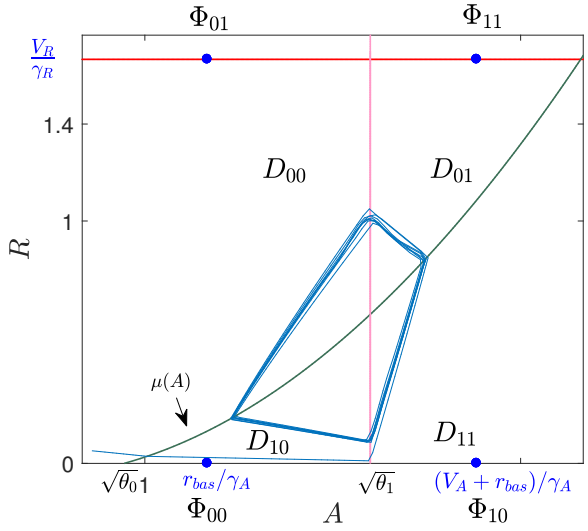

FIGURE 2.6: A trajectory of the PWA system following a periodic orbit with parameter values: $V_A = 0.43\ min^{-1}$, $V_R = 0.3\ min^{-1}$, $\gamma_A = 0.2\ min^{-1}$, $\gamma_R = 0.18\ min^{-1}$, $r_{bas} = 0.3\ min^{-1}$, $\theta_0 = 0.7$, $\theta_1 = 7.84$, $\theta_2 = 0.06$

ii. $$\left| -\gamma \frac{\mu(\sqrt{\theta_1}) - \phi_{ij}^R}{\sqrt{\theta_1} - \phi_{ij}^A} + 2\sqrt{\theta_1}\frac{\theta_2}{\theta_0} \right| < 1, ij \in \{00, 11\}.$$

Conditions (f) establish the sign of the second derivatives of G_{ij} at the point $x = \sqrt{\theta_1}$:

(f) i. $$\left| (\gamma^2 + \gamma) \frac{\mu(\sqrt{\theta_1})}{\phi_{11}^A - \sqrt{\theta_1}} \right| > 2\frac{\theta_2}{\theta_0}(2\gamma\sqrt{\theta_1} + \phi_{11}^A - \sqrt{\theta_1})$$

ii. $$\left| (\gamma^2 + \gamma) \frac{\mu(\sqrt{\theta_1}) - \phi_{01}^R}{(\sqrt{\theta_1} - \phi_{01}^A)^2} - 4\gamma\frac{\theta_2}{\theta_0}\frac{\sqrt{\theta_1}}{\sqrt{\theta_1} - \phi_{01}^A} \right| > 2\frac{\theta_2}{\theta_0}$$

iii. $$(\gamma^2 + \gamma)\frac{\mu(\sqrt{\theta_1})}{\sqrt{\theta_1} - \phi_{00}^A} + 2\frac{\theta_2}{\theta_0}(\sqrt{\theta_1} - \phi_{00}^A) > 4\gamma\sqrt{\theta_1}\frac{\theta_2}{\theta_0}.$$

It can be easily checked that a set of parameters such as indicated in the caption of Fig. 2.6 verifies these conditions.

2.4.2 The first return map of the system

Lemma 1. *The following functions characterize the correspondence between entry and exit points of D_{ij}:*

$$G_{ij}(x) = \left(\frac{\sqrt{\theta_1} - \phi_{ij}^A}{x - \phi_{ij}^A} \right)^{\frac{\gamma_R}{\gamma_A}} (\mu(x) - \phi_{ij}^R) + \phi_{ij}^R \tag{2.12}$$

for $i, j \in \{0,1\}$ referring to the corresponding domain D_{ij}, and defined in the following sets:

- $\{(x, G_{10}(x)) \in \mathbb{R}^2_+ : x \in (\phi^A_{00}, \sqrt{\theta_1}), G_{10}(x) < \mu(x)\}$
- $\{(x, G_{11}(x)) \in \mathbb{R}^2_+ : x \in (\sqrt{\theta_1}, \phi^A_{10}), G_{11}(x) < \mu(x)\}$
- $\{(x, G_{01}(x)) \in \mathbb{R}^2_+ : x \in (\sqrt{\theta_1}, \phi^A_{11}), G_{01}(x) > \mu(x)\}$
- $\{(x, G_{00}(x)) \in \mathbb{R}^2_+ : x \in (\phi^A_{01}, \sqrt{\theta_1}), G_{00}(x) > \mu(x)\}$

Proof. To obtain these functions, note that in each domain D_{ij}, equations (2.10) can be written as

$$\frac{dA}{dt} = \gamma_A(\phi^A_{ij} - A), \quad \frac{dR}{dt} = \gamma_R(\phi^R_{ij} - R).$$

Then, the trajectory crossing D_{ij} from a point (A_0, R_0) to a point (A, R) is given by:

$$\begin{cases} A(t) &= (A(t_0) - \phi^A_{ij})e^{-\gamma_A(t-t_0)} + \phi^A_{ij} \\ R(t) &= (R(t_0) - \phi^R_{ij})e^{-\gamma_R(t-t_0)} + \phi^R_{ij} \end{cases} \tag{2.13}$$

and solving with respect to time yields the equalities

$$e^{-(t-t_0)} = \left(\frac{A - \phi^A_{ij}}{A_0 - \phi^A_{ij}}\right)^{\frac{1}{\gamma_A}} = \left(\frac{R - \phi^R_{ij}}{R_0 - \phi^R_{ij}}\right)^{\frac{1}{\gamma_R}}. \tag{2.14}$$

In addition, for $ij \in \{11, 00\}$, we have $A_0 = \sqrt{\theta_1}$ and $R_0 = \mu(A_0)$. It follows that $R_0 = G_{ij}(A_0)$. Conversely, for $ij \in \{01, 10\}$, let $R = \mu(A)$ and $A = \sqrt{\theta_1}$. Then it follows that $R = G_{ij}(A_0)$. ■

For a trajectory starting at the point $\tilde{P}_2 = (\tilde{A}_2, \tilde{R}_2) = (\tilde{A}_2, \mu(\tilde{A}_2))$ and returning to another point P_2, both at the boundary between domains D_{11} and D_{01}, the first return map of the system can be computed as follows.

Lemma 2. *The Poincaré map of the system (2.10) is given by the function:*

$$G(x) = G^{-1}_{11} \circ G_{10} \circ G^{-1}_{00} \circ G_{01}(x) \tag{2.15}$$

defined on the interval $G : [\sqrt{\theta_1}, \phi^A_{10}) \to [\sqrt{\theta_1}, \phi^A_{10})$.

Proof. Applying the system's solution for each transition in the phase space from $\tilde{P}_2$ to P_2 as it is described in the Proof of Lemma 1 and after some computation follows the Poincaré map of the system.

■

The first and second derivatives of the Poincaré map G, to be used in the next section, can be computed from those of the four crossing maps. The first derivative of each map G_{ij} is given by:

$$\frac{dG_{ij}}{dx} = \left(\frac{\sqrt{\theta_1} - \phi^A_{ij}}{x - \phi^A_{ij}}\right)^{\gamma} \left[-\gamma \frac{\mu(x) - \phi^R_{ij}}{x - \phi^A_{ij}} + 2x\frac{\theta_2}{\theta_0} \right] \tag{2.16}$$

and the second derivative is given by:

$$\frac{d^2G_{ij}}{dx^2} = \left(\frac{\sqrt{\theta_1}-\phi_{ij}^A}{x-\phi_{ij}^A}\right)^{\gamma}\left[(\gamma+\gamma^2)\frac{\mu(x)-\phi_{ij}^R}{(x-\phi_{ij}^A)^2} - 4x\gamma\frac{\theta_2}{\theta_0} + 2\frac{\theta_2}{\theta_0}\right]. \tag{2.17}$$

2.4.3 Existence and uniqueness of limit cycle

By definition, the fixed points $G(x^*) = x^*$ of the Poincaré map indicate the number of periodic orbits of the PWA system (2.10), and their stability indicates the stability of the orbit. Our main result is thus:

Theorem 1. *Assume conditions (a)-(f) hold. Then the first return map (2.15) of system (2.10) has a unique fixed point in the open interval* $(\sqrt{\theta_1}, \phi_0^A)$.

To analyse the fixed points of G, we will first compute the signs of the first and second derivatives of its components, and show that G is a strictly increasing and concave function. The following properties are easy to check:

Lemma 3. *Assume conditions (a)-(f) hold. For each function* G_{ij}, $i, j \in \{0,1\}$, *the following inequalities hold:*

(i) $\dfrac{dG_{ij}}{dx} > 0, \;\; ij \in \{10,01\}$

(ii) $\dfrac{dG_{ij}}{dx} < 0, \;\; ij \in \{00,11\}$

(iii) $\dfrac{d^2G_{ij}}{d^2x} > 0, \;\; ij \in \{10,00\}$

(iv) $\dfrac{d^2G_{ij}}{d^2x} < 0, \;\; ij \in \{11,01\}$

(v) $\left|\dfrac{dG_{ij}}{dx}(\sqrt{\theta_1})\right| > 1, \;\; ij \in \{10,01\}$

(vi) $\left|\dfrac{dG_{ij}}{dx}(\sqrt{\theta_1})\right| < 1, \;\; ij \in \{00,11\}.$

We can now state the monotonicity properties of G (see also Fig. 2.7):

Lemma 4. *Assume conditions (a)-(f) hold. Then map G defined as in (2.15) is an increasing and concave function.*

Proof. First, from Lemma 3 (i) we have that G_{11}, G_{00} are strictly decreasing functions in their domains, and since they are invertible, G_{11}^{-1} and G_{00}^{-1} are also strictly decreasing. Conversely, by Lemma 3 (ii), the functions G_{10}, G_{01} and their inverse functions are strictly increasing in their domains. Therefore, both $G_{11}^{-1} \circ G_{10}$ and $G_{00}^{-1} \circ G_{01}$ are strictly decreasing, meaning that G is itself strictly increasing as a composition of two decreasing functions.

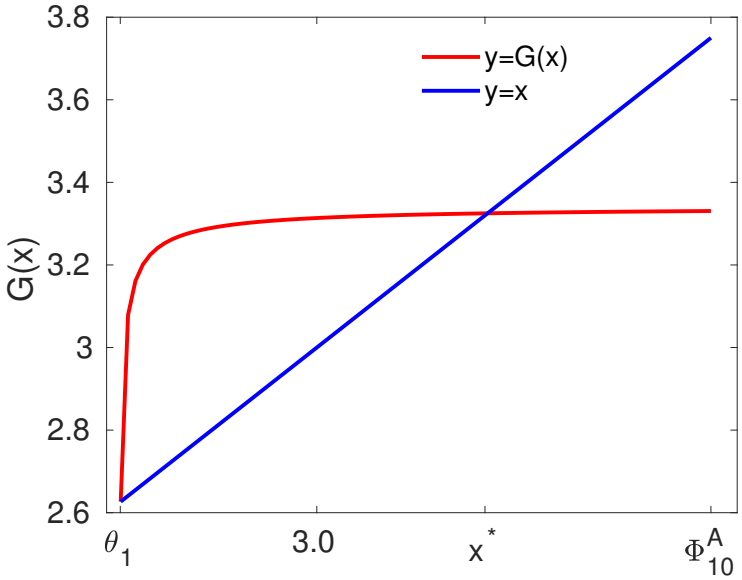

FIGURE 2.7: The map G, defined in the interval $[\sqrt{\theta_1}, \phi_{10}^A)$, computed for the same parameters as in Fig. 2.6. Its fixed points are given by the intersection with the straight line $y = x$. The point $\sqrt{\theta_1}$ corresponds to an unstable fixed point of system (2.10) while x^* corresponds to a locally stable periodic orbit.

For the concavity, recall that the inverse f^{-1} of a strictly monotone convex (resp., concave) function f in an open domain D is concave (resp., convex) in its corresponding domain.

Since G_{10}, G_{00} are convex functions and G_{11}, G_{01} are concave (by Lemma 3 (iii) and (iv)), set $f_1 = G_{00}^{-1} \circ G_{01}$ and note that

$$f_1'' = (G_{00}^{-1})'' \circ G_{01}(G_{01}')^2 + (G_{00}^{-1})' \circ G_{01} G_{01}'' > 0$$

and so f_1 is convex and decreasing as a composition of an increasing and a decreasing function. Similarly

$$f_2'' = [G_{10} \circ f_1]'' > 0$$

so it follows that f_2 is a convex and decreasing function. Lastly, we have that

$$G'' = [G_{11}^{-1} \circ f_2]'' < 0$$

implying that G is concave. ■

Extremal values $G(\sqrt{\theta_1})$ and $G(\phi_{10}^A)$

Before proving our main result, we will evaluate map G at the two endpoints of its interval of definition, that is $\sqrt{\theta_1}$ and ϕ_{10}^A. Let us first study the map at $x = \sqrt{\theta_1}$, which is equivalent to the point $A = \sqrt{\theta_1}$, $R = \mu(\sqrt{\theta_1})$ at the boundary of the four regions. At this point, the system (2.10) must be defined as a differential inclusion and should be written as a convex combination of the vector fields f_{ij} in each of the

four domains D_{ij}:

$$\begin{bmatrix} \dfrac{dA}{dt} \\ \\ \dfrac{dR}{dt} \end{bmatrix} = \sum_{i,j=0}^{1} \alpha_{ij} f_{ij}(\sqrt{\theta_1}, \mu(\sqrt{\theta_1})) \tag{2.18}$$

where $\sum_{i,j=0}^{1} \alpha_{ij} = 1$. It is easy to see that the zero vector is included in this convex combination, hence the point $(\sqrt{\theta_1}, \mu(\sqrt{\theta_1}))$ is a Filippov-type equilibrium point of (2.10) (Filippov, 1960). Moreover, by definition of the partial crossing maps:

$$\frac{G_{ij}(x) - \phi_{ij}^R}{\mu(x) - \phi_{ij}^R} = \left(\frac{\sqrt{\theta_1} - \phi_{ij}^A}{x - \phi_{ij}^A} \right) \frac{\gamma_R}{\gamma_A}$$

it follows that $G_{ij}(\sqrt{\theta_1}) = \mu(\sqrt{\theta_1})$ for all ij, hence $G(\sqrt{\theta_1}) = \sqrt{\theta_1}$ and $\sqrt{\theta_1}$ is a fixed point of the first return map. However, the combination of Lemma 3 (v) and (vi) implies that $G'(\sqrt{\theta_1}) > 0$, which in turn implies that $\sqrt{\theta_1}$ corresponds to an unstable fixed point of (2.10).

At the other endpoint $x = \phi_{10}^A$, by definition of focal point, it follows that $G(\phi_{10}^A) < \phi_{10}^A$, since $\phi_{11}^A = \phi_{10}^A$ and for $A_0 \in D_{11}$ $dA/dt = -\gamma_A(\phi_{11}^A - A)$ implies $A(t;A_0) < \phi_{10}^A$ for all t and $A < A_0$.

Proof of Theorem 1

We want to show that there exists a unique $\sqrt{\theta_1} < x^* < \phi_{10}^A$ such that $x^* = G(x^*)$. From the above discussion, G is strictly increasing and concave in $[\sqrt{\theta_1}, \phi_0^A)$ and satisfies $G(\sqrt{\theta_1}) = \sqrt{\theta_1}$ and $G(\phi_{10}^A) < \phi_{10}^A$. Therefore G intersects the line $y = x$ exactly once in the open interval.

To show that this fixed point x^* is stable, i.e. $dG/dx(x^*) < 1$, consider the function $L(x) = G(x) - x$ on $[\sqrt{\theta_1}, \phi_{10}^A)$. This function has exactly two zeros on this interval, $\sqrt{\theta_1}$ and x^*. By the Intermediate Value Theorem, $L'(x)$ has one zero at $r \in (\sqrt{\theta_1}, x^*)$ and L is decreasing between r and $x^* + \delta$ for some $\delta > 0$ (since $G(x)$ is continous and $G(x) < x$ in (x^*, ϕ_{10}^A)). Therefore, $L'(x) = G'(x) - 1 < 0$ and $0 < G'(x) < 1$ for all $x \in (r, x^* + \delta)$.

2.4.4 Focal points shift due to basal synthesis rate for the repressor

This Section generalizes system (2.10) by adding a basal production rate to the repressor equation. This result will be useful later on in next Chapter Section 3.2.1, where we need to characterize the shift in the focal points due to the network coupling. Define the following PWA system associated with (2.10):

$$\begin{aligned}\frac{dA}{dt} &= V_A s_A^+((A,R);(\theta_0,\theta_2)) - \gamma_A A + r_{bas}\\ \frac{dR}{dt} &= V_R s_R^+(A;\theta_1) - (\gamma_R+\beta)R + \beta C,\end{aligned} \tag{2.19}$$

with s_A^+, s_R^+, as defined in Section 2.3.1; $\beta > 0$ is a constant that controls the shift of ϕ_{ij}^R coordinates in the phase space and $C > 0$ expresses a basal term that remains constant. The other parameters are those of system (2.10).

The system domains are defined as in Section 2.3.1 and the coordinates ϕ_{ij}^R can be computed as a shift of the corresponding focal points R-coordinates of system (2.10):

$$\begin{aligned}\phi_{00}^R = \phi_{10}^R &= \frac{\beta C}{\gamma_R+\beta}\\ \phi_{01}^R = \phi_{11}^R &= \frac{V_R+\beta C}{\gamma_R+\beta}\end{aligned} \tag{2.20}$$

Note that the ϕ_{ij}^A coordinates remain the same as in Table 2.1.

Additionally to parameter conditions (a)-(f), we next introduce conditions on β, for which the location of the focal points (the domain in which ϕ_{ij} is located) is the same as in Table 2.1); these conditions will imply that the system (2.19) also admits a unique periodic solution as shown in Section 2.4.3. Introduce first the notation:

$$a_{bas} = \frac{r_{bas}}{\gamma_A}, \quad a_{max} = \frac{V_A + r_{bas}}{\gamma_A}. \tag{2.21}$$

For system (2.19), the following holds:

(i) $\phi_{00} \in D_{10}$ if and only if $\phi_{00}^R < \mu(a_{bas})$,

(ii) $\phi_{11} \in D_{01}$ if and only if $\phi_{11}^R > \mu(a_{max})$.

From (2.20), these inequalities become:

(i) $\beta < \beta_1(C) := \mu(a_{bas})\gamma_R/(C-\mu(a_{bas}))$, whenever $C > \mu(a_{bas})$,

(ii) $\beta < \beta_2(C) := (\mu(a_{max})\gamma_R - V_R)/(C-\mu(a_{max}))$, whenever $C < \mu(a_{max})$.

Combining these two inequalities, yields the following condition on β:

$$\beta < \begin{cases}\beta_1(C), & \text{if } C > \mu(a_{max})\\ \beta_2(C), & \text{if } C < \mu(a_{bas})\\ \min\{\beta_1(C),\beta_2(C)\}, & \text{if } \mu(a_{bas}) < C < \mu(a_{max})\end{cases} \tag{2.22}$$

If β does not satisfy these conditions, it follows that the shift in R- coordinates of the focal points induces a change in the dynamic of system (2.19) from sustained oscillations to stability: for $C > \mu(a_{max})$, if the condition on β is not satisfied, then ϕ_{00} shifts to its corresponding domain D_{00} and becomes locally stable solution for

the system (2.19). Analogously, for $C < \mu(a_{bas})$ and the corresponding condition on β not satisfied, ϕ_{11} changes location to D_{11} and becomes steady state. Lastly, for $\mu(a_{bas}) < C < \mu(a_{max})$, ϕ_{00} shifts to D_{00} for $\beta > \beta_1$ and ϕ_{11} to D_{11} for $\beta > \beta_2$. In either of these three cases, the periodic solution disappears.

Note: This observation will be used in the next Chapter (Section 3.2.1) to show stability of a network under some conditions.

2.5 Discussion

2.5.1 Applying activity thresholds separation ($\theta_0 < \theta_1$) to the continuous model

As an application of the theoretical analysis in this chapter, we now check the effect of the new parameter inequalities on the dynamics of continuous system.

The analysis of the piecewise system highlights a crucial factor for the existence of a periodic solution: the separation of the activity thresholds. We apply this condition to the continuous system (2.2) providing a new parameter set for the proposed (continuous) model, see Table 2.2.

TABLE 2.2: Parameters of improved Smolen model

$V_A = 12.5\ min^{-1}$	$V_R = 0.3\ min^{-1}$
$\gamma_A = 1\ min^{-1}$	$\gamma_R = 0.2\ min^{-1}$
$\theta_0 = 10$	$\theta_1 = 16$
$r_{bas} = 0.4\ min^{-1}$	$\theta_2 = 0.2$

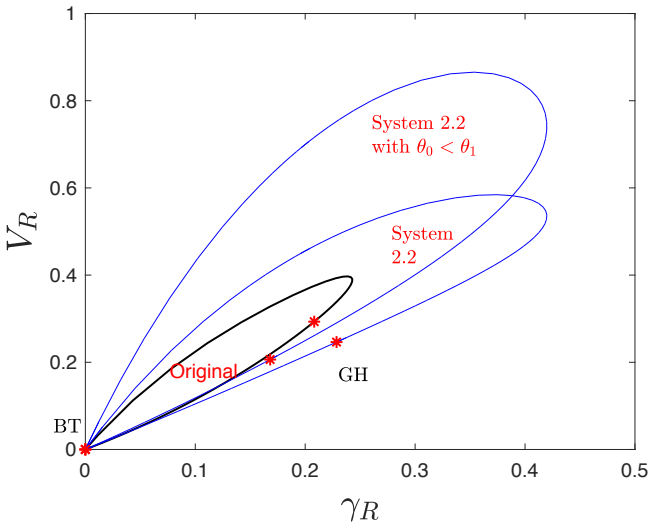

FIGURE 2.8: Two parameter bifurcation diagrams for synthesis and degradation rate of R, for the original model (in black) and for model (2.2) with $\theta_0 = \theta_1$ and $\theta_0 < \theta_1$. Inside of each circle of the parameter values the periodic solutions occur. GH indicates a generalized Hopf point.

We perform bifurcation analysis to establish the parameter space for oscillations. From the bifurcation diagrams we extract information about the influence of the activity thresholds separation ($\theta_0 < \theta_1$) to the oscillations parameter space of system 2.2. Indicatively, Fig. 2.8 depicts two parameter bifurcation analysis for the synthesis and degradation rate of the repressor V_R,γ_R. Comparing the bifurcation diagrams for the three cases: a) original Smolen model, b)proposed model with activity thresholds equal and c)proposed model with thresholds separation, we conclude that the region that admits periodic solution substantially increases for the proposed system (2.2) in case b) with $\theta_0 = \theta_1 = 10$, and extends further in case c) with $\theta_0 = 10, \theta_1 = 16$.

2.5.2 Conclusion

In this chapter we study an improved model of a synthetic biology oscillator using a piecewise affine approximation and prove existence and uniqueness of periodic solution for this PWA system, in a suitable region of parameters. This qualitative characterization of the system allows us to better understand the influence of each parameter on the dynamical behaviour, crucial factors to help guide system design and synthetic implementation.

The two most important steps for the improvement of the system design are: first, separate the activation thresholds. The activator should act much faster on itself than on the repressor ($\theta_0 < \theta_1$). Second, the maximal rate for the activator synthesis $(V_A + r_{bas})/\gamma_A$ should be smaller than the maximal repressor modulating factor $\sqrt{1 + V_R/(\gamma_R\theta_2)}$. Moreover, we apply the parameter condition on the activity thresholds in the associated continuous system, to illustrate further the results of our analysis. Applying the condition $\theta_0 < \theta_1$, the oscillations region increases further. These results can be useful guidelines for synthetic circuit implementation.

Chapter 3

Dynamics in a Network of N Coupled Two-gene Oscillators: the Effect of the Topology of Interactions

As an application of our two-gene oscillator analysis, we then study a network of N identical piecewise affine two-gene oscillators, linked by diffusion of one of the variables. There are still few studies of coupled identical oscillators in a piecewise affine formalism: for instance, Edwards and Gill, 2003 prove synchronization under a weak coupling, and Nicks, Chambon, and Coombes, 2018 study clusters of synchronized elements, with applications to neuron networks. More generally, networks of identical linear systems under diffusive coupling are studied by Scardovi and Sepulchre, 2008, who give conditions for synchronization depending on the communication graph. Sorrentino et al., 2016 and a review by Golubitsky and Stewart, 2016 examine the relationship between network topology and patterns of synchrony among the oscillators, in a more theoretical context.

Motivated by the synchronization of mammalian circadian clocks in tissues and organs, we will consider a network of N two-gene oscillators interconnected according to three different topologies. Experiments have shown that the mammalian suprachiasmatic nucleus (SCN), that consists of neurons and is located in the brain, is the central synchronizer of the circadian rhythms, (Ralph et al., 1990). In parallel, in cultured cells and tissue explants, there have been observed self-sustained and autonomous circadian clocks (Balsalobre, Damiola, and Schibler, 1998), (Yamazaki et al., 2000). The suprachiasmatic nucleus (SCN) is the central circadian synchroniser, sending signals to the rest of the brain and to the pheripheral clocks in the body. The exact means of communication of the clocks in the circadian system is not yet fully understood. In the present work, we investigate the dynamics of a coupled network of identical oscillators with local connection. Thus, for the form of the interaction between the SCN and the peripheral clocks, as a first approach we will consider diffusive exchanges between cells. This hypothesis follows experimental studies implying the presence of this type of interaction in intercellular connections (Silver et al., 1996), (Durand, Park, and Jensen, 2010). Similar way of coupling is also studied in model-based investigations and simulations (Kunz and Achermann, 2003), (Silva, Lopes, and Viana, 2016).

In the context of the hierarchical organisation of the circadian system, we explore a network N two-gene oscillators coupled through diffusion terms. In a first case, we consider one PWA system (2.10) to represent the SCN and the other $N-1$ identical systems as peripheral clocks, leading to an "one-to-all" or "star" topology where

oscillator $i = 1$ is connected to all others, as in Fig. 3.1. In a second case, we consider all oscillators to play identical roles, as in a homogeneous tissue, and study an "all-to-all" topology where each oscillator is connected to all others. As an intermediate case, we will consider randomly chosen connections, within certain parameters.

3.1 PWA oscillator network and location of focal points

Consider N identical oscillators of the form (2.10), with coordinates (A_i, R_i) $i \in \{1,2,\ldots,N\}$, coupled through R_i according to some topology L and a diffusion parameter κ:

$$\begin{aligned} \frac{dA_i}{dt} &= V_A s^+_{A,R}(A_i, R_i; \theta_0, \theta_2) - \gamma_A A_i + r_{bas} \\ \frac{dR_i}{dt} &= V_R s^+_A(A_i; \theta_1) - \gamma_R R_i + \kappa \sum_{j \in \mathscr{L}} (R_j - R_i),\ i = 1,\ldots,N, \end{aligned} \tag{3.1}$$

where the set $\mathscr{L}$ contains all systems j that are connected to i. It will be useful to define the vectors $A = (A_1,\ldots,A_N)'$ and $R = (R_1,\ldots,R_N)'$, as well as the state of the coupled system as $X = (A_1,R_1,\ldots,A_i,R_i,\ldots,A_N,R_N)' \in \mathbb{R}^{2N}_{\geq 0}$. We further define

$$sh_{A,R} = [s^+_A((A_1,R_1);(\theta_0,\theta_2)),\ldots,s^+_A((A_n,R_n);(\theta_0,\theta_2))]'$$

and

$$sh_A = [s^+_A(A_1;\theta_1),\ldots,s^+_A(A_n;\theta_1)]'$$

to be N-dimensional Boolean vector functions, evaluated according to the state X. The coupled system (3.1) can be rewritten as:

$$\begin{aligned} \frac{dA}{dt} &= V_A sh_{A,R} - \Gamma_A A + r_{bas} \\ \frac{dR}{dt} &= V_R sh_A - (\Gamma_R + L)R, \end{aligned} \tag{3.2}$$

where Γ_A, Γ_R are diagonal $N \times N$ matrices with elements γ_A, $\gamma_R > 0$ respectively, and (by abuse of notation) r_{bas} is an N-dimensional vector with elements r_{bas}. L is the symmetric $N \times N$ Laplacian matrix of the connection topology, to be defined for each case. Analogously to Section 2.3.1, we define the domains of system (3.2) as $D_C = D_{c_1} \times \cdots \times D_{c_N}$, where c_i belongs to $\{00,01,10,11\}$, so that each D_{c_i} corresponds to a regular domain of the 2-dimensional system (2.10). The focal points for each domain D_C are denoted by $\phi_C = (\tilde{A}^C, \tilde{R}^C)'$ and they are given by:

$$\begin{aligned} \tilde{A}^C &= V_A \Gamma_A^{-1} sh_{A,R}[D_C] + \Gamma_A^{-1} r_{bas} \\ \tilde{R}^C &= V_R (\Gamma_R + L)^{-1} sh_A[D_C] \end{aligned} \tag{3.3}$$

where $sh_{A,R}[D_C]$ and $sh_A[D_C]$ are the synthesis rate vectors evaluated at domain D_C.

As before, the location of the focal points determines the dynamics of the system. In Section 2.4.3 we have shown that the (single) two-gene oscillator (2.10) admits a unique periodic solution for certain parameter conditions. This periodic solution,

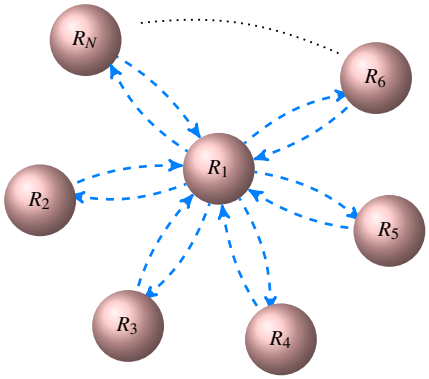

FIGURE 3.1: Star topology scheme: coupling N two-gene oscillators of the form (2.10), through variable R.

which we call $(\varphi_A(t), \varphi_R(t))$, extends to naturally as a solution to the coupled system with $\varphi_A^i(t) = \varphi_A(t)$ and $\varphi_R^i(t)) = \varphi_R(t))$ for all i. This can be seen by taking identical initial conditions for all systems i. Intriguingly, our analysis shows that diffusive coupling generates new locally stable steady states for the coupled system. Notice that only the coordinates $\tilde{R}^C$ depend on the coupling parameter κ, as well as on the number N of oscillators, while $\tilde{A}^C$ are independent of the coupling topology and can be computed for $i = 1,\ldots,N$ as follows

$$\tilde{A}_i^C = \begin{cases} a_{bas}, & D_{C_i} \in \{D_{00}, D_{10}\} \\ a_{max}, & D_{C_i} \in \{D_{11}, D_{01}\} \end{cases} \tag{3.4}$$

where we used notation (2.21). This implies that regular domains D_C whose product includes $\{D_{01}, D_{10}\}$ for some i cannot contain their own focal point ϕ_C. Conversely, for regular domains D_C which are products of D_{00} and D_{11} only, the location of the focal points depends on the value of each $\tilde{R}_i^C$ relative to the curve $\mu(A)$ (see Fig. 2.6), as stated in the next Lemma.

Lemma 5. *For each oscillator i, the following hold:*

(a) Let $D_{c_i} = D_{00}$, $\tilde{R}_i^C \in D_{00}$ if and only if $\tilde{R}_i^C > \mu(a_{bas})$,

(b) Let $D_{c_i} = D_{11}$, $\tilde{R}_i^C \in D_{11}$ if and only if $\tilde{R}_i^C < \mu(a_{max})$.

Consider a regular domain D_C with $D_{c_i} \in \{D_{00}, D_{11}\}$ for all $i = 1,\ldots,N$. Then $\phi_C = (\tilde{A}^C, \tilde{R}^C)' \in D_C$ if and only if either (a) or (b) are satisfied for each i.

The inequalities (a) and (b) follow directly from the expressions (3.4) for $\tilde{A}^C$ and the geometry of the phase space. The result on ϕ_C is an immediate consequence of (a) and (b).

3.2 Star Topology

This simplified interconnection scheme naturally assumes that *SCN* (represented by R_1) is connected to all other peripheral clocks, but the latter do not communicate

among themselves, as in the network depicted in Fig. 3.1. The corresponding Laplacian matrix L is defined as

$$L = \kappa \begin{pmatrix} N-1 & -1 & -1 & \dots & -1 \\ -1 & 1 & 0 & \dots & 0 \\ -1 & 0 & 1 & \dots & 0 \\ \vdots & & & & \vdots \\ -1 & 0 & 0 & \dots & 1 \end{pmatrix} \tag{3.5}$$

In each of the 4^N regular domains of the coupled system the coordinates of the focal points can be computed as in (3.3), where the matrix $(\Gamma_R + L)^{-1}$ is strictly positive and has the form

$$\begin{bmatrix} Q & S & S & \cdots & S \\ S & P & T & \cdots & T \\ S & T & P & \cdots & T \\ \vdots & \vdots & \vdots & & \vdots \\ S & T & T & \cdots & P \end{bmatrix} \tag{3.6}$$

where the entries are given by:

$$\begin{aligned} S &= \frac{\kappa}{\gamma_R(\gamma_R + N\kappa)} \\ Q &= \frac{\gamma_R}{\gamma_R(\gamma_R + N\kappa)} + S \\ T &= \frac{\kappa}{\gamma_R + \kappa} S \\ P &= \frac{(\gamma_R + \kappa)^2 + (N-2)\gamma_R\kappa}{\kappa^2} T. \end{aligned} \tag{3.7}$$

Based on Lemma 5, we can now show that new steady states may be generated due to the coupling scheme. In addition, using (3.7), we can estimate the number of these new steady states in terms of the coupling parameter and the number of oscillators in the network. Introduce the notation:

$$D_{00} \times (D_{11}^m \times D_{00}^{N-m-1})_{prm}, \;\; D_{11} \times (D_{11}^{m-1} \times D_{00}^{N-m})_{prm}$$

to denote products of m domains of the form D_{11} and $N-m$ of the form D_{00}, where only the first component D_{c1} is fixed, and the other components are any permutation of the remaining domains. For example, in the case $N = 3$, $m = 2$ we have: $D_{00} \times D_{11} \times D_{11}$ and $D_{11} \times D_{11} \times D_{00}$, $D_{11} \times D_{00} \times D_{11}$.

Theorem 2. *Consider system (3.2) in a star-coupled topology, with L defined as in (3.5). Assume that conditions (a)-(f) hold.*

Case (i) Define the positive integers:

$$\begin{aligned} m_{min} &= \left\lceil \frac{1}{TV_R} \mu(a_{bas}) \right\rceil \\ m_{max} &= \left\lfloor \frac{1}{TV_R} \mu(a_{max}) - \frac{(\gamma_R + \kappa)^2 + (N-2)\gamma_R\kappa}{\kappa^2} + 1 \right\rfloor. \end{aligned} \tag{3.8}$$

If $m_{min} < m_{max}$, then system (3.2) has exactly $\sum_{m=m_{min}}^{m_{max}} (N-1)/(m!(N-m-1)!)$ locally stable steady states corresponding to focal points $\phi_C \in D_C = D_{00} \times (D_{11}^m \times D_{00}^{N-m-1})_{prm}$.

Case (ii) Define the positive integers:

$$\begin{aligned} m_{min} &= \left\lceil \frac{1}{TV_R}\mu(a_{bas}) - \frac{\gamma_R}{\kappa} \right\rceil \\ m_{max} &= \left\lfloor \frac{1}{TV_R}\mu(a_{max}) - \frac{\gamma_R}{\kappa} - \frac{1}{\gamma_R+\kappa}\frac{1}{T}\max\left\{\frac{\gamma_R}{V_R}\mu(a_{max}), 1\right\} \right\rfloor. \end{aligned} \tag{3.9}$$

If $m_{min} < m_{max}$, then system (3.2) has exactly $\sum_{m=m_{min}}^{m_{max}} (N-1)!/((m-1)!(N-m)!)$ locally stable steady states corresponding to focal points $\phi_C \in D_C = D_{11} \times (D_{11}^{m-1} \times D_{00}^{N-m})_{prm}$.

Case (iii) Let

$$\hat{\kappa} = \begin{cases} max\left\{ \dfrac{\gamma_R(\mu(a_{max})\gamma_R - V_R)}{V_R - N\gamma_R\mu(a_{max})}, \dfrac{\gamma_R^2\mu(a_{bas})}{V_R - N\gamma_R\mu(a_{bas})} \right\}, \text{ if } N \le N^* \\ \dfrac{V_R}{\mu(a_{max}) - \mu(a_{bas})} - \gamma_R, \text{ if } N > N^* \end{cases}$$

with $N^* = \lceil \frac{V_R}{\gamma_R\mu(a_{bas})} - \frac{\gamma_R(\mu(a_{max})-\mu(a_{bas}))}{V_R-\gamma_R(\mu(a_{max})-\mu(a_{bas}))} \rceil$. Then no new steady states exist for any $\kappa \le \hat{\kappa}$.

Proof. First, recall that a focal point ϕ_C is a locally stable state if and only if it belongs to its own domain D_C: since the eigenvalues of the matrices $-\Gamma_A$ and $-(\Gamma_R + L)$ have strictly negative real part, the Hurwitz condition holds, hence the focal points that lie in their own domains are locally asymptotically stable. Second, Lemma 5 provides the conditions required to guarantee $\phi_C \in D_C$. Consider a general domain D_C consisting of the product of m regions of the form D_{11} and $N-m$ of the form D_{00}, in any order. Since oscillator 1 has a special role, we need to consider two cases, depending on whether $c_1 = 00$ or $c_1 = 11$:

Case (i) $D_C = D_{00} \times (D_{11}^m \times D_{00}^{N-m-1})_{prm}$**.** In this case, the vector $sh_A[D_C]$ has m entries equal to 1, and (3.6) and (3.3) lead to

$$\begin{aligned} \tilde{R}_1^C &= mSV_R \\ \tilde{R}_i^C &= \begin{cases} (P+(m-1)T)V_R, & \text{if } sh_{A,i} = 1,\ i = 2,\ldots,N \\ mTV_R, & \text{if } sh_{A,i} = 0,\ i = 2,\ldots,N. \end{cases} \end{aligned}$$

By Lemma 5, the conditions to guarantee $\phi_C \in D_C$ become

$$\begin{aligned} mSV_R &> \mu(a_{bas}) \\ (P+(m-1)T)V_R &< \mu(a_{max}) \\ mTV_R &> \mu(a_{bas}) \end{aligned}$$

From (3.7), it follows that $S > T$ so, combining these inequalities leads to

$$\frac{1}{TV_R}\mu(a_{bas}) < m < 1 + \frac{1}{TV_R}\mu(a_{max}) - \frac{P}{T},$$

and (3.7) shows that $P/T = ((\gamma_R+\kappa)^2 + (N-2)\gamma_R\kappa)/\kappa^2$ which yields $m_{min} < m < m_{max}$. If there exists an integer m in this interval, this means that any choice of m oscillators in D_{11} implies that the corresponding focal point belongs to D_C. Now, there are several ways of choosing m oscillators among the N. In this first case, $D_{c_1} = D_{00}$ is fixed, so the formula is "$N-1$ choose m", that is $(N-1)!/(m!(N-1-m)!)$ ways for each m. Since there is one focal point for each of these choices and this is valid for any integer m in the interval $[m_{min}, m_{max}]$, obtain the given sum for the total number of new steady states.

Case (ii) $D_C = D_{11} \times (D_{11}^{m-1} \times D_{00}^{N-m})_{prm}$**.** The coordinates $\tilde{R}^C$ of the focal points are now given by

$$\begin{aligned} \tilde{R}_1^C &= (Q+(m-1)S)V_R \\ \tilde{R}_i^C &= \begin{cases} (S+P+(m-2)T)V_R, & \text{if } sh_{A,i}=1,\ i=2,\ldots,N \\ (S+(m-1)T)V_R, & \text{if } sh_{A,i}=0,\ i=2,\ldots,N. \end{cases} \end{aligned}$$

Applying Lemma 5 yields,

$$\begin{aligned} (Q+(m-1)S)V_R &< \mu(a_{max}) \\ (S+P+(m-2)T)V_R &< \mu(a_{max}) \\ (S+(m-1)T)V_R &> \mu(a_{bas}). \end{aligned}$$

Combining the first two inequalities

$$m < \min\left\{1 + \frac{1}{SV_R}\mu(a_{max}) - \frac{Q}{S},\ 2 + \frac{1}{TV_R}\mu(a_{max}) - \frac{P+S}{T}\right\},$$

using (3.7) to obtain $Q/S = 1+\gamma_R/\kappa$, $(S+P)/T = 2+\gamma_R/\kappa + 1/(\kappa S)$

$$m < \min\left\{\frac{1}{SV_R}\mu(a_{max}) - \frac{\gamma_R}{\kappa}, \frac{1}{TV_R}\mu(a_{max}) - \frac{\gamma_R}{\kappa} - \frac{1}{\kappa S}\right\},$$

and noticing that $T/S = \kappa/(\gamma_R+\kappa) = 1-\gamma_R/(\gamma_R+\kappa)$ yields $m_{min} < m < m_{max}$. In this case, the first oscillator is fixed at $D_{c_1} = D_{11}$ so the formula becomes "$N-1$ choose $m-1$", that is $(N-1)!/((m-1)!(N-m)!)$ for each m.

We note that if the inequalities

$$\begin{aligned} QV_R &< \mu(a_{max}) \\ (S+P+T)V_R &> \mu(a_{max}) \\ SV_R &> \mu(a_{bas}) \end{aligned} \tag{3.10}$$

are satisfied and $m_{min} \geq m_{max}$ for the values defined in (3.8), then there is exactly one locally stable steady state for the system (3.2), that is of the form $D_C = D_{11} \times (D_{00})^{N-1}$. This derives from the inequalities satisfied in Case (ii), for $m = 1$.

Case (iii) To prove the last statement of Theorem 2, observe that $\hat{\kappa}$ is the value of κ that renders $m_{min} > m_{max}$ for the values as defined by (3.8) and (3.10), that is the intersection of

$$\begin{aligned} \Big\{ \frac{1}{TV_R}\mu(a_{max}) - \frac{P}{T} + 1 < \frac{1}{TV_R}\mu(a_{bas}) \Big\} \\ \cap \Big\{ QV_R > \mu(a_{max}) \Big\} \\ \cap \Big\{ SV_R < \mu(a_{bas}) \Big\} \end{aligned} \tag{3.11}$$

gives an interval for κ such that no focal point belongs to its own domain. Solving $\mu(a_{max})/TV_R - P/T + 1 < \mu(a_{bas})/TV_R$ with respect to κ and using (3.7) yields the value of $\hat{\kappa}_c = V_R/(\mu(a_{max}) - \mu(a_{bas})) - \gamma_R$, which is constant $\forall N$. Solving $SV_R < \mu(a_{bas})$ with respect to N for $\hat{\kappa}_c$ to obtain

$$N^* = \lceil \frac{V_R}{\gamma_R \mu(a_{bas})} - \frac{\gamma_R(\mu(a_{max}) - \mu(a_{bas}))}{V_R - \gamma_R(\mu(a_{max}) - \mu(a_{bas}))} \rceil,$$

that is the maximum value of N for which, the value of $\hat{\kappa}$ is given by solving $\{QV_R > \mu(a_{max})\} \cap \{SV_R < \mu(a_{bas})\}$ with respect to κ. ■

Example 1: $N = 2$. System (3.2) has 16 regular domains and the corresponding focal points are given in Table (3.1).

In this case, for a coupling constant $\kappa = 0.25$, and the other parameters as in Fig. 2.6, we have $S = 2.0425$, $T = 1.1875$, $Q = 3.5131$, $P = 3.5131$, $\mu(a_{bas}) = 0.1336$, $\mu(a_{max}) = 1.0865$, $\hat{\kappa} = 0.21$ and the bounds (3.8) and (3.9):

$$0.375 < m < 1.0914$$
$$QV_R = 1.05 < \mu(a_{max}) \text{ and } SV_R = 0.6127 > \mu(a_{bas}).$$

According to Theorem 2, $m = 1$ thus implying at most $1!/(1!0!) = 1$ new steady state in D_{0011} and $1!/(0!1!) = 1$ new steady state in D_{1100}, in agreement with Table 3.1. The value of $\hat{\kappa}$ also agrees with simulations, see Fig. 3.3.

Example 2: $N = 10$. Similarly, the computations of the m bounds in Theorem 2 case (i) yield $1.4783 < m < 4.3013$, thus $m_{min} = 2$, and $m_{max} = 4$. We expect $\sum_{j=2}^{4}(9)!/((j)!(9-j)!) = 246$ steady states in domains of the form $D_{00} \times (D_{11})^4 \times (D_{00})^{N-5}$. Applying the inequalities of case (ii) to obtain $0.7583 < m < 3.5813$, with $m_{min} = 1$ and $m_{max} = 3$, we expect $\sum_{j=1}^{3}(9)!/((j-1)!(10-j)!) = 46$ steady states in domains of the form $D_{11} \times (D_{11})^3 \times (D_{00})^{N-3}$. Our estimations are exact as it is illustrated by comparison with numerical computations in Fig. 3.2.

3.2.1 Star-coupled network stabilization

In this section we show that the star topology does not admit "mixed" dynamics: if any of the two-dimensional systems converges to a steady state, then all the network stabilizes.

TABLE 3.1: Focal points of 2 systems coupled and their corresponding location in the domains for $\kappa = 0.25$.

Φ_{1010}	D_{1111}	Φ_{1011}	D_{1111}
Φ_{1001}	D_{1100}	Φ_{1000}	D_{1110}
Φ_{1110}	D_{1111}	Φ_{1111}	D_{0101}
Φ_{1101}	D_{0100}	Φ_{1100}	D_{1100}
Φ_{0110}	D_{0011}	Φ_{0111}	D_{0001}
Φ_{0101}	D_{0000}	Φ_{0100}	D_{0000}
Φ_{0010}	D_{1011}	Φ_{0011}	D_{0011}
Φ_{0001}	D_{0000}	Φ_{0000}	D_{1010}

Theorem 3. *Consider system (3.2) in a star-coupled topology, with L defined as in (3.5). Assume that conditions (a)-(f) hold. If any 2D system k converges to a steady state (away from the domain boundaries), then the full network converges to a steady state.*

Proof. Suppose that 2D system $k \neq 1$, converges a to steady state in a regular domain, $\tilde{R}_k = constant$. Then, from (3.4), there are two possible values for $\tilde{A}_k$:

$$\tilde{A}_k = \begin{cases} a_{bas}, & \text{which implies } sh_{A,R} = 0 \text{ and } sh_A = 0 \\ a_{max}, & \text{which implies } sh_{A,R} = 1 \text{ and } sh_A = 1. \end{cases}$$

For simplicity we denote $\delta_j = (sh_A)_j \in \{0,1\}$.

By assumption, $\tilde{R}_k$ must remain constant (or within an interval of length ε as small as desired), δ_k remains fixed, and $\dot{R}_k \approx 0$, thus (3.1) implies:

$$\kappa L_{kk}\tilde{R}_k + \gamma_R \tilde{R}_k \approx V_R \delta_k(t) + \kappa \sum_{j \in \mathscr{L}} \tilde{R}_j, \tag{3.12}$$

Since oscillator k is only connected to system $j = 1$, from (3.3) and (3.5), it follows that $L_{kk} = 1$ and $\sum_{j\in\mathscr{L}} \tilde{R}_j = \tilde{R}_1$. Solving (3.12) with respect to $\tilde{R}_1$ gives :

$$\tilde{R}_1 \approx \frac{\kappa + \gamma_R}{\kappa}\tilde{R}_k - \frac{V_R}{\kappa}\delta_k(t) \tag{3.13}$$

Since both $\tilde{R}_k$ and $\delta_k(t)$ are fixed, the latter implies that $\tilde{R}_1 = constant$, and so $(A_1(t), R_1(t))$ converges to a steady state.

Next, for an oscillator i of the coupled network, with $i \neq 1, k$, from (3.1) it holds that

$$\frac{dR_i}{dt} = V_R \delta_i(t) - (\gamma_R + \kappa)R_i + \kappa \tilde{R}_1. \tag{3.14}$$

Since $\tilde{R}_1$ remains constant and the coupling parameter κ is fixed, the term $\kappa\tilde{R}_1$ acts like a basal term for all components R_i, $i = 2, \ldots, N$. This implies that systems

(A_i, R_i) become decoupled, and are described by the following equations:

$$\begin{aligned} \frac{dA_i}{dt} &= V_A s^+_{A,R}(A_i, R_i; \theta_0, \theta_2) - \gamma_A A_i + r_{bas} \\ \frac{dR_i}{dt} &= V_R s^+_A(A_i; \theta_1) - (\gamma_R + \kappa) R_i + \kappa \tilde{R}_1, \end{aligned} \tag{3.15}$$

This implies that each i-th system (3.15) is equivalent to system (2.19) with $\beta = \kappa$, $C = \tilde{R}_1$ and other parameters as in Fig. 2.6.

Since there are at least two oscillators in the network (k and 1) that converge to steady states, it holds that $\kappa > \hat{\kappa}$ (Theorem 2). From Lemma 5, it follows that either $\mu(a_{bas}) < \tilde{R}_1$ or $\tilde{R}_1 < \mu(a_{max})$. Recalling (2.22), we have that

$$\begin{aligned} \tilde{R}_1 > \mu(a_{max}) \quad &\Rightarrow \beta_1(\tilde{R}_1) < \frac{\gamma_R \mu(a_{bas})}{\mu(a_{max}) - \mu(a_{bas})} < \hat{\kappa}, \\ \tilde{R}_1 < \mu(a_{bas}) \quad &\Rightarrow \beta_2(\tilde{R}_1) < \frac{V_R - \gamma_R \mu(a_{max})}{\mu(a_{max}) - \mu(a_{bas})} < \hat{\kappa}, \end{aligned}$$

with the $\hat{\kappa}$ expression for N sufficiently large.

For the range $\tilde{R}_1 \in (\mu(a_{bas}), \mu(a_{max}))$, note that $\beta_1(C)$ is a decreasing function in the interval $(\mu(a_{bas}), +\infty)$, with $\lim_{C \to \mu(a_{bas})} \beta_1(C) = +\infty$ and, conversely, $\beta_2(C)$ is an increasing function in the interval $(0, \mu(a_{max})$ with $\lim_{C \to \mu(a_{max})} \beta_2(C) = +\infty$. Therefore, in the interval $C \in (\mu(a_{bas}), \mu(a_{max}))$, the two functions intersect at a single point $\hat{C}$ and it is easy to check that:

$$\min\{\beta_1(\tilde{R}_1), \beta_2(\tilde{R}_1)\} < \beta_1(\hat{C}) = \beta_2(\hat{C})$$

with

$$\beta_1(\hat{C}) = \beta_2(\hat{C}) = \frac{V_R - \gamma_R(\mu(a_{bas}) - \mu(a_{max}))}{\mu(a_{bas}) - \mu(a_{max})} \equiv \hat{\kappa}.$$

Thus, from (2.22), the i-th system (3.15) does not admit a periodic solution, meaning that all systems in the star-coupled network converge to a (locally) stable steady state.

■

3.3 All-to-all topology

An alternative configuration mimics the network of interconnections that might be found between the cells in a living tissue, where each cell communicate with all the others. This is a fully symmetrical network, since no oscillator can be distinguished from another. The corresponding $\Gamma_R + L$ matrix and its inverse are:

$$\Gamma_R + L = \kappa(NI - \mathbf{11'}) + \gamma_R I \tag{3.16}$$

$$(\Gamma_R + L)^{-1} = \frac{1}{N\kappa + \gamma_R} I + \frac{\kappa}{\gamma_R(N\kappa + \gamma_R)} \mathbf{11'}, \tag{3.17}$$

where I is the $N \times N$ identity matrix, **1** is the vector with all entries equal to 1 and **11'** is the matrix with all entries 1.

As for the star topology, we can count the number of new steady states due to the coupling. Since all oscillators have an equal role, let $(D_{11}^m \times D_{00}^{N-m})_{prm}$ denote any permutation of m D_{11} and $N-m$ D_{00} domains.

Theorem 4. *Consider system (3.2) coupled in an all-to-all topology, with L defined as in (3.16). Assume that conditions (a)-(f) hold. Define:*

$$\begin{aligned} m_{min} &= \left\lceil \frac{\gamma_R}{\kappa} \frac{N\kappa+\gamma_R}{V_R} \mu(a_{bas}) \right\rceil \\ m_{max} &= \left\lfloor \frac{\gamma_R}{\kappa} \Big(\frac{N\kappa+\gamma_R}{V_R} \mu(a_{max}) - 1 \Big) \right\rfloor, \end{aligned} \tag{3.18}$$

If $m_{min} < m_{max}$, then system (3.2) has exactly $\sum_{m=m_{min}}^{m_{max}} N!/(m!(N-m)!)$ locally stable steady states corresponding to focal points $\phi_C \in D_C = (D_{11}^m \times D_{00}^{N-m})_{prm}$. Furthermore, let

$$\hat{\kappa} = \frac{1}{N} \Big(\frac{V_R}{\mu(a_{max}) - \mu(a_{bas})} - \gamma_R \Big) \tag{3.19}$$

then none of the focal points corresponds to a steady state for any $\kappa \leq \hat{\kappa}$.

Proof. As in the proof of Theorem 2, we will provide conditions such that regular domains of the form $D_C = (D_{11}^m \times D_{00}^{N-m})_{prm}$ contain their own focal points. In this case, all oscillators play a similar role. By (3.3) and (3.16), the $\tilde{R}^C$ coordinates of the focal point of D_C are given by

$$\tilde{R}_i^C = \begin{cases} V_R \dfrac{\kappa}{\gamma_R(N\kappa+\gamma)} m, & \text{if } sh_{A,i} = 0 \\ V_R \dfrac{1}{N\kappa+\gamma_R} + V_R \dfrac{\kappa}{\gamma_R(N\kappa+\gamma_R)} m, & \text{if } sh_{A,i} = 1. \end{cases}$$

By Lemma 5, the conditions to guarantee that $\phi_C \in D_C$

$$\begin{aligned} V_R \frac{\kappa}{\gamma_R(N\kappa+\gamma_R)} m &> \mu(a_{bas}) \\ V_R \frac{1}{N\kappa+\gamma_R} + V_R \frac{\kappa}{\gamma_R(N\kappa+\gamma_R)} m &< \mu(a_{max}), \end{aligned}$$

immediately yield the values (3.18). Since the interconnection scheme is fully symmetric, the maximal number of new steady states equals all the possible combinations of the form D_C, that is $N!/(m!(N-m)!)$, for each $m_{min} \leq m \leq m_{max}$.

The value $\hat{\kappa}$ is the highest value that implies $m_{min} > m_{max}$ in (3.18). It follows by solving the inequality with respect to κ:

$$\gamma_R(\gamma_R + N\kappa)(\mu(a_{max}) - \mu(a_{bas})) - V_R\gamma_R < 0.$$

■

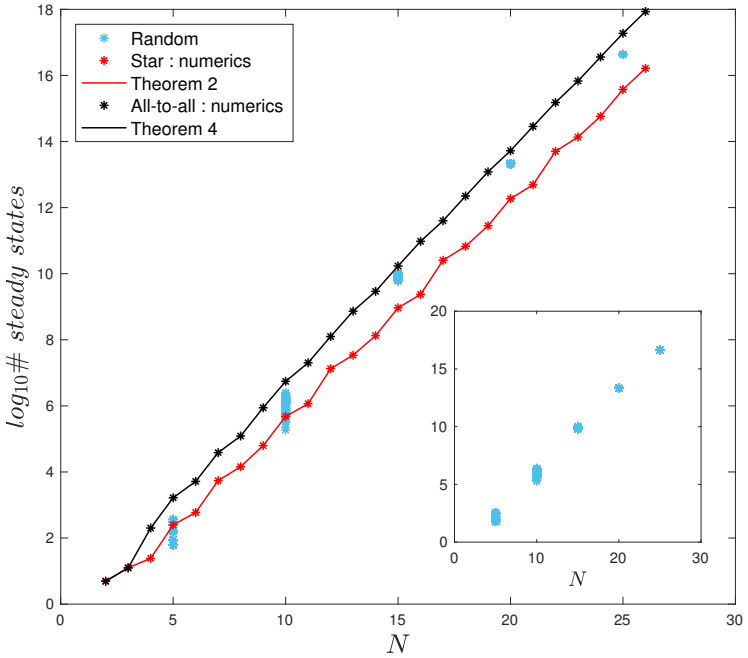

FIGURE 3.2: The number of new steady states (log scale) generated by each topology.

A fundamental difference arises between the star and the all-to-all topology: the upper bound on the diffusion constant decreases to zero with N in the all-to-all topology, while it remains constant in the star topology (Fig. 3.3). For large N, we can expect to avoid new steady states in the star topology by assigning a small but finite and reasonable diffusion constant (on the order of the degradation constants); however, steady states will appear for sufficiently large N in all-to-all topology, possibly contributing to disrupt synchronization of the oscillators to the periodic orbit. In any case, the periodic orbit is preserved: in the last section we give the basin of attraction for the periodic solution. Therefore, considering clusters of cells connected in all-to-all topology, for a reasonable number of cells in each cluster the oscillations are preserved regardless the large number of the steady states generated by the coupling, see Fig.3.4.

3.4 Random topology

Star and all-to-all topologies are standard network architectures in graph theory with numerous applications. When it comes to biology, in particular to intercellular coupling, it becomes important to explore a larger class of interconnection structures.

In the work of Hafner, Koeppl, and Gonze, 2012, a comprehensive mathematical model of the circadian clock is used to simulate the cells inside the SCN with different types of interconnections.

The results of this study suggest that cells with problematic oscillatory behaviour synchronize more efficiently in a random topology than in other topologies tested. Motivated by this result, we introduce a random topology for the network (3.2), with degree of connectivity d. The cell i is randomly bidirectionally connected to cell j,

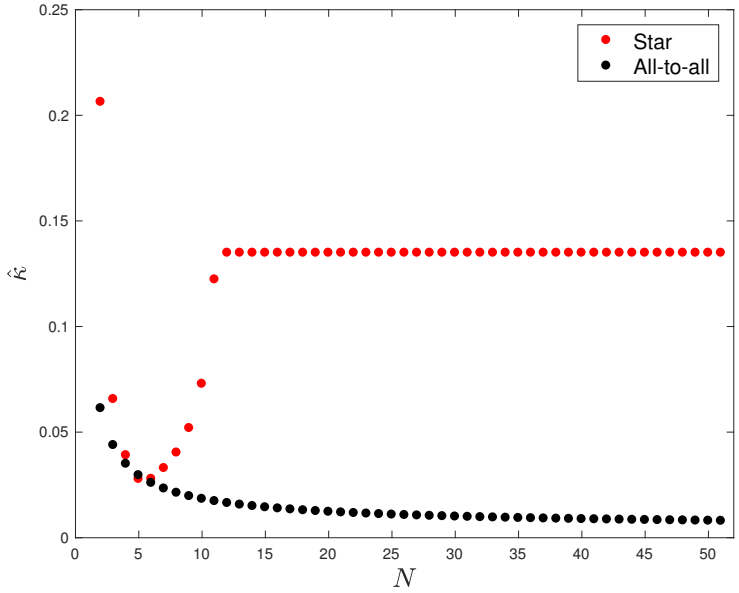

FIGURE 3.3: The upper bound $\hat{\kappa}$ on the diffusion constant that guarantees no new steady states for $\kappa < \hat{\kappa}$.

with $i, j = 1, \ldots, N$, $i \neq j$, and each cell (node) has exactly d connections (edges). We will denote this bidirectional connection as : $i \leftrightarrow j$. The elements of the Laplacian matrix L are defined as

$$l_{kj} = \begin{cases} \kappa(N-1-d), & j = k \\ -\kappa, & \text{if } j \leftrightarrow k, j \neq k, \end{cases}$$

The numerical results for the total number of new locally stable steady states in random connected networks of N oscillators, with degree of connectivity fixed for each network at $25\% - 50\%$ of N, are illustrated in Fig. 3.2, along with the corresponding numbers for the two other topologies.

The comparison of the total number of steady states for the three topologies, shows that random connections generate more steady states than star topology but less than all-to-all. This is an intuitively reasonable result since, for the average degree of connectivity δ, for the three types of connections, we have that $\delta_{star} < \delta_{random} < \delta_{all-to-all}$.

3.5 Initial conditions to guarantee convergence to the periodic solution

The generation of new stable steady states due to the diffusive coupling may be a disrupting factor in a network where the goal is synchronization towards the biological rhythm present in each single cell. Thus, in addition to the lower bound on the coupling constant, which prevents the generation of new stable steady states, it is also crucial to define initial conditions that guarantee convergence to the periodic orbit. Due to the specific form of the domains of system (2.10), and consequently of system (3.1) (that are defined by the quadratic curve $\mu(A)$), the explicit definition

TABLE 3.2: Phase space of system (3.1) partitioned in three regions to test convergence of initial conditions. Parameters as in Fig. 2.6, $l_\theta(A) = cA + b$, $c = 0.8482$, $b = -0.7082$.

Zones	
1	$\{R_i \in [0, V_R/\gamma_R), A_i \leq l_\theta^{-1}(R_i)\}$
2	$\{R_i \in [0, V_R/\gamma_R), A_i > l_\theta^{-1}(R_i) \cap (\sqrt{\theta_1} + \varepsilon, \mu^{-1}(R_i))\}$
3	$A_i \in (\sqrt{\theta_1} + \varepsilon, \mu^{-1}(V_R/\gamma_R)), R_i \in [0, \mu(A_i))$

TABLE 3.3: Percentage of the initial conditions that lead the trajectories to the steady states, $N = 10$, $\kappa = 0.25$, and the initial states for each system to slightly vary as: $(A_i, R_i) = \alpha(A_1, R_1)$, with $(A_1, R_1) \in$ zone j, $\alpha \in [0.8, 1.2]$, $i = 2, \ldots N$ and $j = 1, 2, 3$.

Topology	Star	All-to-all	Random
Zone 1	0%	0%	0 %
Zone 2	15.2 %	43.6 %	27 - 39 %
Zone 3	4.7%	25.8%	15 - 21.7 %

of the basins of attraction for the limit cycle and the locally stable steady states is not straightforward. Instead, numerical simulations were performed to identify the basins of attraction for the two types of attractors in three regions (zones) of the phase space, as defined in Table 3.2. Table 3.3 shows the percentage of initial conditions that converge to the steady states in each zone.

To facilitate the characterization of our results, first we define the line $l_\theta(A) = cA + b$, that passes through the point $(\sqrt{\theta_0}, 0)$ and intersects the R-nullcline $A = \sqrt{\theta_1}$ and the R threshold-line $R = V_R/\gamma_R$, with $c = V_R/\gamma_R(\sqrt{\theta_1} - \sqrt{\theta_0})$ and $b = -V_R\sqrt{\theta_0}/\gamma_R(\sqrt{\theta_1} - \sqrt{\theta_0})$. This line is used to define the zones of Table 3.2.

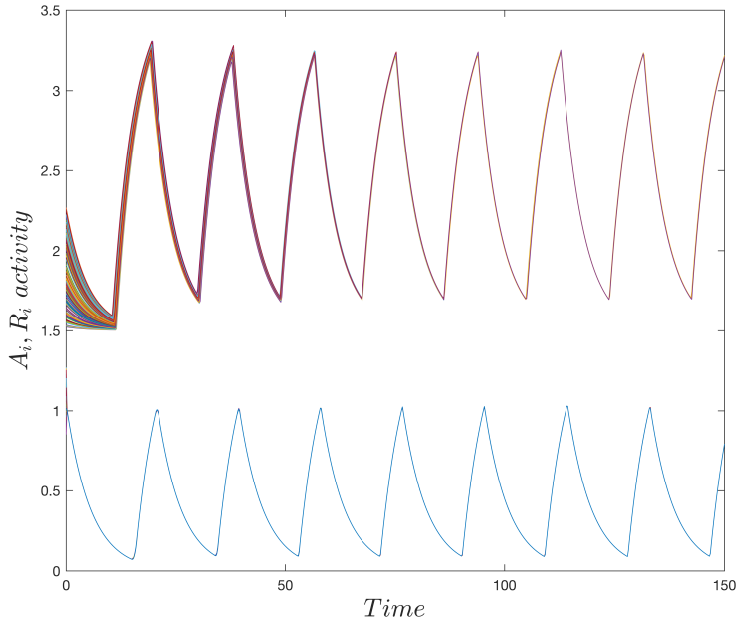

FIGURE 3.4: Activity in time of $N = 200$ coupled two-gene oscillators of the form (2.10) in all-to-all topology, initial conditions in zone 1, $\kappa = 0.25$ and other parameters as in Fig. 2.6. Trajectories converge to the periodic solution.

The results of Table 3.3 imply that trajectories starting in zone 1 have the highest probability to oscillate, with 100 % of the initial conditions tested leading to the periodic orbit. We note that the other two zones both intersect the basins of attraction of more than one attractor. Initial conditions in the region

$$C = \{(A,R) \in \mathbb{R}^{2N}_{\geq 0}\}, R_i \in [0, V_R/\gamma_R), A_i \leq l_\theta^{-1}(R_i), i = 1, \ldots N \tag{3.20}$$

lead trajectories of system (3.1) to the periodic solution, for the three topologies tested. Indicatively for star topology, initial conditions in zone 1 are depicted in Fig. 3.5; trajectories starting from the marked superimposed points (A_i, R_i) converge to the periodic orbit.

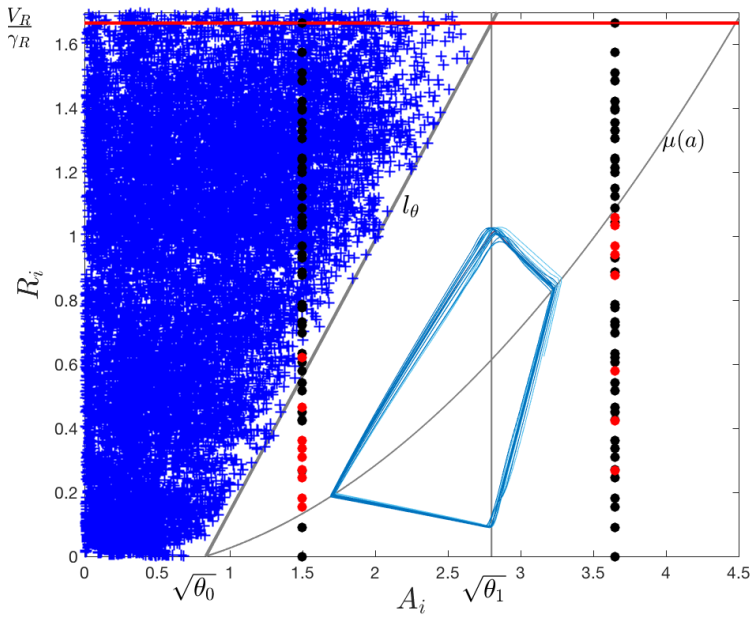

FIGURE 3.5: For all initial conditions tested in zone 1 (blue + symbols), trajectories converge to the periodic orbit. Here are shown the numerical tests for star topology with $N = 10$.

3.6 Discussion

Interconnection of identical oscillators generates new dynamics A network of synthetic oscillators was next constructed by connecting N identical elements through diffusive coupling, organized according to different interconnection structures: one-to-all or star, all-to-all and random. All three forms of interconnection preserve the periodic orbit but acquire additional attractors: new locally stable steady states. We give the exact total number of the new stable states, which increases with the number N of the systems in the network. In addition, we provide a lower bound on the diffusion constant that prevents the generation of new steady states due to the coupling. Numerical simulations show that oscillators synchronize towards some (new) stable steady states in groups, i.e. some oscillators converge to the same stable state and therefore form a group or "cluster". Indicatively see for instance, in Fig. 3.6 for $N = 5$, we observe convergence to locally stable steady states in two groups for all to all topology, and in three groups for star topology. Similar behavior is also observed in the analysis of Nicks, Chambon, and Coombes, 2018 for PWA systems. Cluster synchronization patterns and their properties are analytically studied by Sorrentino et al., 2016 in a more general framework. We also identify a region of the state space which prevents convergence to any of the steady states, for the three forms of interconnections applied. Numerical simulations show that, in the case of convergence to the periodic orbit, the N systems synchronize both in period and in phase, even for a small value of the coupling constant. An interesting question to be addressed in future work is whether the coupled systems still synchronize if the individual systems are not identical but have different parameters and periods.

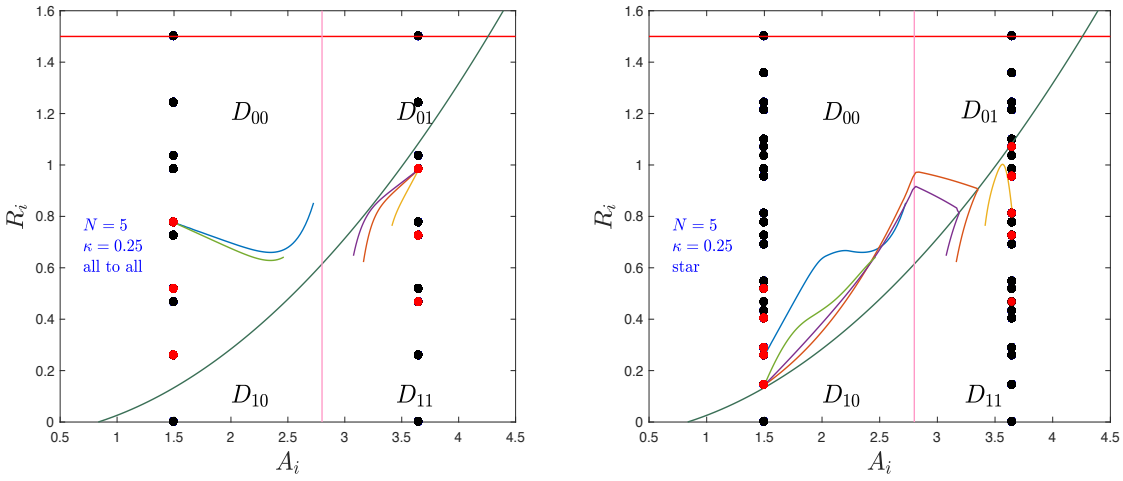

FIGURE 3.6: Projection of the activity of A_i, R_i, i=1,...,5 simultaneously: phase portrait of the coupled system for $\kappa = 0.25$. Trajectories of the system converge to locally stable steady states in two groups for all to all topology (left) and three groups for star (right). Red dots indicate the locally stable steady states.

Network topologies and robustness of oscillations The three interconnection topologies lead to similar qualitative dynamical behaviours and raise the problem of the robustness of the periodic behavior, when the goal is, for instance, the synchronization of a cluster of cells to the same periodic rhythm. The analysis of the new steady states and their basins of attraction indicates that, for a large amount of initial conditions, the network elements will not synchronize to a similar asymptotic behaviour. Star topology has fewer new steady states and a finite lower bound on the diffusion constant that prevents locally stable steady states and guarantees the existence of periodic oscillations. Moreover, this lower bound has physiologically reasonable values and is independent of the number of cells in the network. In constrast, the all-to-all topology creates locally stable steady states for any value of diffusion constant, for sufficiently large N. This analysis indicates that a star interconnection, resembling a central synchronizer with peripheral clocks, has the capacity to more robustly maintain a synchronized oscillatory behaviour, while in an all-to-all network, representing identical cells in a homogeneous tissue, it will be difficult to synchronize to a periodic orbit as the number of cells increases. In random interconnections, reminiscent of a network of circadian oscillators inside the SCN, the total number of locally stable states lies in between the corresponding numbers of the two other topologies, making this type of connection more robust to oscillations than all-to-all topology.

Conclusion Our results show that the architecture of interconnections induces new dynamics in a network of identical oscillators, creating new steady states and interfering with synchronization properties, which can be undesirable in synthetic biology applications. Our analysis provides useful guiding lines for choosing network design and implementation showing that, by carefully adjusting the coupling

strength or tuning initial conditions, it is still possible to synchronize the network of N biological oscillators, in all architectures. However, a star-shaped network has the potential to more robustly maintain oscillators synchronized.

Acknowledgments We gratefully thank Luca Scardovi for many interesting and useful discussions on the coupling and synchronization of oscillators, during his extended visit to Inria.

Chapter 4

Period response to different interconnection schemes for two coupled genetic oscillators

Biological complex mechanisms with oscillatory behavior are often modeled by high dimensional nonlinear ODEs systems, which makes the analysis and understanding the dynamics of the system difficult. In this chapter, we consider two reduced models that mimic the oscillatory dynamics of the cell cycle and the circadian clock, and study their coupling from a synthetic biology perspective. Moreover, we study the capacity for mutual period regulation and control of the coupling between the two reduced oscillators.

4.1 Introduction

Biological oscillators often involve a complex network of interactions, as in the case of circadian rhythms or cell cycle. Mathematical modeling and especially model reduction help to understand the main mechanisms behind oscillatory behavior. Low dimensional systems can be found at the core of oscillatory dynamics, such as a basic 3-dimensional negative feedback loop or a 2-dimensional negative loop with self-regulation (Smolen, Baxter, and Byrne, 1998). Moreover, both of these systems have been synthetically constructed in living cell environment and indeed shown to oscillate (Elowitz and Leibler, 2000, Stricker et al., 2008, Purcell et al., 2010).

A new challenge in synthetic biology is to study the behavior of an oscillator when coupled to another system (Tomazou et al., 2018, Perez-Carrasco et al., 2018). Interesting questions include the tuning capacity and period control for the coupled system. In this context, we perform a model-based investigation for the coupling between two oscillators, mimicking the cell cycle and circadian clock. This analysis aims to contribute to gain further intuition on the interactions between these oscillators (Feillet et al., 2015) and their mutual regulation of the period of oscillations.

A simple model proposed by Smolen, Baxter, and Byrne, 1998, consists of two *transcriptional factors* that compete with each other in a negative feedback loop, possibly generating oscillatory behavior. Such a system is able to describe complex autonomous mechanisms like the *circadian clock*, in terms of their function and properties, i.e. oscillatory behavior, feedback, autoregulation of the transcriptional factors.

A two-dimensional model for the cell cycle was recently proposed by Almeida et al., 2017. It represents the concentration of cyclin B and a complex APC that promotes exit from mitosis. This model was calibrated from experimental data and its region of oscillations can also be characterized in terms of the parameters.

A short outline of this chapter is as follows: in Sections 2 and 3 we introduce the two models with an improved version of Smolen oscillator. Section 4 contains the coupling schemes for the two models. Section 5 explores the coupled system dynamics and its period response. Lastly, in Section 6 we give an overall view of our results and some aspects for their application in synthetic biology.

4.1.1 The Smolen oscillator models the circadian clock

One version of the Smolen oscillator Smolen, Baxter, and Byrne, 1998 was implemented using the gene lacI as a repressor and araC as an activator (see Stricker et al., 2008, Purcell et al., 2010). In this study we consider the improved Smolen model as described in 2.1.1.

To establish that (2.2) can be interpreted as a minimal mammalian clock model we consider that the activator A represents the fundamental protein BMAL1 which activates the transcription of several clock proteins, including REV-ERBα, PER and CRY. In turn, there is also an auxiliary loop of REV-ERBα which inhibits BMAL1 making it a good candidate for the repressor R. The proteins CRY and PER form a complex (PC) which binds to BMAL1 to inhibit the transcription of genes that are regulated by CLOCK-BMAL1, as well as their own transcription (autoregulation) Ye et al., 2014. Describing in a simplified way, BMAL1 and PC mutually inhibit each other's activities by binding. The positive self-regulation of A can be interpreted as the result of this double negative loop.

4.1.2 A cell cycle reduced model

The reduced model of the mammalian cell cycle developed by Almeida et al., 2017 is a system of two variables: MPF (*mitosis promoting factor*) which is a cyclin-Cdk complex that phosphorylates multiple proteins during mitosis phase, and APC:cdc20, (subunit of the *anaphase-promoting complex*) which is a large complex of proteins that promote exit from mitosis phases through MPF and other kinases degradation. The network consists of an activator (MPF) and an inhibitor (APC:cdc20), both of them crucial components of cell division. This two-variable model was calibrated from experimental data, Pomerening, Kim, and Ferrell, 2005 and shown to reproduce the observations in a very reasonable way. The two dimensional model is as follows:

$$\begin{aligned}
\frac{d[APC:cdc20]}{dt} &= V_m[MPF] - V_k[APC:cdc20] \\
\frac{d[MPF]}{dt} &= S_{GF} + V_c \frac{\overline{MPF_{max}} - [MPF]}{\overline{MPF_{max}} - [MPF] + k_c} \frac{[MPF]^m}{[MPF]^m + k_m^m} \\
&\quad - V_w \frac{[MPF]}{[MPF] + k_w} \frac{k_n^n}{[MPF]^n + k_n^n} \\
&\quad - \gamma_1 [APC:cdc20][MPF],
\end{aligned}$$

with parameters given in Table 4.1. Very briefly, the constant S_{GF} represents growth factor, the term in V_c represents the positive feedback loop involving cdc25, while the term in V_w represents the double negative loop involving wee1.

TABLE 4.1: Parameters of cell cycle model

$V_m = 0.0168\ min^{-1}$	$V_k = 0.0107\ min^{-1}$
$S_{GF} = 5.6917\ min^{-1}$	$V_c = 225.71\ min^{-1}$
$V_w = 747.61\ min^{-1}$	$\overline{MPF_{max}} = 284.1087$
$k_c = 130.3331$	$k_m = 98.5219$
$k_w = 137.9830$	$k_n = 0.1164$
$\gamma_1 = 0.0162\ min^{-1}$	$m, n = 2$

4.2 Interactions between the two oscillators

In mammalians, it is known that the circadian clock affects the cell cycle, and more recently there has been evidence that the cell cycle may also directly affect the clock Feillet et al., 2014. Thus, in addition to their specific characteristics as biological processes, a very important aspect to be studied is their interaction: in some tissues, the pace with which the cell divides into two daughter cells (*mitosis phase*) is regulated by the cell circadian clock, Feillet et al., 2014, Ünsal-Kaçmaz et al., 2005. More precisely, the regulation of one specific kinase-inhibitor of the cell cycle,*Wee1*, by the clock genes, has been observed and explains the circadian control of cell cycle division Gérard and Goldbeter, 2012, Matsuo et al., 2003.

4.2.1 A scheme for bidirectional coupling

To model the interaction from the circadian clock to the cell cycle we have that: the activator A in the Smolen model, that stands for the complex CLOCK/BMAL1, influences the cell cycle through activation of the kinase Wee1 that inhibits MPF, Gérard and Goldbeter, 2012 , Matsuo et al., 2003.

The influence of the cell cycle on the clock is less clear, but an hypothesis is that of Feillet et al., 2015: the protein MPF inhibits the nuclear receptor REV-ERBα that is assumed as the component R (repressor) of the Smolen oscillator. We mention that there is no specific evidence on the form of clock regulation by the cell cycle, see in Feillet et al., 2015, so our current study will explore several possibilities for coupling schemes. A general scheme for bidirectional coupling between the two oscillators is shown in Fig. 4.1.

4.2.2 Period-response analysis

To better analyse the period response of the coupled system, and to identify whether either of the oscillators has a dominant contribution, we develop the following criteria.

We characterize the two systems as controller and follower comparing the 3 period values, the cell cycle period T_{cc}, the Smolen oscillator period T_{Smolen} and the coupled system period T_{bi}. Then define:

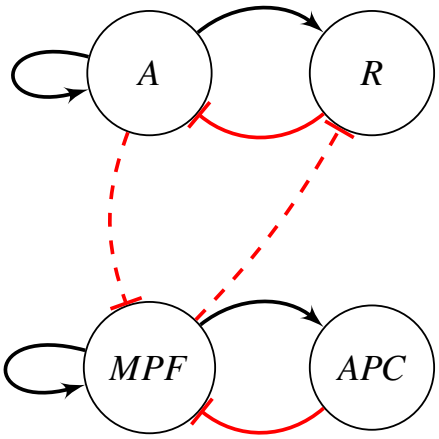

FIGURE 4.1: Cell cycle and Smolen oscillator coupled network.

Definition 1. *Let* $T_{min} = min\{T_{cc}, T_{Smolen}, T_{bi}\}$, $T_{max} = max\{T_{cc}, T_{Smolen}, T_{bi}\}$ *and* T_{int} *be the intermediate of the three period values. Then the controller is defined to be the oscillator with the period closer to that of the coupled system:*

(a) If $T_{bi} = T_{min}$ *or* $T_{bi} = T_{int}$ *and*

$$\frac{T_{bi}}{T_{max}} \ll min\left\{\frac{T_{bi}}{T_{int}}, \frac{T_{min}}{T_{bi}}\right\}$$

then the controller is the oscillator with lower period.

(b) If $T_{bi} = T_{min}$ *or* $T_{bi} = T_{int}$ *and*

$$\frac{T_{bi}}{T_{max}} \gg max\left\{\frac{T_{bi}}{T_{int}}, \frac{T_{min}}{T_{bi}}\right\}$$

then the controller is the oscillator with higher period.

(c) If $T_{bi} = T_{max}$ *and* $\frac{T_{int}}{T_{max}} \approx 1$ *then the controller is the oscillator with higher period.*

(d) If $T_{bi} = T_{min}$ *or* $T_{bi} = T_{int}$ *and*

$$\left|\frac{T_{min}}{T_{int}} - \frac{T_{min}}{T_{max}}\right| < \varepsilon \text{ or } \left|\frac{T_{min}}{T_{int}} - \frac{T_{int}}{T_{max}}\right| < \varepsilon$$

for $\varepsilon = 0.1$*, then no oscillator is considered as controller.*

4.3 Two coupling mechanisms

Following the discussion in Section 3, we investigate two general cases: the oscillators affect each other through synthesis or through degradation rates.

4.3.1 Coupling through synthesis rate

First, we consider the case where the clock acts on the cyclin complex MPF synthesis rate, i.e. BMAL1/CLOCK modulates parameter V_c, which expresses the activation of the kinase cdc25. The coupling is expressed through a saturation function:

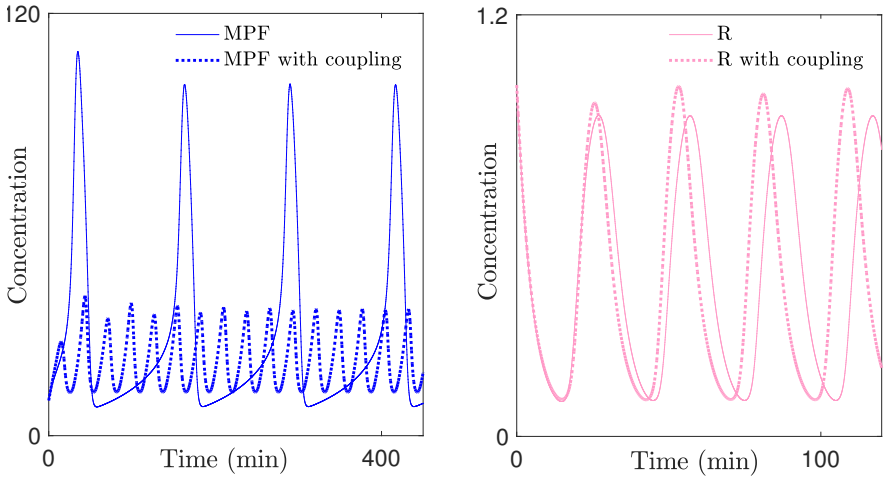

FIGURE 4.2: Activity of variables MPF (cell cycle) and R (clock), with or without couplig (respectively, solid and dashed lines). Strong coupling from the side of the clock, initial period $T_{Smolen} = 30$ min, $T_{cc} = 126.77$ min, period of the coupled system: $T_{bi} = 27.78$ min. Coupling parameters used: $v_1, v_2 = 1.5$, $\delta_1 = 1.5$, $\delta_2 = 100$.

$$C_1 = v_1 \frac{\delta_1}{\delta_1 + A} \tag{4.1}$$

where δ_1 represents the coupling strength and v_1 guarantees that the concentrations remain at sufficient levels. The term C_1 multiplies V_c.

Conversely, the complex MPF acts on REV-ERBα synthesis rate by inhibition:

$$C_2 = v_2 \frac{\delta_2}{\delta_2 + MPF} \tag{4.2}$$

The term C_2 multiplies V_R in (2.2).

We study the interaction between the two oscillators as a function of the coupling strength. First, our results show that, through bidirectional coupling the two oscillators lock at phase 1:1. Second, varying the coupling parameters, the clock tends to play the role of controller, see Fig. 4.3, top. Indicatively, for v_1, $v_2 = 1.2$, and for coupling strengths $\delta_1 = 0.5$ and $\delta_2 = 100$, (corresponding to 0.14 % of the maximum value of A and 91.65 % of the maximum value of MPF in the uncoupled systems), there is strong effect from the clock and weaker from the cell cycle : $\frac{T_{bi}}{T_{cc}} = 0.22$ while $\frac{T_{bi}}{T_{Smolen}} = 0.92$.

In this case, we see that varying the coupling strength from the side of clock δ_1, the period of the coupled system stays close to that of the clock. Thus, according to Definition 4.2.2, the clock is the controller in this case, with $\frac{T_{bi}}{T_{Smolen}} \approx 1$, Fig. 4.3 top. We also observe that δ_2 (cell cycle $\rightarrow$ clock) does not greatly affect the qualitative period response.

4.3.2 Coupling through degradation

We now investigate the case where the clock acts directly on the degradation rate of the MPF component of the cell cycle. The coupling term now is expressed through an increasing function since A promotes degradation rate of MPF:

$$C_1 = v_1 \frac{A}{\delta_1 + A} \tag{4.3}$$

This function will multiply the term $-\gamma_1$APC MPF, in MPF equation of cell cycle model.

Likewise, MPF now promotes the degradation rate of the REV/ERB-α. The coupling term will be:

$$C_2 = v_2 \frac{MPF}{\delta_2 + MPF} \tag{4.4}$$

The term C2 will multiply the degradation rate $-\gamma_R$ R, in R equation of the Smolen model, see (2.2).This scheme of interactions allows a wider range of period responses, as illustrated in Fig. 4.3, bottom. For instance, we now present a case where both oscillators strongly contribute to the coupling. With coupling parameters $v_1, v_2 = 1$, $\delta_1 = 0.5$, $\delta_2 = 100$ and uncoupled periods $T_{Smolen} = 30$ min, $T_{cc} = 126.77$ min, the period of the coupled system is $T_{bi} = 63.68$ min, with ratios: $\frac{T_{bi}}{T_{cc}} = 0.5$ and $\frac{T_{Smolen}}{T_{bi}} = 0.43$. Two ratios are very close so, according to Definition 4.2.2, none of the oscillators is a controller.

In this case, the coupled system period varies with both δ_1 and δ_2 (Fig. 4.3, bottom). We see that the cell cycle is able to play the role of the controller, as δ_2 increases and δ_1 remains low. This result can be interpreted as a stronger action from the cell cycle on the coupling: $\delta_1 \leq 0.5$, is less than the minimum concentration value of the uncoupled A and $\delta_2 \leq 109.1$ lower than the maximum uncoupled MPF, so it is likely that the term C_2 (4.4) contributes to significantly decrease the degradation rate of R. The latter results in the decrease of concentration of A, which finally can only weakly inhibit the cell cycle through MPF. In a simplified way, weak action from the side of clock allows the cell cycle to control the coupled system period; indicatively, our results show $\frac{T_{bi}}{T_{cc}} \approx 1$, for $\delta_2 = 100$ and $0.2 < \delta_1 \leq 0.5$, Fig. 4.3 bottom. Conversely, the clock is the controller with $\frac{T_{bi}}{T_{Smolen}} \geq 0.6$, for certain coupling parameter intervals, Fig. 4.3 bottom.

4.3.3 Analysis of Controller-follower results

To interpret the controller - follower results in both coupling cases, we extract information from the bifurcation analysis for the synthesis and degradation parameters of the two systems. (Bifurcation analysis performed using Matcont.)

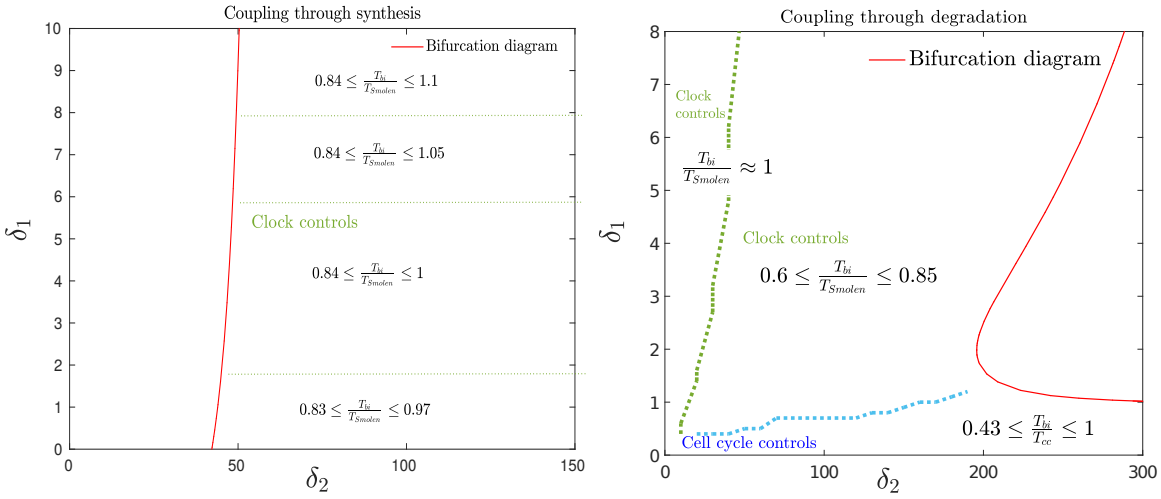

FIGURE 4.3: Coupled system period - response in the two interaction cases, as the coupling strengths δ_1, δ_2 vary. Remaining parameters used: see Table 2.2 for the Smolen model, Table 4.1 for the cell cycle, v_1,v_2 =1.

Cell cycle controls For a deeper analysis of this scenario, we perform bifurcation analysis for the synthesis and degradation parameters of the uncoupled Smolen system. In Fig. 4.4 right we indicate the parameter region where the uncoupled Smolen oscillates. We note that for the initial $V_A = 12.5\ min^{-1}$ the system becomes stable for $\gamma_R < 0.077\ min^{-1}$. Hence, as the coupling strength δ_2 from the side of cell cycle increases the term $-\gamma_R C_2$ decreases and the system has no longer periodic solutions. The cell cycle in this case is able to play the role of the controller when the Smolen system is close to exit the oscillatory region. For instance, if $\delta_2 = 80$ ($\delta_1 = 0.5$), we have that $-\gamma_R C_2 < 0.14$ and $\dfrac{T_{bi}}{T_{cc}} = 0.8$, see Fig. 4.5 (bottom).

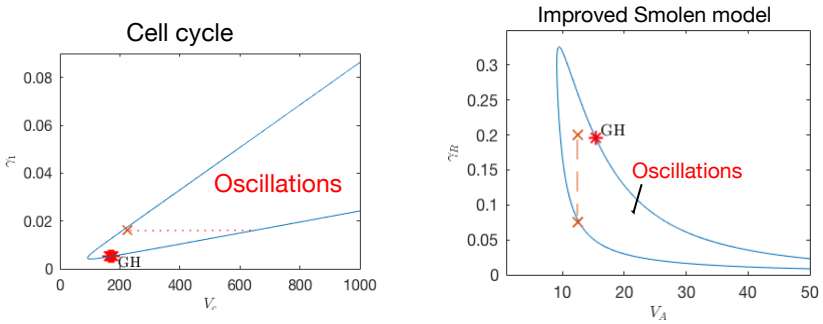

FIGURE 4.4: Bifurcation analysis for cell cycle synthesis and degradation parameters (left) and the improved Smolen model (right). The red stars indicate Generalized Hopf points.

Clock controls As we observe in Fig.4.4 (left) the uncoupled cell cycle becomes

stable for $\gamma_1 < 6.4 \times 10^{-3}$ if $V_c = 225.71\ min^{-1}$. In the case of coupling through degradation, the term C_1 (4.3) becomes very small as δ_1 increases, (Fig. 4.5 top), thus it forces the cell cycle to become stable: for $\delta_1 > 1$, ($\delta_2 = 100$) we have that $-\gamma_1 C_1 < 5 \times 10^{-3}$. Under these coupling parameter conditions, the clock is the controller with $\frac{T_{bi}}{T_{Smolen}} \geq 0.7$, Fig. 4.3 bottom. This observation can be interpreted as: the clock is more likely to be the controller of the coupled system period when the cell cycle starts to loose its instability (i.e. loose its periodic orbit) due to the coupling strength.

In the case of coupling through MPF synthesis rate the cell cycle looses instability much faster than in the case of degradation: the initial γ_1 value is 0.0162 min^{-1} and for $V_c < 210\ min^{-1}$ system (4.1) has no longer periodic behavior, see the bifurcation analysis in Fig. 4.4 left. Since the initial V_c value is 225.71 min^{-1} the term $V_c C_1$ decreases immediately as δ_1 increases, C_1 as in (4.1). Altogether, this analysis suggests that an oscillator A becomes a controller when its coupling term induces oscillator B to enter a parameter region where sustained oscillations disappear.

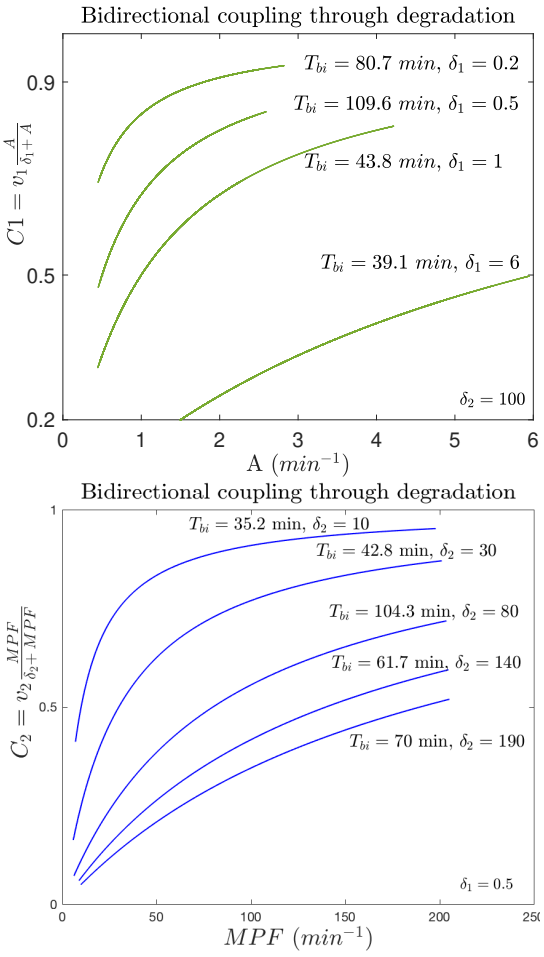

FIGURE 4.5: The term C_1 in coupling through degradation, as a function of the activator A concentration amplitude (top) v_1, $v_2 = 1$, $\delta_2 = 100$. The term C_2 in coupling through degradation, as a function of MPF concentration amplitude (bottom) v_1, $v_2 = 1$, $\delta_1 = 0.5$.

4.3.4 Effect of Synthesis rate parameters

We now investigate the effect on the coupled system period of varying each oscillator period. This is done separately by varying the synthesis rate parameters V_c of MPF and V_A of A.

In Fig. 4.6 (top), we observe that increasing V_c the coupled system period remains constant for both interaction cases. However, in the case of coupling through degradation, the coupled system period is greater than in case of coupling through synthesis. An interesting observation is that even when the cell cycle is at a stable steady state (for $V_c < 209\ min^{-1}$), the coupled system manifests oscillations in both interaction cases.

Varying now the synthesis rate of A (at bottom of Fig. 4.6), we notice that for $V_A > 12\ min^{-1}$ the uncoupled clock period increases and so does the coupled period. The latter is strongly controlled by the clock when the coupling is through synthesis rate. In the case where the coupling is through degradation rate, T_{bi} takes higher values reflecting the cell cycle contribution.

It is surprising though, that for $V_A > 15.5\ min^{-1}$ the clock (Smolen system) is at a stable steady state, whereas the coupled system oscillates with period around 50 min. In this way the cell cycle forces the clock (Smolen system) to oscillate. This observation can be interpreted as the capacity of the cell cycle to induce oscillations of the coupled system even when the clock is at a steady state.

In the bifurcation diagram for the parameters V_A, γ_R of Fig. 4.4 we observe that as γ_R reaches values lower than $0.02\ min^{-1}$ the interval for periodic solutions of V_A shifts to the right and increases. Indeed, with coupling through degradation rate, the term $-\gamma_R C_2$ decreases as δ_2 increases, see Fig. 4.5 bottom, C_2 as in (4.4). For example, for $\delta_1 = 1$ and $\delta_2 = 100 \Rightarrow 0.05 < -\gamma_R C_2 < 0.7$, so R degradation rate decreases allowing V_A to take higher values in the oscillatory region, see Fig. 4.4 right. Thus, although the uncoupled Smolen system is at a stable steady state, the coupled system oscillates as it is shown in Fig. 4.6 (bottom).

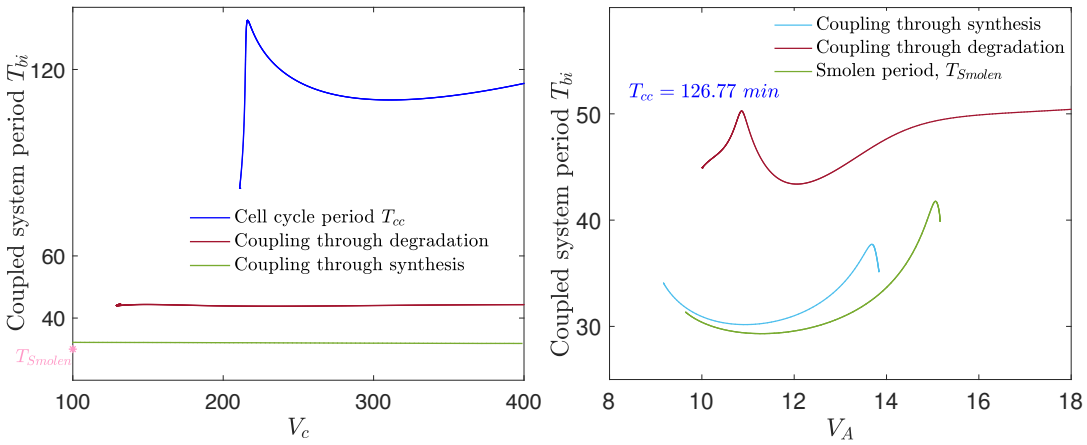

FIGURE 4.6: Coupled system period as a function of V_c (synthesis rate of MPF) and V_A (synthesis rate of A, right) in the two interaction cases. Coupling parameters used: $\nu_1, \nu_2 = 1$, $\delta_1 = 1$, $\delta_2 = 100$.

4.4 Conclusion

In this chapter we present a model-based investigation of the cell cycle and circadian clock coupling, using two reduced models. We consider two bidirectional schemes for the coupled system and observe that: (i) generally, in the case of coupling through synthesis rates, the coupled system closely follows the clock period, (ii) in the case of coupling through degradation rates, the cell cycle may have a higher contribution on the coupling. In either scheme, it is interesting to note that each of the oscillators can alone induce oscillations in the coupled system, implying that the coupling contributes to increase the parameter region where oscillations happen.

Many different coupling schemes remain to be discussed and tested. However, the current analysis provides some indications on how to couple the two systems so that the joint periodic behavior is improved and also suggests ways of regulating the period of the coupled system through one of the oscillators. These are promising directions to consider in the context of synthetic biology.

Chapter 5

Coupled synthetic genetic oscillators: comparison and analysis of period tunability and control

Recent developments in synthetic biology engineering include the improvement of synthetic circuit design, the precise control of the output and the implementation of coupled circuits with robust oscillatory behaviour. In our work we consider a theoretic coupling scheme for the bidirectional interaction of two classic synthetic oscillators.Using different pairs of classic oscillators (an improved Smolen oscillator, coupled with either a cell cycle model or a repressilator), we compare the effect of the same coupling scheme on the period response of the coupled system, in terms of the properties of each individual oscillator. In our methodology we use computational tools and bifurcation analysis,to propose tuning of the coupling parameters and period control of the coupled circuit through bidirectional coupling.

5.1 Introduction

Research in synthetic biology aim to understand the function of complex biological processes utilizing minimal circuits that capture the basic characteristics of heterogeneous mechanisms. To improve the performance of a synthetic circuit implementation, external control is required to better support the actions of the biologists/scientists/researchers. The efficient design of a synthetic circuit combined with the comprehension of the system dynamics, has the most important contribution to the improvement and the robustness of the system performance in a living-cell environment (Del Vecchio, Dy, and Qian, 2016,Hsiao, Swaminathan, and Murray, 2018).

Biological oscillators and their coupling are part of these complex mechanisms in living organisms, such as calcium oscillations, NFκB oscillations, circadian rhythms, cell cycle, and others (Tsai et al., 2008). Among these, the interactions between the mammalian cell cycle and circadian clock have been a topic of much recent research but many unknown questions still remain (Gérard and Goldbeter, 2012 , Matsuo et al., 2003, Feillet et al., 2015). Experimental and theoretical studies seek to understand possible ways that the oscillators interact and their potential for sustained oscillations as a coupled system.

Recent studies in synthetic bio-engineering (Tomazou et al., 2018,Perez-Carrasco et al., 2018) focus on recasting and improvement of synthetic circuit design through coupling approaches. In our previous work (Firippi and Chaves, 2019), we study

the bidirectional coupling of two synthetic genetic oscillators, an improved Smolen oscillator (Smolen, Baxter, and Byrne, 1998), and a reduced model of the mammalian cell cycle calibrated from experimental data (Almeida et al., 2017). Our results aimed at giving directions on the implementation dynamical behavior of the coupled circuit where the coupling scheme was based on the experimental observations of Feillet et al., 2015.

For the implementation of a circuit that consists of several systems-components linked to each other, it is crucial to provide controllable design of each individual system along with predictions on the system response to the coupling scheme and strength. In this context, we seek to study in more detail the mechanism behind the coupled period response in a coupled system of two synthetic oscillators. In particular, we wish to explore the relationship between the properties of each oscillator (period length, peak amplitude, form of the oscillations) and those of the coupled system (control-follower classification, period control, etc.). More specifically, choosing a coupling scheme where the oscillators regulate each other's degradation rates, as in our previous work, we now apply this scheme to a different pair of classic synthetic oscillators: the same improved configuration of the Smolen oscillator (as in Firippi and Chaves, 2019) and a specific form of the *repressilator*, introduced by Elowitz and Leibler, 2000. We study the coupled system response to the control on the degradation rate of the repressilator by the Smolen system. We provide coupling parameters range for controller-follower analysis of the coupled period response.

Furthermore, our results show the capacity of the studied coupling scheme to induce a joint period which is larger than both the initial uncoupled periods.

5.2 Three classic synthetic genetic oscillators

We investigate the coupling of the improved version of the Smolen model (2.2) and a classic genetic oscillator, a form of repressilator, Elowitz and Leibler, 2000. One of the goals in this chapter is to provide a comparison of the coupling behavior of different pairs of oscillators, to explore how the properties of the coupled system are related to the properties of the individual systems. To do this, it is useful to first recall some of the characteristics of each of the three oscillators to be used in this chapter: the improvement Smolen oscillator, a reduced model of the cell cycle, and the repressilator.

The improved Smolen oscillator and the cell cycle model are those studied in Chapter 4.

The repressilator is a well known synthetic circuit that consists of three genes in a negative feedback loop generating oscillations. It was first implemented in *E. coli* by Elowitz and Leibler, 2000. In this work we use a specific form of the repressilator where one gene repressses an other gene of the network, as illustrated in the following scheme:

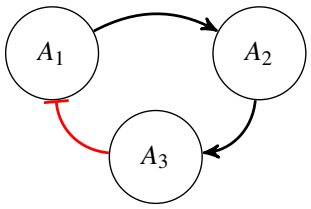

FIGURE 5.1: A form of repressilator.

The model is described by the following system of ODEs:

$$\begin{aligned} \frac{dA_1}{dt} &= V_1 \frac{k_3^3}{k_3^3 + A_3^3} - \gamma_1 A_1 \\ \frac{dA_2}{dt} &= V_2 \frac{A_1^3}{k_1^3 + A_1^3} - \gamma_2 A_2 \\ \frac{dA_3}{dt} &= V_3 \frac{A_2^3}{k_2^3 + A_2^3} - \gamma_3 A_3 \end{aligned} \tag{5.1}$$

We denote $T_{repress}$ the period of the repressilator. The following Table contains the parameters used for the repressilator model:

TABLE 5.1: Parameters of repressilator

Case I & II	$V_1 = 0.2\ min^{-1}$	$V_2 = 3\ min^{-1}$	$V_3 = 3\ min^{-1}$	
Case I & II	$\theta_1 = 3$	$\theta_2 = 2$	$\theta_3 = 2$	
Case I	$\gamma_1 = 0.08\ min^{-1}$	$\gamma_2 = 0.1\ min^{-1}$	$\gamma_3 = 0.1\ min^{-1}$	$T_{repress} = 40.7$
Case II	$\gamma_1 = 0.03\ min^{-1}$	$\gamma_2 = 0.1\ min^{-1}$	$\gamma_3 = 0.1\ min^{-1}$	$T_{repress} = 54.54\ min$

5.2.1 Parameter sensitivity and birfucation analysis

Fig. 5.2 shows the form of the oscillations and peak amplitudes for all variables of each oscillator. The cell cycle is close to a relaxation oscillator while the repressilator has quite symmetric sinusoidal-like oscillations. The form of the Smolen oscillatory solutions is in between. All three oscillators have one variable which exhibits a much larger peak amplitude.

Fig. 5.3 shows the period sensitivity for variations in the degradation rate of the regulated variable, within a region admitting oscillations. The regulated variables are, respectively, MPF, A_1 and R, for the cell cycle, the repressilator, and the Smolen oscillators. The corresponding degradation rates will be the connection points of the coupling scheme (see Figs. 4.1 and 5.5) It follows that, although exhibiting different period ranges, each of the three oscillators admits roughly a 25% change in its period in response to a two-fold increase in the degradation rate of the regulated variable.

From the numerical analysis of the repressilator, we conclude that the system period is significantly more sensitive to variations of the degradation parameters (γ_i), than to variations of the synthesis rates (V_i). As observed in Fig. 5.3, the repressilator has the capacity for larger period: as the degradation rate increases 6-fold, the period

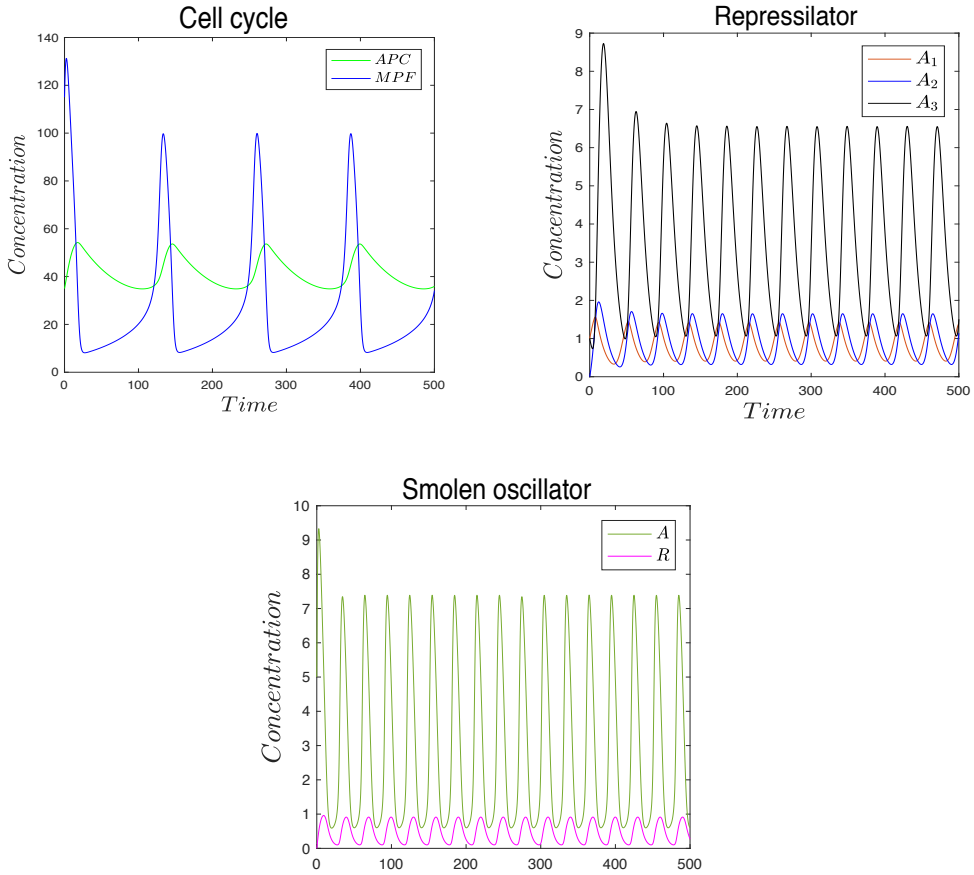

FIGURE 5.2: Solutions of the three classic oscillators along time: Cell cycle (top left), repressilator (top right), Smolen oscillator (bottom). The corresponding periods: $T_{cc} = 126.77$ min, $T_{repress} = 40.7$ min, $T_{Smolen} = 30$ min. The parameters used for the numerical simulations are those of Tables 4.1, 5.1/Case I, 2.2.

decreases to about half. In particular, the period can be tuned by the degradation parameters γ_i,$i = 1,2,3$.

To characterize the parameter regions for oscillations, we perform bifurcation analysis for the synthesis and degradation parameters of the regulated variable, as illustrated in Fig. 5.4. The two-parameter bifurcation diagrams show that the repressilator admits a much larger region of oscillatory behavior. For the repressilator, the synthesis parameter V_1 has a weaker effect on establishing osccillatory behavior.

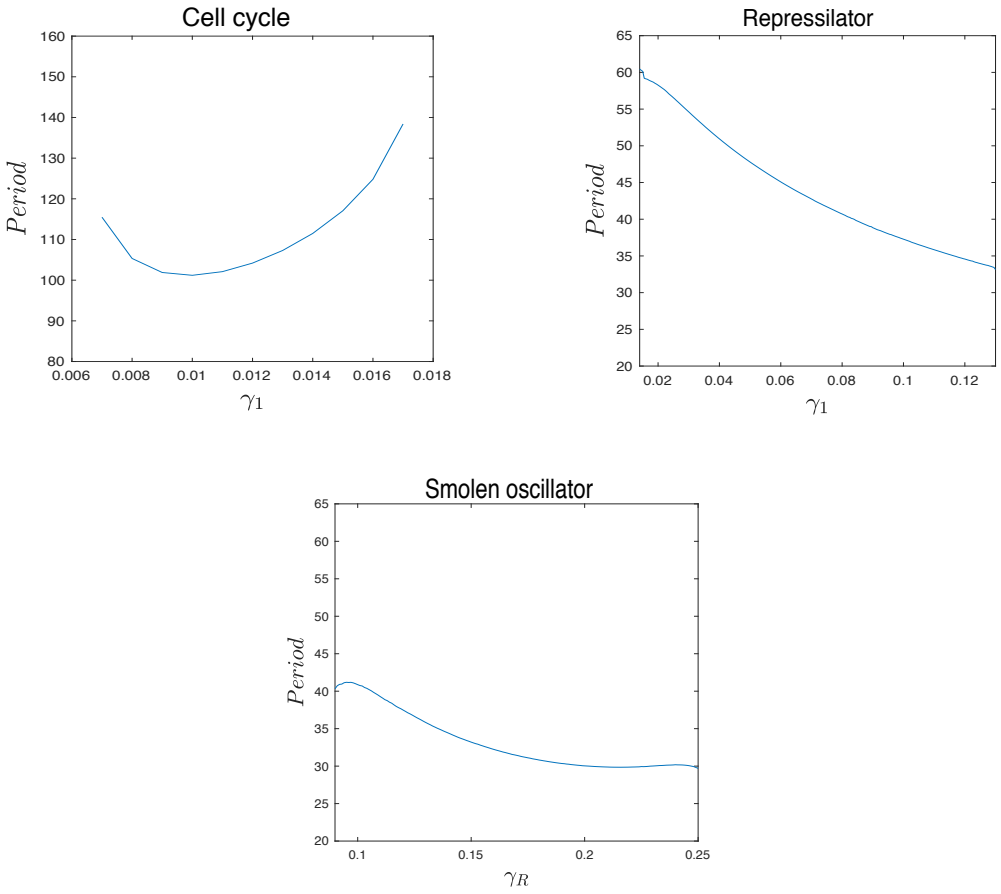

FIGURE 5.3: Period of the Cell cycle model, the repressilator and the Smolen oscillator, T_{cc},$T_{repress}$,T_{Smolen}, as a function of the involved in the corresponding coupling schemes degradation parameters.

In Chapter 4, we study the period-response of the cell cycle - Smolen coupled system, using the information from the two-parameter bifurcation analysis. Our conclusion is that the controller of the coupled system period is more likely to be the system that has more *robust* individual oscillatory behaviour than the other, in the sense that its parameters are further away from the boundary between the oscillatory and stability regions.

As we observe in Fig. 5.4, the Smolen system parameters (red cross) are inside the region for sustained oscillations defined by parameters (V_R,γ_R), whereas the cell cycle model parameters (red cross)are very close to the stability boundary on an extreme value of the V_C parameter. In analogy with the study of Chapter 4 and for a more meaningful comparison of coupled systems behaviors, two different values of γ_1 are chosen for the repressilator: one for robust oscillations (Case 1) and the other close to the stability boundary (Case 2). Two separate sets of numerical experiments will be performed for the repressilator-Smolen coupling.

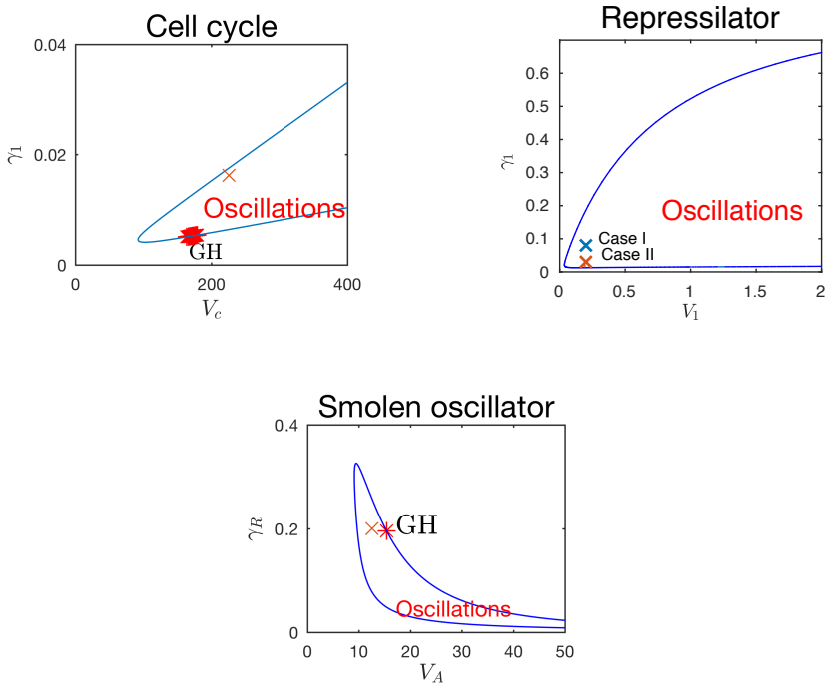

FIGURE 5.4: Bifurcation analysis for cell cycle synthesis and degradation involved parameters (top left), the repressilator model (top right) and the Smolen oscillator (bottom). The red stars indicate Generalized Hopf points.

5.2.2 One bidirectional coupling scheme

Comparison of the two coupling schemes for the cell cycle-Smolen oscillator (Chapter 4) indicate that the coupling through degradation rates has a richer dynamical behavior than the coupling through synthesis rates. In addition, as remarked in Section 5.2.1, the period of the repressilator is more sensitive to degradation parameters. Thus, from now on, we focus more on the coupling through the degradation rates of the regulated variables (respectively, MPF, A_1 and R, for the cell cycle, the repressilator, and the Smolen oscillators.

To choose the regulated variables, we consider that A_1 and MPF play analogous roles, since both are repressed by the previous component and activate the next component of their respective models. Therefore, in the coupling scheme of Fig. 5.5, A_1 is regulated by A and regulates R.

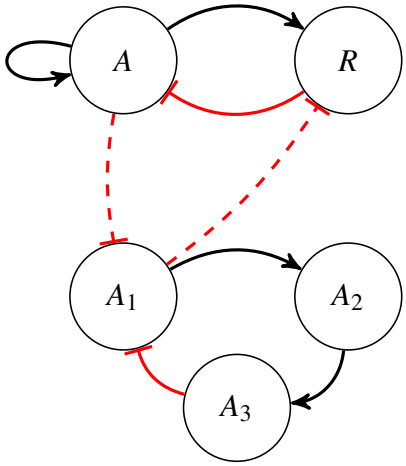

FIGURE 5.5: Smolen oscillator and repressilator coupled network.

To express the coupling strength we use the parameters δ_i, $i = 1,2$ along with v_i that express the maximum regulation rate of the given component. The coupling terms are expressed by saturation functions as follows:

$$C_1 = v_1 \frac{A}{\delta_1 + A} \tag{5.2}$$

where activator A increases the degradation rate of the repressilator component A_1, thus the term C_1 multiplies the degradation rate γ_1 in system 5.1.Likewise,

$$C_2 = v_2 \frac{A_1}{\delta_2 + A_1} \tag{5.3}$$

represents the inhibition of the repressor R by component A_1, where C_2 multiplies the degradation rate γ_R, in 2.2.

We note that the parameter values for the Smolen model are those of Table 2.2.

5.3 Period-response for the coupled Smolen-repressilator system

In this section, we describe two separate experiments performed for the coupling of the improved Smolen oscillator and repressilators: first with the repressilator parameter values for sustained oscillations (Case I) and second with the repressilator to be very close to enter the region of stability (Case II), as it is the case for the cell cycle model.

For the *controller-follower* analysis we recall the criteria (1) used in Section 4.2.2.

5.3.1 Controller-follower analysis under strong coupling

The repressilator parameters used for the numerical simulations can be found in Table 5.1, while those for the improved Smolen are given in Table 2.2.

Case I. The value of the degradation rates is chosen so that the parameter set of each system is well within the region for sustained oscillations (see Table 5.1 and Fig. 5.4).

We investigate the coupled period response to bidirectional coupling for the parameters range δ_1 and δ_2, using strong coupling constants $v_1 = 10$ and $v_2 = 1$. To establish the range of the coupling parameters δ_1, $\delta_2 > 0$ we consider the maximal concentration rates of the Smolen system activator A and the repressilator activator A_1, $max\{A\}$ and $max\{A_1\}$ respectively. The region in which the coupled system admits sustained oscillations is defined approximately by the following intervals : $\delta_1 \in [12\%, 128.6\%]max\{A\}$, $\delta_2 \in [5.34\%, 64.1\%]max\{A_1\}$. In these intervals, for all parameter sets tested, the two systems lock in a 1:1 period ratio. Moreover, both systems have the capacity to play the role of controller in certain regions of δ_1, δ_2, as shown in Fig. 5.6.

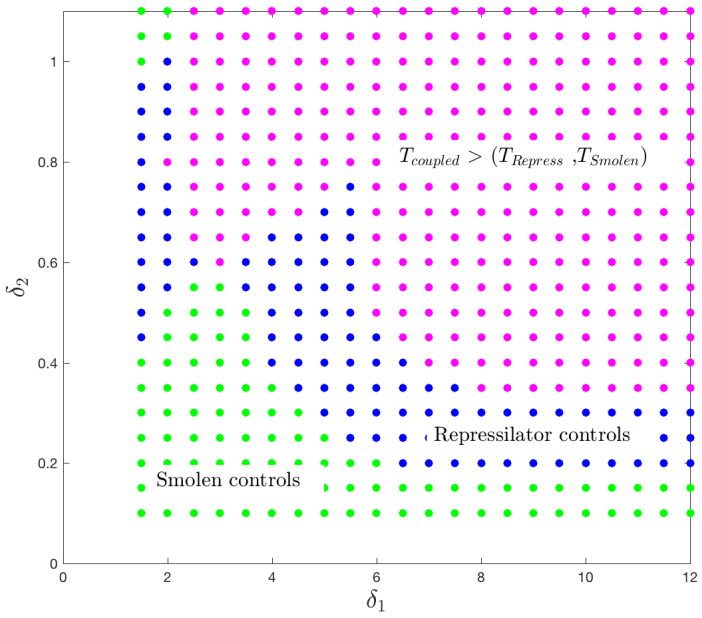

FIGURE 5.6: Coupling parameter regions for controller-follower results, $v_1 = 10$, $v_2 = 1$.

An interesting observation here is that, for mutually strong coupling effects (i.e., both δ_1 and δ_2 large), corresponding to lower degradation rates for each system, the joint period of the coupled system increases (upper right region in Fig. 5.6), i.e. the coupled period appears to be larger than the two individual periods. In this rose-colored region, the controller-follower analysis is not conclusive, and a new type of coupled dynamical behavior emerges, to be further explored below in Section 5.3.2.

Case II. Now, for the repressilator system, the degradation rate γ_1 is chosen so as the system dynamics is very close to the boundary between the oscillatory and stability regions (see Fig. 4.4). In this configuration, it may be expected that the coupling link (through the term $\gamma_1 C_1(t)$) will "force" the repressilator towards the stability region, an analogous situation to that obtained in Chapter 4, for the Smolen - cell cycle coupling.

Regarding the controller-follower analysis, for the coupling parameter range δ_1, δ_2 as depicted in Fig. 5.7, we observe that the Smolen system plays the role of controller for a wider region than in Case I.

This capacity of the Smolen system to be the controller in a wider region can be interpreted as the result of the choice of low γ_1: by pushing the repressilator out of its oscillatory region, it becomes easier for the Smolen system to set its own period to the oscillations.

This response can be compared to the results of Section 4.3.3, where the set of parameters of the cell cycle was also very close to the boundary between oscillatory behavior and stability, thus allowing the Smolen system to be the controller in a wide region of coupling parameters.

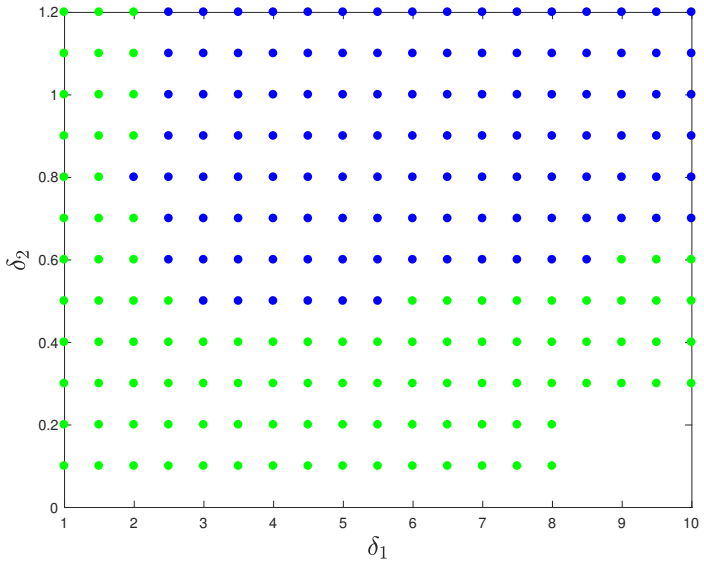

FIGURE 5.7: Coupling parameter regions: Smolen system controls in the green region and repressilator in the blue, $\nu_1 = 10$, $\nu_2 = 1$.

The controller-follower analysis illustrates the crucial role that plays each system individual dynamics in the response to the coupling. More specifically, our results indicate that when one of the two systems is closer to the stability boundary than the other, then it allows the latter to take over and be the controller of the coupled joint period.

Furthermore, comparing the results of Cases I and II, another intriguing observation is that the larger joint period occurs when both systems as individuals admit sustained oscillations, to be explored in the next section.

5.3.2 Strong coupling of two robust oscillators

From our controller-follower analysis of Case I, Fig. 5.6, we extract the qualitative information that for a wide coupling parameter range the coupled system obtains a joint period larger than both the individual periods. Indicatively, in Fig. 5.8 we observe the two coupled systems locked in a larger period value than those of each

individual system. This observation suggests the idea that a new system is generated from the coupling of two systems with robust oscillatory behaviour.

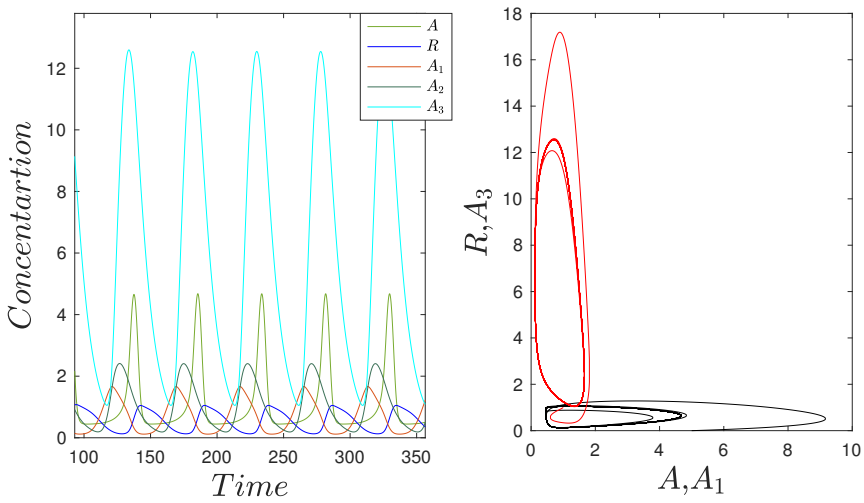

FIGURE 5.8: Left: Activity of the coupled system towards time. Right: the phase portrait of the coupled system. Initial repressilator period $T_r = 40.70$ min ($\gamma_1 = 0.08$, Case I), initial Smolen period, $T_{Smolen} = 30$ min. Coupling parameters $\delta_1 = 10$, $\delta_2 = 0.8$, $v_1 = 10$, $v_2 = 1$. Coupled joint period: 48 min.

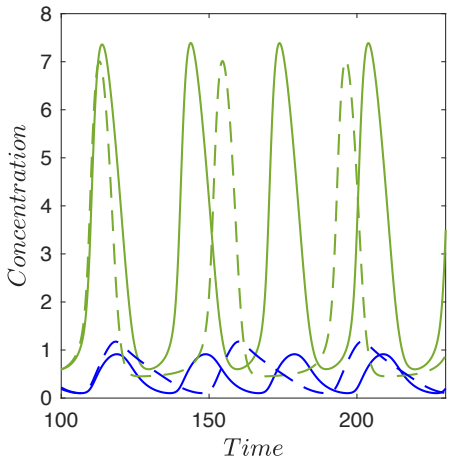

FIGURE 5.9: Activity of the coupled Smolen system before and after coupling (dashed), as a comparison of the amplitude of the limit cycle. Original periods: $T_{Smolen} = 30$ min, $T_{repress} = 47.7$ min. Coupling parameters $\delta_1 = 10$, $\delta_2 = 0.9$, $v_1 = 10$, $v_2 = 1.5$. Coupled period: 41.7 min.

We now investigate the sensitivity of the coupled system period (for the 1:1 locked period case) to variations of the regulated degradation parameters. Variations of the degradation rates result in change -increase or decrease- of the individual

period for each system. However, as we observe in Fig. 5.3, the Smolen oscillator period appears to be relatively robust to variations of the degradation parameter γ_R. Whereas this is not the case for variations of the degradation rate γ_1 for the repressilator that appears to admit a wider period range.

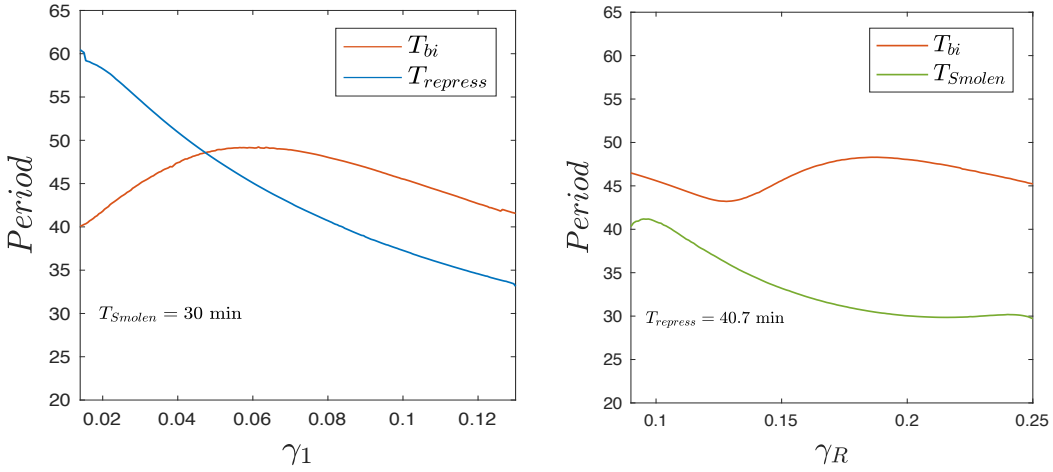

FIGURE 5.10: Coupled joint period and the individual period of each system as a function of γ_1 (degradation rate of A_1, right) and γ_R (degradation rate of R,left). Coupling parameters used: $\nu_1 = 10$, $\nu_2 = 1$, $\delta_1 = 10$, $\delta_2 = 0.8$. $T_{repress}$ and T_{Smolen} refer to the individual periods that remain fixed in each experiment.

The coupled systems lock in a 1:1 period ratio, and their common period is robust with respect to variations of the two regulated degradation parameters, γ_1 and γ_R. More specifically, the coupled period T_{bi} varies from 40 min to 49.2 min for the range of γ_1 degradation rate.

Similarly, T_{bi} takes values from 43 min to 48.3 min in the interval for oscillations of γ_R. This result indicates that the coupled system of two robust oscillators (Case I) for large coupling parameters, evolves as a new system with larger period, relatively robust to variations of individual systems parameters. This larger period is due in part to the strong coupling that implies lower degradation rates (higher δ_i imply $C_i(t)$ lower than 1, which multiply γ_1 and γ_R).

Comparison of the time solutions in Figs. 5.2 and 5.8(right) shows that, in the coupled system, the Smolen variables A, R becomes closer to a relaxation oscillator with variable A exhibiting a wide low platform followed by a very narrow peak. Note also that the variable R has a very slow degradation (due to the term $\gamma_R C_2(t)$ with low $C_2(t)$), reflected in a longer descent after the maximal peak. The fact that R takes longer to decrease is responsible for the wider low platform of A and, consequently, for a longer period of the variables A, R. The repressilator variables still have a sinusoidal form, but their period locks in a 1:1 ratio to that of A, R

These results point to a new application of the coupling of synthetic circuit, which is to obtain a large period oscillator from two low period oscillators. Motivated by this outcome, we next consider the Smolen oscillator with a larger individual period,

and discuss its effect on the period of the coupled system as a function of the coupling parameter δ_2.

5.3.3 Coupled dynamics in the case of a controller with large period

Following the discussion in the previous section, we now investigate the coupling using an alternative parameter set for the Smolen oscillator, (in **??**, we explain in more detail our choice of parameters), implying in particular a larger period $T_{Smolen} \approx$ 92 min.

To test the effect of this new controller configuration in the period of the coupled system, we vary δ_2 from very small to very large values, corresponding respectively to a small to large decrease in the R degradation rate. As illustrated in Fig. 5.11, the coupled system appears to admit a joint period significantly larger than the periods of the two component systems. As before, two experiments were performed, (Case I and II): first, for initial repressilator period $T_{repress} = 40.7$ min (the red circles), the coupled joint period increases to approximately 144 min for $\delta_2 > 0.65$. Second, for $T_{repress} = 54.5$ min (the blue circles) we notice a joint period that overpasses the 100 min for $\delta_2 > 0.1$ and goes up to 139 min for $\delta_2 = 0.7$.

These results confirm the observations of Section 5.3.1 showing that, as the coupling parameter increases and the degradation term becomes smaller, the joint period of the coupled system may increase by more than 50% relative to the periods of the uncoupled systems. In this case, the slow degradation of the repressor R implies a slow activation of the variable A, which also slows down inhibition of A_1, thereby entraining an increase in the period of the coupled system.

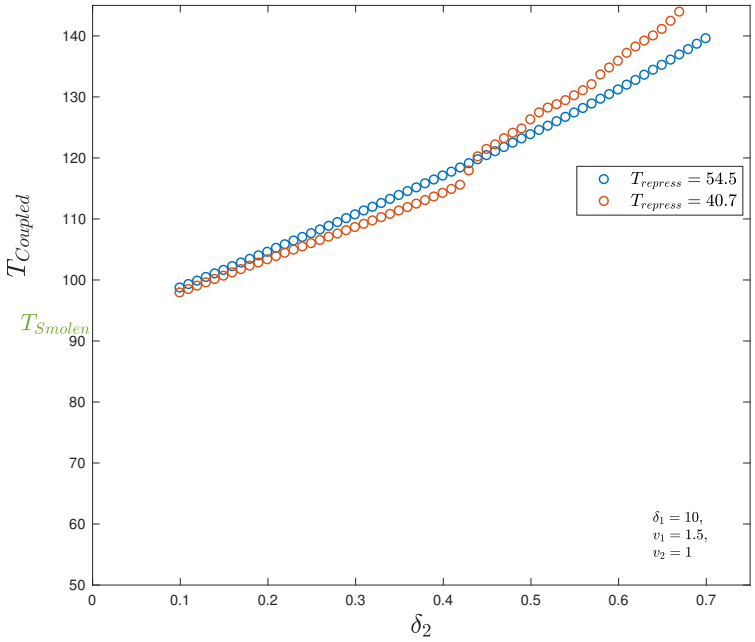

FIGURE 5.11: Coupled period as a function of the coupling parameter δ_2. Other parameters (for strong coupling): $\delta_1 = 10$, $v_1 = 1.5$, $v_2 = 1$. Initial uncoupled periods: $T_{Repress} = 54.5$ (blue), 40.7 (red), $T_{Smolen} =$ 92 min.

Fig. 5.12 illustrates the activity of the coupled system with larger (joint) period. Remarkably, the form of the activity curves of the Smolen system components, reveals a response (to the coupling) similar to that of a time delay: narrow peak and plateau; the amplitude is not greatly affected, Fig. 5.9 and Fig. 5.13.

However, here the overall dynamics has already been tuned due to the increase of Smolen individual period ($T_{Smolen} = 92$ min). In the first comparison (Fig.5.9), where the Smolen system is still fast, the effect of "slowing down" the rhytmicity of the activator is more apparent.

These observations might indicate that the coupling through the repressilator (a symmetric oscillator) introduces to the Smolen system, (which is characterized by a much higher concentration of the activator), a sort of time delay.

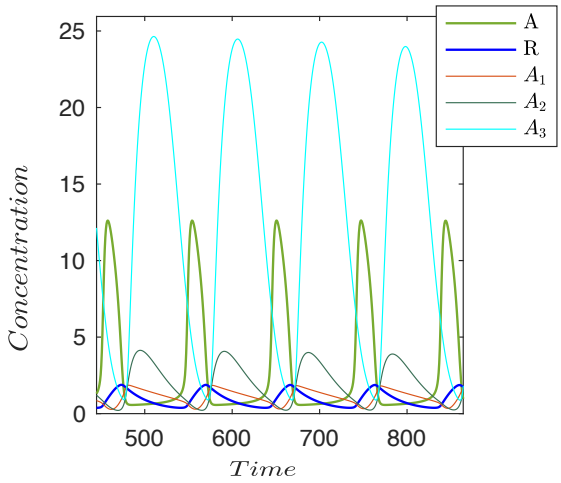

FIGURE 5.12: Time solution of the coupled system with $T_{coupled} = 109.3\ min$. Individual periods: $T_{Repress} = 54.5$, $T_{Smolen} = 92$ min, coupling parameters: $v_1 = 5$, $v_2 = 1$, $\delta_1 = 0.3$, $\delta_2 = 15$

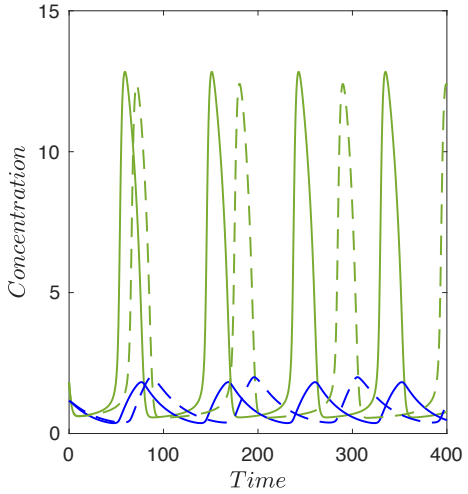

FIGURE 5.13: Time solution of the uncoupled (solid line) and coupled (dashed) Smolen system in an amplitude comparison. Periods: $T_{Smolen} = 92$ min and $T_{coupled} = 109.3\ min$. Coupling parameters: $v_1 = 5$, $v_2 = 1$, $\delta_1 = 0.3$, $\delta_2 = 15$

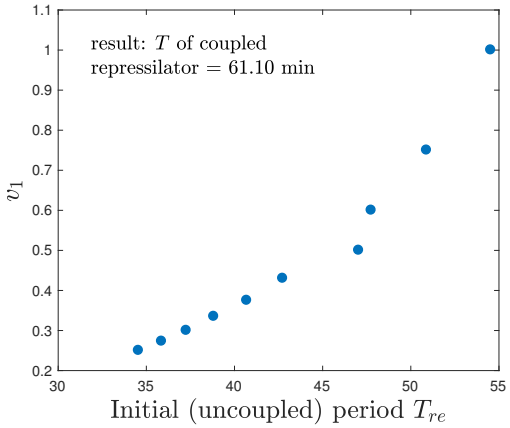

FIGURE 5.14: The range of the repressilator period and the corresponding coupling parameter value v_1 for period 61.10 min. The Smolen system period is fixed at 30 min. Other parameters: $\delta_1 = 1$, $\delta_2 = 0.1$, $v_2 = 1$.

5.3.4 Weak coupling dynamics

Finally, we briefly analyze the case of weak coupling parameters, setting $v_1 = 1$ (as opposed to $v_1 = 10$ in Case I and II) but keeping $v_2 = 1$. The use of a much smaller coupling constant, in particular $v_1 = 1$, results in a coupled system composed of two oscillators with different frequencies. Although the coupling is bidirectional, the fact that v_1 is small implies that the Smolen system is only weakly affected by the repressilator, and thus the Smolen system period in the coupled system is hardly changed relative to its individual period. In contrast, the repressilator is under strong regulation of the Smolen system and its period can be tuned by the coupling constant v_1.

Fig. 5.14 essentially reflects the fact that $\gamma_1 v_1$ is a single parameter in the coupled system equations. While γ_1 changes the period of the individual repressilator, v_1 can be used to maintain the same period for the coupled system.

TABLE 5.2: Comparison of dynamical properties of oscillators and different coupled pairs.

Model	Dynamics	Coupling Schemes with Smolen oscillator
Smolen Oscillator	much higher concentration of the activator	*Diffusion coupling.* Generation of new system dynamics: steady states, unstable limit cycles.
Cell Cycle Reduced Model	relaxation oscillator	*Coupling through synthesis rates.* Controller: the more robust oscillator of the two systems, i.e. Smolen oscillator. *Coupling through degradation rates.* 1. Controller-follower for both systems, 2. Smolen oscillator (more robust) controls for a wider coupling parameter range.
Repressilator	symmetric oscillations	*Coupling through degradation rates.* Case I, repressilator as robust oscillator: 1. controller-follower for both systems, 2. the coupled system admits a new period for a wide coupling parameter range. Case II, repressilator close to stability: 1.controller-follower for both systems, 2. Smolen oscillator, that is more robust compared to repressilator in this case, controls for a wider coupling parameter range.

5.4 Conclusion

Table 5.2 presents the oscillators studied throughout this thesis, characterized by their individual dynamics, as well as a synopsis of the coupling results for the different pairs of oscillators tested. Namely, in Chapter 3 we investigate the coupling of N piecewise Smolen oscillators by diffusion, and the main result is the generation of new dynamics for the network. In Chapters 4 and 5, we study the coupling of pairs of synthetic circuits, the Smolen oscillator with a reduced cell cycle model (Chapter 4) and the repressilator (Chapter 5). In the referred table, we include a synopsis of the results and some important observations: the coupling schemes studied (coupling through synthesis and degradation), the capacity of the systems to control the coupled period as a relation to the individual dynamics, and the new periodic behavior that is generated by the coupling (new joint period).

In this Chapter, we investigate the effects of the same coupling scheme on the dynamical behavior of two different pairs of synthetic oscillators. This schemes exploits the potential of the degradation rates to tune the period of an oscillator. Applying bidirectional coupling for different parameter sets and strengths of the coupling

constants, we present mainly two new intriguing observations along with a result that agrees with the study in Chapter 4.

Strong bidirectional coupling results in a coupled system where both systems are locked in a 1:1 period ratio. Defining as the controller the system that succeeds in forcing its own individual period to the coupled system, we conclude that the Smolen system is more likely to act as a controller when the repressilator is close to the stability region. This observation closely agrees with the results of the cell cycle and Smolen oscillator coupling scheme in our previous study.

However, when both systems admit robust oscillations (that is, the parameter sets are well away from the boundary with the stability region), it is surprising to see that the coupled system period obtains a value (possibly much) larger than both the individual periods, and for a wide range of coupling parameter.

This can be an interesting direction for the development and implementation of coupling strategies for synthetic oscillators or even the coupling between a synthetic and a "natural" oscillator. The possibility of regulating the period of a given oscillator over a large range of values is very appealing for chronotherapy approaches (Lévi, 2001,Gery and Koeffler, 2010, Bernard et al., 2010). For disease treatment it is important for the biologist and the biomedical engineer to have several possibilities for regulating the system response. Here, the regulation or control is performed by the means of another synthetic oscillator.

Another interesting observation concerns the weak coupling configuration. In this case, the coupled oscillators do not lock into a 1:1 ratio but have different frequencies: the period of the repressilator is about twice the period of the Smolen oscillator. The latter is only weakly affected by the coupling and continues to oscillate with approximately its individual period.

The numerical results presented in this Chapter suggest new ways to tune or control the period of an oscillator by coupling it with a second oscillator with suitable dynamical properties. These ideas can be useful in the context of synthetic biology and chronotherapy strategies.

Chapter 6

Discussion and Perspectives

6.1 General discussion and conclusion

In this thesis we studied coupling schemes of biological oscillators representing the circadian clock and the cell cycle in the context of synthetic biology. We developed strategies to improve the synthetic circuit design and methods to couple two oscillators for joint coupled period provided by one of the systems-contributors. We also studied analytically the outcome of different network topologies in the dynamics of N two-gene piecewise oscillators. Finally, we simulated coupling scenaria for pairs of three synthetic models, to investigate the dynamics and period response of the systems as individuals and of the coupled circuit.

Improvement of synthetic circuit design: increase of the potential for oscillations

The first step was the study of a two-gene synthetic oscillator (Smolen oscillator), for which we propose a system modification that serves as enhancement of its oscillatory behavior. We propose the elimination of the negative loop that acts on the repressor. The model becomes a two-variable negative feedback loop, with a positive auto-regulatory loop on the activator. This configuration appears often in biological systems, as reviewed in Tsai et al., 2008, where it is suggested that a positive loop in a negative feedback loop can induce the robustness of oscillations, and more importantly the tunability of the period without affecting the overall amplitude. This implies that the dynamics of the proposed system, that is negative feedback loop with one positive auto-regulation, is likely to fulfill conditions for robust oscillatory behavior and controllable period. Indeed, period tunability without affecting the amplitude manifests itself in the coupling of the proposed two-gene oscillator -variant of Smolen model- with the repressilator. Furthermore, a topologically equivalent model -considerably more detailed though- was also introduced by Tigges et al., 2009 to model the mammalian circadian clock.

Bifurcation analysis for the variant model, shows that oscillations emerge through a Hopf bifurcation. The latter was also observed by Smolen, Baxter, and Byrne, 1999 and so we see the conservation of system qualitative dynamical characteristics regardless the removal of the negative self-loop. In fact, with this alternative configuration the periodic solution is effectively preserved and more importantly, the corresponding parameter space significantly increases. Our objective is to propose an improved version of a model that has already shown oscillatory capacity for in

vivo implementation (Stricker et al., 2008), so as to induce its potential for robust performance.

In a second step, we provide mathematical analysis of the proposed variant system introducing a piecewise affine approximation of the model. In this framework, we analytically prove the existence of a unique periodic solution under appropriate parameter conditions, from which we identify those that may further promote the capability of sustained oscillations for the continuous system.

Ultimately, from the analysis of the Smolen oscillator utilizing both analytical and computational tools, we exploit qualitative information for the model parameters for periodic solution and we make variations to the parameters accordingly.

Coupling of N identical piecewise systems: maintenance of oscillations and generation of new steady states

The analysis of the two-gene oscillator in the context of piecewise affine formalism is followed by the study of a network of N identical two-gene oscillators, inspired by the network of biological oscillators in circadian rhythms. The main characteristics of the circadian oscillators that is crucial to preserve for the normal functionality of the biological clock and the mechanisms it regulates, is the sustained rhythmicity and synchronization.

We investigate the effect of three network topologies, "all-to-all", "one-to-all" and "random", on the coupled system dynamics under diffusive coupling. Our analysis of the two more "strictly" defined schemes of interconnection (all-to-all and one-to-all), show that new stable steady states occur through the coupling. The type of systems that we study (PWA) combined with a diffusive linear connection, allow to explicitly compute the number of the new stable steady states for a given number of systems in the network, in both interconnections (all-to-all and one-to-all).

Furthermore, we also provide the exact lower bound for the coupling parameter for the two topologies, for which the appearance of the steady states is prevented. For the one-to-all topology, our computations point that the lower bound is independent from the number of the coupled oscillators and reasonable in terms of biology. On the contrary, in the case of a global connection (all-to-all) this lower bound becomes small as the number of the oscillators increases. An interpretation of the latter is that with all to all connection of the oscillators, it is possible to lose oscillatory behavior for the coupled system, due to the generation of a large number of steady states. This observation implies that a more locally oriented connection (one-to-all) is an advantage for robust oscillations and synchronization in a network of oscillators.

In the case of random links between the oscillators, numerical simulations show results that might be intuitively expected: the number of the new steady states lies between the two others. Indeed, the all-to-all and one-to-all topologies set, respectively, upper and lower limits on the number of stable steady states, on the order of $10^{\frac{4}{5}N-2}$ for the former.

The new steady states form different patterns of protein expression throughout the network. Convergence of the network solutions to one of these steady states implies that distinct groups of oscillators converge to distinct protein expression levels (see Fig. 3.6) In our numerical results, we observe clusters of oscillators that synchronize

to the same values. Some results concerning the synchronization of clusters of oscillators in a network, for coupled piecewise systems, are also found in the analysis of Nicks, Chambon, and Coombes, 2018. Also, the phenomenon of synchronization in "clusters" is analyzed in other theoretical studies of coupled systems, as in the work of Sorrentino et al., 2016 (see also the review of Golubitsky and Stewart, 2016).

The topologies and coupling schemes tested serve as investigations of a coupled network of oscillators that may be biologically interpreted as individual neural cells in the SCN or a central pacemaker linked to peripheral oscillators. However, the study of the dynamics of a coupled network comprising N oscillators belongs to a more general context.

On the whole, our results can be later exploited as directions and predictions for synthetic biology applications.

Coupling of two topologically equivalent circuits for synthetic biology: period response to different coupling schemes

The circadian rhythms, the organization of which motivated us for the study of N identical oscillators, is also related to an other biological oscillator, the cell cycle. In this thesis, we investigated this relationship in model-based contexts for synthetic biology.

In our study, the Smolen oscillator represents the circadian clock. For the cell cycle we use a two-gene model, developed for synthetic biology applications and calibrated from experimental data. Although we studied the coupling of two topologically equivalent circuits -negative feedback loop of two genes with additional positive loop on the activator-, our results indicate that only the Smolen oscillator (as circadian clock) is capable of entrainement of the cell cycle model, in both coupling schemes tested. This result may be related to systems' individual dynamics: the Smolen oscillator admits sustained and robust oscillations in terms of parameters, whereas the cell cycle system is very close to the stability boundary. Other studies that develop sufficient conditions for effective synchronization and entrainement as a result of forced to damped oscillations (in a network of N identical oscillators) can be found in the computational studies of Gonze et al., 2005, Bernard et al., 2007.

We introduced a "controller-follower" classification which, roughly, indicates that the controller system is the one whose natural (uncoupled) period is closer to the period of the coupled system. Our exploration towards the control of the coupled system period indicates that a bidirectional connection through the degradation rates of the two systems yields a wider range for the coupled period response, than the coupling through synthesis rates. In the former case, both systems play the role of the controller for appropriate coupling parameter conditions. As a first approach to comprehend this behavior, bifurcation analysis of the two systems show that the more robust oscillator forces the other to exit the region of susteained oscillations, thus "enslaving" it. This observation may be useful not only as a prediction for the way of implementing a coupled synthetic circuit, but also as a control tool.

To conclude, our simulations show that both systems can play th role of controller -at least for the coupling scheme where the systems are connected through degradation rates. This general result agrees with experimental observations for mutual influence between the two mechanisms, circadian clock and cell cycle.

Combining two synthetic oscillators: an improved (larger) joint period

Recent designs in bio-engineering include coupling of synthetic elements or circuits so as the synthetic elements acquire combined or more complex dynamics, in order to generate novel genetic modules (see also the discussion in Introduction §1.6). In this context, we studied the coupling of two synthetic circuits with oscillatory capacity, the Smolen oscillator and the repressilator.

We performed simulations testing the coupling through degradation rates for a robust and non-robust repressilator in terms of choice of parameters. Our results complement the observations of the previous coupling scenario (circadian clock/cell cycle), pointing towards the fact that the more robust oscillator controls the coupled period. More importantly, for a repressilator close to stability region, the coupled system obtains a new -larger from both individuals- period. Additionally, for weak bidirectional coupling, the Smolen system appears to regulate the repressilator period to double of its individual period; this observation highlights the capacity of the Smolen system to tune the period of the repressilator.

The dynamics of the coupled system along time, for the cases where the coupled period increases, reveals that the Smolen system, behaves closer to a relaxation oscillator, with the activator showing a very narrow peak with fast decrease towards a low expression level. This observation can be interpreted as the effect of time delay. Our results also suggest that the period of the proposed system can be moderated without significantly affecting the maximal amplitude. This delay effect may be introduced through the coupling with the repressilator system. For comparison, in the study of Stricker et al., 2008, time delay was established to the implemented circuit of Smolen oscillator to effectively regulate the system period without compromising the amplitude of oscillations. On top of that, the robustness of oscillations was also enhanced by the time delay. These are directions for exploration in future work.

To conclude, the observations reflected by the numerical results of the coupling of the two synthetic circuits provide suggestions for further study and analysis on how to combine two oscillators and use their respective characteristics for period control through the coupling with an other system.

6.2 Perspectives

Two-gene synthetic oscillators implementation

From a synthetic biology perspective, we studied a circuit and suggested directions to increase the prospects that its implementation shows sustained oscillatory behavior. In fact, the first steps towards implementing this circuit in living cellular environment are taking place in the laboratory of Frank Delaunay. Interestingly, preliminary experiments appear to support oscillations (unpublished data). Furthermore, we fitted the proposed model to experimental observations on the concentration levels of the activator, as a part of preliminary work (see Appendix A). In addition, we also tested different parameter sets in order to obtain different forms of the orbits, such as, narrower versus wider peaks, or difference between maximal amplitudes of both variables. On the whole, our results concerning the improvement of system design with

robust oscillatory behavior as a desired functionality, constitute testable predictions. As new experimental data becomes available, more complete parameter estimations of the model can be performed, to provide more accurate information and predictions for future work in synthetic biology.

Dynamical behavior and synchronization in a network of N oscillators

Exploring the coupling of more than two oscillators in a network with certain topology, reveals observations that can be useful for further analysis alongside with synthetic biology applications. To be more specific, in the study of the coupled network of N two-gene (piecewise) oscillators, our simulations show that initiating the systems with a certain difference between the concentrations of the components, namely higher levels for the repressors and lower for the activators, the coupled network yields oscillations despite the existence of multiple (locally stable) steady states. From a more theoretical perspective, a control strategy so as the system is initiated within the bassin of attraction for the periodic solution would be of interest for analytical study. From synthetic biology perspective, a possible way to control/lead the systems towards the periodic orbit, would be by promotion of the repressor's activity through external cue.

Induction of certain circadian genes can be attained by serum shock (Balsalobre, Damiola, and Schibler, 1998) or other drug treatments, for instance foskolin and dexamethasone. In the work of (Yagita and Okamura, 2000), foskolin has shown to effectively promote the rhythmic activity of *Per1* and other circadian genes. Also, in the study of Balsalobre et al., 2000, there is experimental evidence that dexamethasone acts on *Per1* of peripheral clocks. However, this drug does not have the same effect on the SCN neurons (Balsalobre et al., 2000). The clock gene *Per1* combined with *Cry* proteins, inhibits the *Bmal1* transcriptional activator of the circadian clock, therefore its role in the generation of circadian oscillations could be represented by the repressor R in the Smolen model. Thus, focusing on the abstract representation of the central clock synchronizer (SCN) and the peripheral clocks that we studied in this thesis, a suggestion with the potential to be tested for in vivo implementation, would be a drug treatment on the repressor. In this way, the repressor could initially reach higher concentration levels, and therefore increase the chances for synchronized oscillations of the coupled system.

From a theoretical perspective, our analysis can be further continued to search for and prove appropriate conditions for synchronization. Numerical simulations for large number of systems-contributors, reveal synchronization in phase and in period for the coupled oscillators under diffusive coupling, for three type of connections.

Dynamical behavior and synchronization for coupled continuous systems

This thesis was mainly concerned with the analysis of oscillators in the piecewise affine framework. An immediate question is whether simmilar results also apply for the continuous case. As an extension of this thesis work it will be interesting to explore diffusive coupling for the continuous two-gene system 2.2. Preliminary

-numerical- results of this coupling scheme are briefly presented in Appendix B, highlighting new dynamics, namely co-existence of limit cycles and synchronization. These results are similar to other studies of synchronization in networks of biological oscillators, that we already mentioned (Sorrentino et al., 2016, Nicks, Chambon, and Coombes, 2018). Furthermore, experimental observations as well, reveal collective "cooperative" behavior in neural cells. It will be interesting to further analyze the coupled system, proving sufficient conditions for synchronization and characterization of its dynamics.

Period control for the coupled system

Another topic that could be further developed is the comparison between the dynamical behavior of different pairs of coupled oscillators, as started in Chapter 5. It would be interesting to do a more systematic characterization of the links between the natural properties of individual oscillators and the corresponding induced properties in a coupled pair. For instance, to better understand and extend the characterization of properties such as the “controller-follower” definition. In the light of our numerical experiments, these properties may provide new means for controlling and tuning the period of synthetic oscillators, as well as give intuition on the coupling properties of different physical oscillators.

Preliminary studies: comparison with experimental observations

Diffusive coupling of two-gene oscillators: the continuous case

This preliminary study is a complement to Chapter 3, where we studied analytically the diffusive coupling of N piecewise two-gene oscillators. Here, we explore numerically the same way of coupling for two continuous systems.

B.1 Bidirectional coupling of two oscillators

Considering two identical systems (2.2) interconnected by diffusive coupling through the repressor R, leads to the coupled network illustrated in Fig. B.1.

The bifurcation diagram for the coupling parameter κ_B is depicted in Fig. B.2. As we can observe, for $\kappa_B > 0.1$ the system undergoes a pitchfork bifurcation: in addition to the initial stable periodic solution of system (2.2), two new unstable steady states are generated (in blue). Our results indicate the generation of different new steady states due to the diffusive coupling. First, for low κ_B, we observe synchronization of the coupled system in a stable limit cycle, as a continuation of the original periodic orbit. Second, there exists a point $\kappa_B \approx 0.08$ where new unstable states appear, implying two new periodic orbits; third, for $\kappa_B > 0.55$, the two additional steady states become stable and coexist with a stable limit cycle. An example of the coupled system trajectories for $\kappa_B = 0.4$ is shown in Fig. B.3, and for $\kappa_B = 1$ in Fig. B.4. These are interesting observations in terms of the system dynamics analysis, and useful for the design of synthetic systems.

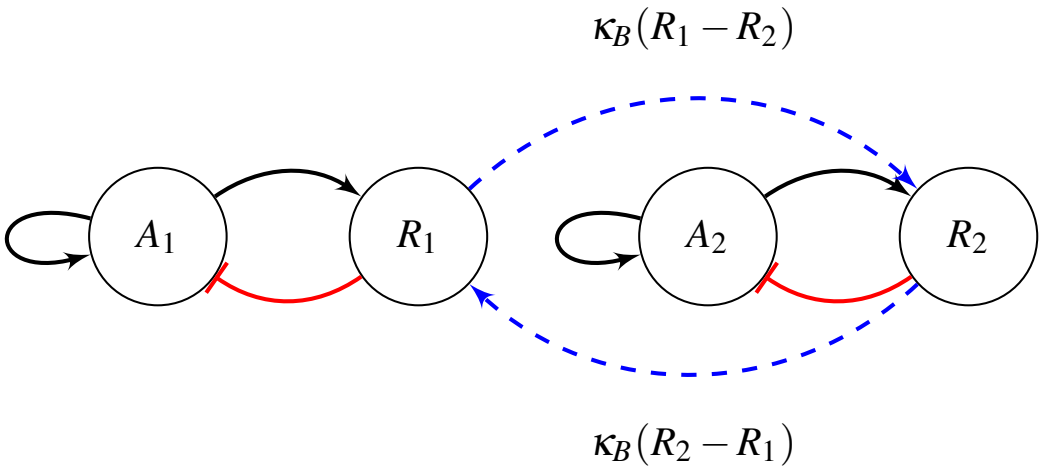

FIGURE B.1: Coupled oscillators of the form (2.2).

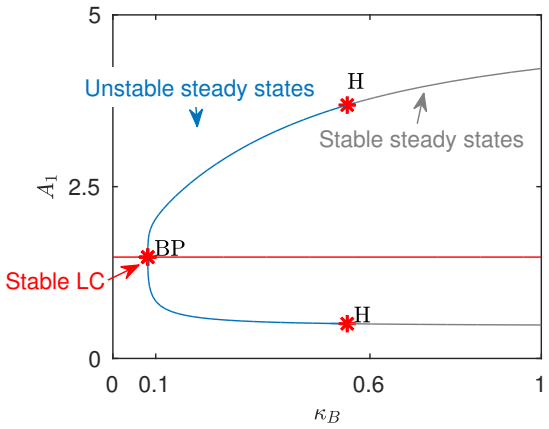

FIGURE B.2: Bifurcation diagram for the coupling parameter κ_B. LC: Limit cycle, BP: Branch point, H: Hopf bifurcation.

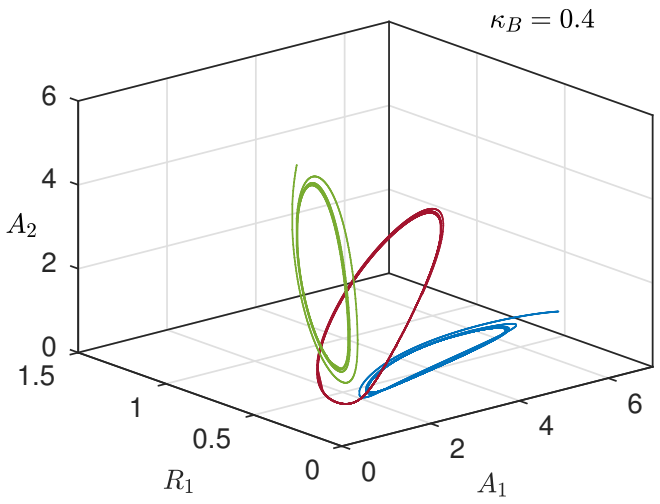

FIGURE B.3: Projection of the phase portrait of the coupled system for $\kappa_B = 0.4$: different trajectories converge to two new stable limit cycles and the original one, depending on the initial conditions.

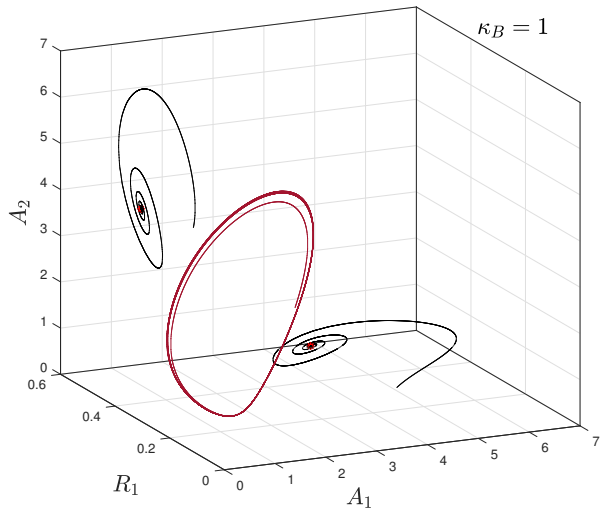

FIGURE B.4: Phase portrait of the coupled system for $\kappa_B = 1$: trajectories converge to two stable steady states and one stable limit cycle depending on the initial conditions.

B.2 Network of N coupled two-gene oscillators

We now consider a network associated to that of Chapter 3, but for the continuous proposed model, as we present above for $N = 2$. We perform numerical tests to explore the dynamics of the coupled system with respect to the network topology and the strength of the interconnection. To obtain intuition, we performed numerical simulations to explore the effect in the coupled system response of two factors separately: i)for a range of the coupling parameter and ii)for a range of number of systems-contributors.

In general, our results suggest that for sufficiently large coupling constant (in terms of biology) and relatively narrow connections, the oscillators in the network synchronize in the same periodic orbit. Likewise for global connection (all to all) under weak coupling ($\kappa = 0.01$), the network yield synchronized oscillations, indicatively see Fig. B.6. In star topology, as the number of oscillators becomes larger, the central element (R_1 interconnected with all others) seems to desynchronize from the other oscillators for relatively strong coupling ($\kappa = 0.15$) Fig. B.5, from our computations they do synchronize in period though.

The above observations also related to the initial conditions. Depending on the region in which the coupled system is initiated, it is possible to have diverse behaviors: synchronized oscillations under suitable conditions for the coupling constant and the network topology, or loss of oscillations after a period of time, or immediate stabilization, are some of the behaviors observed in the numerical tests.

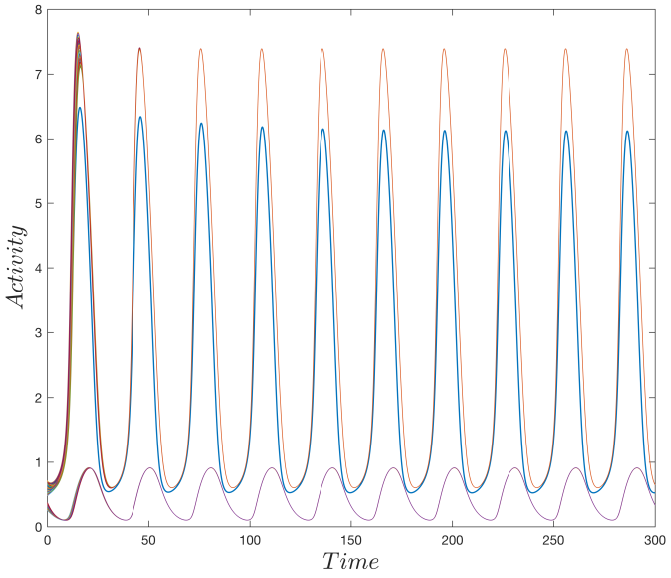

FIGURE B.5: Network of $N = 100$ oscillators with star connection and coupling constant $\kappa = 0.15$, towards the periodic solution.

In general, the numerical results suggest that, for stronger connection either in terms of coupling constant or network topology, the oscillations can be rapidly eliminated. In other words, for strong exchanges between the systems or for a big network of robust oscillators, it is likely for the oscillations to be compromised.

However, we have to take into account possible numerical errors introduced by the coupling, thus one cannot conclude for the dynamical properties of such a network relying solely on results provided by numerical simulations.

In a more general context, the results that we quote here, may constitute interesting observations pointing out directions or give intuition for analysis.

Note: Numerical simulations in this section were performed using the parameter set of Table 2.2.

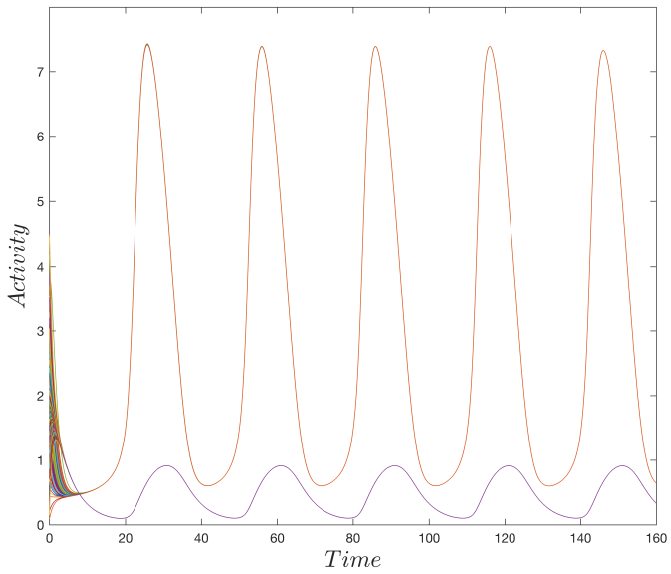

FIGURE B.6: Network of $N = 100$ oscillators with all to all connection and coupling constant $\kappa = 0.01$, towards the periodic solution (zoom to a short time frame).

Bibliography

Almeida, S., M. Chaves, and F. Delaunay (2020). "Control of synchronization ratios in clock/cell cycle coupling by growth factors and glucocorticoids". In: *Royal Society Open Science* 7.2, p. 192054. DOI: 10.1098/rsos.192054. URL: https://doi.org/10.1098/rsos.192054.

Almeida, Sofia et al. (July 2017). "A comprehensive reduced model of the mammalian cell cycle". In: *IFAC-PapersOnLine* 50, pp. 12617–12622. DOI: 10.1016/j.ifacol.2017.08.2204.

Ashwin, P. (1992). "Identical Oscillator Networks with Symmetry". In: *Coupled Oscillating Neurons. Perspectives in Neural Computing*. Ed. by Mannion C.L.T. Taylor J.G. Springer, London.

Atkinson, Mariette R. et al. (2003). "Development of Genetic Circuitry Exhibiting Toggle Switch or Oscillatory Behavior in Escherichia coli". In: *Cell* 113.5, pp. 597–607. DOI: 10.1016/S0092-8674(03)00346-5. URL: https://doi.org/10.1016/S0092-8674(03)00346-5.

Aton, Sara J et al. (Apr. 2005). "Vasoactive intestinal polypeptide mediates circadian rhythmicity and synchrony in mammalian clock neurons". In: *Nature neuroscience* 8.4, pp. 476–483. DOI: 10.1038/nn1419. URL: https://pubmed.ncbi.nlm.nih.gov/15750589.

Balsalobre, A et al. (2000). "Resetting of circadian time in peripheral tissues by glucocorticoid signaling." eng. In: *Science* 289.5488, pp. 2344–2347. ISSN: 0036-8075 (Print); 0036-8075 (Linking). DOI: 10.1126/science.289.5488.2344.

Balsalobre, Aurélio, Francesca Damiola, and Ueli Schibler (1998). "A Serum Shock Induces Circadian Gene Expression in Mammalian Tissue Culture Cells". In: *Cell* 93.6, pp. 929 –937. ISSN: 0092-8674. DOI: https://doi.org/10.1016/S0092-8674(00)81199-X. URL: http://www.sciencedirect.com/science/article/pii/S009286740081199X.

Bernard, Samuel et al. (Apr. 2007). "Synchronization-Induced Rhythmicity of Circadian Oscillators in the Suprachiasmatic Nucleus". In: *PLOS Computational Biology* 3.4, e68–. URL: https://doi.org/10.1371/journal.pcbi.0030068.

Bernard, Samuel et al. (Mar. 2010). "Tumor Growth Rate Determines the Timing of Optimal Chronomodulated Treatment Schedules". In: *PLOS Computational Biology* 6.3, e1000712–. URL: https://doi.org/10.1371/journal.pcbi.1000712.

Bieler, Jonathan et al. (2014). "Robust synchronization of coupled circadian and cell cycle oscillators in single mammalian cells." eng. In: *Mol Syst Biol* 10.7, p. 739. ISSN: 1744-4292 (Electronic); 1744-4292 (Print); 1744-4292 (Linking). DOI: 10.15252/msb.20145218.

Brancaccio, Marco et al. (Nov. 2014). "Network-Mediated Encoding of Circadian Time: The Suprachiasmatic Nucleus (SCN) from Genes to Neurons to Circuits, and Back". In: *The Journal of Neuroscience* 34.46, p. 15192. DOI: 10.1523/JNEUROSCI.3233-14.2014. URL: http://www.jneurosci.org/content/34/46/15192.abstract.

Brophy, Jennifer and Christopher Voigt (Apr. 2014). "Principles of Genetic Circuit Design". In: *Nature methods* 11, pp. 508–520. DOI: 10.1038/nmeth.2926.

Bruce Alberts Alexander Johnson, Julian Lewis Martin Raff Keith Roberts and Peter Walter (2002). *Molecular Biology of the Cell*. Vol. 4th edition. New York: Garland Science. URL: https://www.ncbi.nlm.nih.gov/books/NBK26887/.

Casey, Richard, Hidde de Jong, and Jean-Luc Gouzé (2006). "Piecewise-linear Models of Genetic Regulatory Networks: Equilibria and their Stability". In: *Journal of Mathematical Biology* 52.1, pp. 27–56. ISSN: 1432-1416. DOI: 10.1007/s00285-005-0338-2.

Chen, Bolun, Jan R Engelbrecht, and Renato Mirollo (2017). "Cluster synchronization in networks of identical oscillators with α-function pulse coupling." eng. In: *Phys Rev E* 95.2-1, p. 022207. ISSN: 2470-0053 (Electronic); 2470-0045 (Linking). DOI: 10.1103/PhysRevE.95.022207.

Cheng, Allen A. and Timothy K. Lu (2012). "Synthetic Biology: An Emerging Engineering Discipline". In: *Annual Review of Biomedical Engineering* 14.1, pp. 155–178. DOI: 10.1146/annurev-bioeng-071811-150118. URL: https://doi.org/10.1146/annurev-bioeng-071811-150118.

Conrad, Emery et al. (2008). "Rate constants rather than biochemical mechanism determine behaviour of genetic clocks". In: *Journal of The Royal Society Interface* 5.suppl_1, S9–S15. DOI: 10.1098/rsif.2008.0046.focus. URL: https://doi.org/10.1098/rsif.2008.0046.focus.

Czeisler, C A et al. (1999). "Stability, precision, and near-24-hour period of the human circadian pacemaker." eng. In: *Science* 284.5423, pp. 2177–2181. ISSN: 0036-8075 (Print); 0036-8075 (Linking). DOI: 10.1126/science.284.5423.2177.

Del Vecchio, Domitilla, Aaron J. Dy, and Yili Qian (2016). "Control theory meets synthetic biology". In: *Journal of The Royal Society Interface* 13.120, p. 20160380. DOI: 10.1098/rsif.2016.0380. URL: https://doi.org/10.1098/rsif.2016.0380.

Durand, Dominique M, Eun-Hyoung Park, and Alicia L Jensen (Aug. 2010). "Potassium diffusive coupling in neural networks". In: *Philosophical transactions of the Royal Society of London. Series B, Biological sciences* 365.1551, pp. 2347–2362. DOI: 10.1098/rstb.2010.0050. URL: https://pubmed.ncbi.nlm.nih.gov/20603356.

Edwards, R. and P. Gill (2003). "On synchronization and cross-talk in parallel networks". In: *Dyn. Contin.Discrete Impuls. Syst. Ser. B Appl. Algorithms* 10, pp. 287–300.

El Cheikh, R., S. Bernard, and N. El Khatib (2014). "Modeling circadian clock–cell cycle interaction effects on cell population growth rates". In: *Journal of Theoretical Biology* 363, pp. 318–331. DOI: https://doi.org/10.1016/

j.jtbi.2014.08.008. URL: http://www.sciencedirect.com/science/article/pii/S0022519314004561.

Elowitz, Michael B. and Stanislas Leibler (Jan. 2000). "A synthetic oscillatory network of transcriptional regulators". In: *Nature* 403.6767, pp. 335–338. URL: http://dx.doi.org/10.1038/35002125.

Feillet, Céline et al. (July 2014). "Phase locking and multiple oscillating attractors for the coupled mammalian clock and cell cycle". In: *Proceedings of the National Academy of Sciences of the United States of America* 111.27, pp. 9828–9833. DOI: 10.1073/pnas.1320474111. URL: http://www.ncbi.nlm.nih.gov/pmc/articles/PMC4103330/.

Feillet, Celine et al. (2015). "Coupling between the Circadian Clock and Cell Cycle Oscillators: Implication for Healthy Cells and Malignant Growth". In: *Frontiers in Neurology* 6, p. 96. ISSN: 1664-2295. DOI: 10.3389/fneur.2015.00096. URL: https://www.frontiersin.org/article/10.3389/fneur.2015.00096.

Filippov, A. F. (1960). *Differential equations with discontinuous right-hand side*. Vol. 19. Mathematics and its Applications. Dordrecht, Boston, London: Kluwer Academic Publishers, pp. 99–128.

Firippi, E. and M. Chaves (2020). "Topology-induced dynamics in a network of synthetic oscillators with piecewise affine approximation". In: *Chaos: An Interdisciplinary Journal of Nonlinear Science* 30.11, p. 113128. DOI: 10.1063/5.0020670. URL: https://doi.org/10.1063/5.0020670.

Firippi, Eleni and Madalena Chaves (Jan. 2019). "Period - control in a coupled system of two genetic oscillators for synthetic biology". In: *IFAC-PapersOnLine* 52, pp. 70–75. DOI: 10.1016/j.ifacol.2019.12.238.

Gardner, Timothy, Charles Cantor, and James Collins (Feb. 2000). "Construction of a Genetic Toggle Switch in Escherichia coli". In: *Nature* 403, pp. 339–42. DOI: 10.1038/35002131.

Gaucher, Jonathan, Emilie Montellier, and Paolo Sassone-Corsi (2018). "Molecular Cogs: Interplay between Circadian Clock and Cell Cycle". In: *Trends in Cell Biology* 28.5, pp. 368–379. DOI: https://doi.org/10.1016/j.tcb.2018.01.006. URL: http://www.sciencedirect.com/science/article/pii/S0962892418300151.

Gekakis, N et al. (1998). "Role of the CLOCK protein in the mammalian circadian mechanism." eng. In: *Science* 280.5369, pp. 1564–1569. ISSN: 0036-8075 (Print); 0036-8075 (Linking). DOI: 10.1126/science.280.5369.1564.

Gérard, Claude and Albert Goldbeter (May 2012). "Entrainment of the Mammalian Cell Cycle by the Circadian Clock: Modeling Two Coupled Cellular Rhythms". In: *PLoS Computational Biology* 8.5. Ed. by Edmund J Crampin, e1002516. DOI: 10.1371/journal.pcbi.1002516. URL: http://www.ncbi.nlm.nih.gov/pmc/articles/PMC3364934/.

Gery, Sigal and H Philip Koeffler (Mar. 2010). "Circadian rhythms and cancer". In: *Cell cycle (Georgetown, Tex.)* 9.6, pp. 1097–1103. DOI: 10.4161/cc.9.6.11046. URL: https://pubmed.ncbi.nlm.nih.gov/20237421.

Glass, L and S A Kauffman (1973). "The logical analysis of continuous, non-linear biochemical control networks." eng. In: *J Theor Biol* 39.1, pp. 103–129. ISSN: 0022-5193 (Print); 0022-5193 (Linking).

Glass, Leon (Mar. 2001). "Synchronization and rhythmic processes in physiology". In: *Nature* 410.6825, pp. 277–284. URL: http://dx.doi.org/10.1038/35065745.

Goldbeter, Albert (2008). "Biological rhythms: clocks for all times". In: *Current biology : CB* 18.17, R751–R753. DOI: 10.1016/j.cub.2008.06.044. URL: http://europepmc.org/abstract/MED/18786378.

Golubitsky, Martin and Ian Stewart (2016). "Rigid patterns of synchrony for equilibria and periodic cycles in network dynamics". In: *Chaos: An Interdisciplinary Journal of Nonlinear Science* 26.9, p. 094803. DOI: 10.1063/1.4953664. URL: https://doi.org/10.1063/1.4953664.

Gonze, Didier et al. (July 2005). "Spontaneous synchronization of coupled circadian oscillators". In: *Biophysical journal* 89.1, pp. 120–129. DOI: 10.1529/biophysj.104.058388. URL: https://pubmed.ncbi.nlm.nih.gov/15849258.

Goodwin, Brian C. (1963). *Temporal organization in cells : a dynamic theory of cellular control processes*. ISBN: 0122893506 9780122893506.

Govaerts, Willy, Yuri A. Kuznetsov, and Annick Dhooge (2005). "Numerical Continuation of Bifurcations of Limit Cycles in MATLAB". In: *SIAM J. Scientific Computing* 27, pp. 231–252.

Guantes, Raúl and Juan F Poyatos (Mar. 2006). "Dynamical principles of two-component genetic oscillators". In: *PLoS computational biology* 2.3, e30–e30. DOI: 10.1371/journal.pcbi.0020030. URL: https://pubmed.ncbi.nlm.nih.gov/16604190.

Hafner, Marc, Heinz Koeppl, and Didier Gonze (Mar. 2012). "Effect of Network Architecture on Synchronization and Entrainment Properties of the Circadian Oscillations in the Suprachiasmatic Nucleus". In: *PLOS Computational Biology* 8.3, pp. 1–16. DOI: 10.1371/journal.pcbi.1002419. URL: https://doi.org/10.1371/journal.pcbi.1002419.

Harmer, SL, S Panda, and SA Kay (2001). "Molecular bases of circadian rhythms". In: *Annual review of cell and developmental biology* 17, pp. 215–253. DOI: 10.1146/annurev.cellbio.17.1.215. URL: http://europepmc.org/abstract/MED/11687489.

Hastings, Michael H, Elizabeth S Maywood, and Marco Brancaccio (2018). "Generation of circadian rhythms in the suprachiasmatic nucleus." eng. In: *Nat Rev Neurosci* 19.8, pp. 453–469. ISSN: 1471-0048 (Electronic); 1471-003X (Linking). DOI: 10.1038/s41583-018-0026-z.

Hasty, J. et al. (2002). "Synthetic Gene Network for Entraining and Amplifying Cellular Oscillations". In: *Phys. Rev. Lett.* 88, p. 148101.

He, Fei, Ettore Murabito, and Hans Westerhoff (Apr. 2016). "Synthetic biology and regulatory networks: Where metabolic systems biology meets control engineering". In: *Journal of The Royal Society Interface* 13, p. 20151046. DOI: 10.1098/rsif.2015.1046.

Herzog, Erik D. (2007). "Neurons and networks in daily rhythms". In: *Nature Reviews Neuroscience* 8.10, pp. 790–802. DOI: 10.1038/nrn2215. URL: https://doi.org/10.1038/nrn2215.

Hsiao, V., A. Swaminathan, and R. M. Murray (2018). "Control Theory for Synthetic Biology: Recent Advances in System Characterization, Control Design, and Controller Implementation for Synthetic Biology". In: *IEEE Control Systems Magazine* 38.3, pp. 32–62. DOI: 10.1109/MCS.2018.2810459.

Hunt, Tim and Paolo Sassone-Corsi (2007). "Riding Tandem: Circadian Clocks and the Cell Cycle". In: *Cell* 129.3, pp. 461–464. DOI: https://doi.org/10.1016/j.cell.2007.04.015. URL: http://www.sciencedirect.com/science/article/pii/S0092867407005211.

Jong, Hidde de (2002). "Modeling and Simulation of Genetic Regulatory Systems: A Literature Review". In: *Journal of Computational Biology* 9.1, pp. 67–103. DOI: 10.1089/10665270252833208. URL: https://doi.org/10.1089/10665270252833208.

Khapre, Rohini V., William E. Samsa, and Roman V. Kondratov (Sept. 2010). "Circadian regulation of cell cycle: Molecular connections between aging and the circadian clock". In: *Annals of Medicine* 42.6, pp. 404–415. DOI: 10.3109/07853890.2010.499134. URL: https://doi.org/10.3109/07853890.2010.499134.

Komin, N. et al. (2011). "Synchronization and entrainment of coupled circadian oscillators". In: *Interface Focus* 1.1, pp. 167–176. DOI: 10.1098/rsfs.2010.0327. URL: https://doi.org/10.1098/rsfs.2010.0327.

Kunz, Hanspeter and Peter Achermann (2003). "Simulation of circadian rhythm generation in the suprachiasmatic nucleus with locally coupled self-sustained oscillators". In: *Journal of theoretical biology* 224.1, pp. 63–78. DOI: 10.1016/s0022-5193(03)00141-3. URL: http://europepmc.org/abstract/MED/12900204.

Lévi, F (2001). "Circadian chronotherapy for human cancers." eng. In: *Lancet Oncol* 2.5, pp. 307–315. ISSN: 1470-2045 (Print); 1470-2045 (Linking). DOI: 10.1016/S1470-2045(00)00326-0.

Matsuo, Takuya et al. (2003). "Control Mechanism of the Circadian Clock for Timing of Cell Division in Vivo". In: *Science* 302.5643, pp. 255–259. ISSN: 0036-8075. DOI: 10.1126/science.1086271. eprint: http://science.sciencemag.org/content/302/5643/255.full.pdf. URL: http://science.sciencemag.org/content/302/5643/255.

Matthews, Paul C., Renato E. Mirollo, and Steven H. Strogatz (1991). "Dynamics of a large system of coupled nonlinear oscillators". In: *Physica D: Nonlinear Phenomena* 52.2, pp. 293–331. DOI: https://doi.org/10.1016/0167-2789(91)90129-W. URL: http://www.sciencedirect.com/science/article/pii/016727899190129W.

Mirollo, Renato E. and Steven H. Strogatz (1990). "Synchronization of Pulse-Coupled Biological Oscillators". In: *SIAM Journal on Applied Mathematics* 50.6, pp. 1645–1662. DOI: 10.1137/0150098. URL: https://doi.org/10.1137/0150098.

Mohawk, Jennifer A, Carla B Green, and Joseph S Takahashi (2012). "Central and peripheral circadian clocks in mammals". In: *Annual review of neuroscience* 35, pp. 445–462. DOI: 10.1146/annurev-neuro-060909-153128. URL: https://pubmed.ncbi.nlm.nih.gov/22483041.

Müller, Stefan et al. (2006). "A generalized model of the repressilator." eng. In: *J Math Biol* 53.6, pp. 905–937. ISSN: 0303-6812 (Print); 0303-6812 (Linking). DOI: 10.1007/s00285-006-0035-9.

Nicks, Rachel, Lucie Chambon, and Stephen Coombes (2018). "Clusters in nonsmooth oscillator networks". In: *Phys. Rev. E* 97, p. 032213.

Panda, Satchidananda (2016). "Circadian physiology of metabolism". In: *Science* 354.6315, pp. 1008–1015. ISSN: 0036-8075. DOI: 10.1126/science.aah4967. eprint: https://science.sciencemag.org/content/354/6315/1008.full.pdf. URL: https://science.sciencemag.org/content/354/6315/1008.

Perez-Carrasco, Ruben et al. (2018). "Combining a Toggle Switch and a Repressilator within the AC-DC Circuit Generates Distinct Dynamical Behaviors". In: *Cell Systems* 6.4, 521–530.e3. DOI: 10.1016/j.cels.2018.02.008. URL: https://doi.org/10.1016/j.cels.2018.02.008.

Pett, J Patrick et al. (Dec. 2016). "Feedback Loops of the Mammalian Circadian Clock Constitute Repressilator". In: *PLoS computational biology* 12.12, e1005266–e1005266. DOI: 10.1371/journal.pcbi.1005266. URL: https://pubmed.ncbi.nlm.nih.gov/27942033.

Pett, J Patrick et al. (2018). "Co-existing feedback loops generate tissue-specific circadian rhythms". In: *Life Science Alliance* 1.3. DOI: 10.26508/lsa.201800078. eprint: https://www.life-science-alliance.org/content/1/3/e201800078.full.pdf. URL: https://www.life-science-alliance.org/content/1/3/e201800078.

Pomerening, Joseph R., Sun Young Kim, and James E Ferrell (2005). "Systems-Level Dissection of the Cell-Cycle Oscillator: Bypassing Positive Feedback Produces Damped Oscillations". In: *Cell* 122, pp. 565–578.

Potvin-Trottier, Laurent et al. (2016). "Synchronous long-term oscillations in a synthetic gene circuit." eng. In: *Nature* 538.7626, pp. 514–517. ISSN: 1476-4687 (Electronic); 0028-0836 (Print); 0028-0836 (Linking). DOI: 10.1038/nature19841.

Preitner, Nicolas et al. (2002). "The orphan nuclear receptor REV-ERBalpha controls circadian transcription within the positive limb of the mammalian circadian oscillator." eng. In: *Cell* 110.2, pp. 251–260. ISSN: 0092-8674 (Print); 0092-8674 (Linking). DOI: 10.1016/s0092-8674(02)00825-5.

Purcell, Oliver et al. (2010). "A comparative analysis of synthetic genetic oscillators." In: *J R Soc Interface* 7.52, pp. 1503–1524. ISSN: 1742-5662 (Electronic); 1742-5689 (Print); 1742-5662 (Linking). DOI: 10.1098/rsif.2010.0183.

Ralph, MR et al. (1990). "Transplanted suprachiasmatic nucleus determines circadian period". In: *Science* 247.4945, pp. 975–978. ISSN: 0036-8075. DOI: 10.1126/science.2305266. eprint: https://science.sciencemag.org/content/247/4945/975.full.pdf. URL: https://science.sciencemag.org/content/247/4945/975.

Reppert, Steven M. and David R. Weaver (2002). "Coordination of circadian timing in mammals". In: *Nature* 418.6901, pp. 935–941. DOI: 10.1038/nature00965. URL: https://doi.org/10.1038/nature00965.

Sato, Trey K et al. (2004). "A functional genomics strategy reveals Rora as a component of the mammalian circadian clock." eng. In: *Neuron* 43.4, pp. 527–537.

ISSN: 0896-6273 (Print); 0896-6273 (Linking). DOI: 10.1016/j.neuron.2004.07.018.

Scardovi, Luca and Rodolphe Sepulchre (2008). *Synchronization in Networks of Identical Linear Systems*. arXiv: 0805.3456 [math.OC].

Silva, F. A. dos S., S. R. Lopes, and R. L. Viana (2016). "Synchronization of biological clock cells with a coupling mediated by the local concentration of a diffusing substance". In: *Communications in Nonlinear Science and Numerical Simulation* 35.Complete, pp. 37–52. DOI: 10.1016/j.cnsns.2015.11.003.

Silver, Rae et al. (1996). "A diffusible coupling signal from the transplanted suprachiasmatic nucleus controlling circadian locomotor rhythms". In: *Nature* 382.6594, pp. 810–813. DOI: 10.1038/382810a0. URL: https://doi.org/10.1038/382810a0.

Smolen, P, D A Baxter, and J H Byrne (1999). "Effects of macromolecular transport and stochastic fluctuations on dynamics of genetic regulatory systems." eng. In: *Am J Physiol* 277.4, pp. C777–90. ISSN: 0002-9513 (Print); 0002-9513 (Linking). DOI: 10.1152/ajpcell.1999.277.4.C777.

Smolen, Paul, Douglas A. Baxter, and John H. Byrne (1998). "Frequency selectivity, multistability, and oscillations emerge from models of genetic regulatory systems". In: *American Journal of Physiology - Cell Physiology* 274.2, pp. C531–C542. ISSN: 0363-6143. eprint: http://ajpcell.physiology.org/content/274/2/C531.full.pdf. URL: http://ajpcell.physiology.org/content/274/2/C531.

Sorrentino, Francesco et al. (Apr. 2016). "Complete characterization of the stability of cluster synchronization in complex dynamical networks". In: *Science Advances* 2, e1501737–e1501737. DOI: 10.1126/sciadv.1501737.

Stricker, Jesse et al. (2008). "A fast, robust and tunable synthetic gene oscillator." eng. In: *Nature* 456.7221, pp. 516–519. ISSN: 1476-4687 (Electronic); 0028-0836 (Linking). DOI: 10.1038/nature07389.

Teng, Zhidong et al. (2014). "Birhythmicity and Hard Excitation from Coupled Synthetic Feedback Loops". In: *Journal of Applied Mathematics* 2014, p. 694854. DOI: 10.1155/2014/694854. URL: https://doi.org/10.1155/2014/694854.

Tigges, Marcel et al. (2009). "A tunable synthetic mammalian oscillator". In: *Nature* 457.7227, pp. 309–312. DOI: 10.1038/nature07616. URL: https://doi.org/10.1038/nature07616.

Tigges, Marcel et al. (May 2010). "A synthetic low-frequency mammalian oscillator". In: *Nucleic acids research* 38.8, pp. 2702–2711. DOI: 10.1093/nar/gkq121. URL: https://pubmed.ncbi.nlm.nih.gov/20197318.

To, Tsz-Leung et al. (2007). "A Molecular Model for Intercellular Synchronization in the Mammalian Circadian Clock". English. In: *Biophysical Journal* 92.11, pp. 3792–3803. DOI: 10.1529/biophysj.106.094086.

Tomazou, Marios et al. (2018). "Computational Re-design of Synthetic Genetic Oscillators for Independent Amplitude and Frequency Modulation". In: *Cell Systems* 6.4, 508 –520.e5. ISSN: 2405-4712. DOI: https://doi.org/10.1016/j.cels.2018.03.013. URL: http://www.sciencedirect.com/science/article/pii/S2405471218301108.

Traynard, Pauline et al. (2016). "Model-based investigation of the circadian clock and cell cycle coupling in mouse embryonic fibroblasts: Prediction of RevErb-αup-regulation during mitosis". In: *Biosystems* 149, pp. 59–69. DOI: http://dx.doi.org/10.1016/j.biosystems.2016.07.003. URL: http://www.sciencedirect.com/science/article/pii/S0303264716301162.

Tsai, Tony Yu-Chen et al. (2008). "Robust, tunable biological oscillations from interlinked positive and negative feedback loops." eng. In: *Science* 321.5885, pp. 126–129. ISSN: 1095-9203 (Electronic); 0036-8075 (Print); 0036-8075 (Linking). DOI: 10.1126/science.1156951.

Tyler, Jonathan, Anne Shiu, and Jay Walton (2019). "Revisiting a synthetic intracellular regulatory network that exhibits oscillations". In: *Journal of Mathematical Biology* 78.7, pp. 2341–2368. DOI: 10.1007/s00285-019-01346-3. URL: https://doi.org/10.1007/s00285-019-01346-3.

Tyson, John J et al. (Aug. 2008). "Biological switches and clocks". In: *Journal of the Royal Society, Interface* 5 Suppl 1.Suppl 1, S1–S8. DOI: 10.1098/rsif.2008.0179.focus. URL: https://pubmed.ncbi.nlm.nih.gov/18522926.

Ünsal-Kaçmaz, Keziban et al. (2005). "Coupling of Human Circadian and Cell Cycles by the Timeless Protein". In: *Molecular and Cellular Biology* 25.8, pp. 3109–3116.

Wang, Ruiqi, Zhujun Jing, and Luonan Chen (2005). "Modelling periodic oscillation in gene regulatory networks by cyclic feedback systems". In: *Bulletin of Mathematical Biology* 67.2, pp. 339–367. DOI: 10.1016/j.bulm.2004.07.005. URL: https://doi.org/10.1016/j.bulm.2004.07.005.

Weber, Wilfried and Martin Fussenegger (Nov. 2011). "Emerging biomedical applications of synthetic biology". In: *Nature reviews. Genetics* 13, pp. 21–35. DOI: 10.1038/nrg3094.

Welsh, David K, Joseph S Takahashi, and Steve A Kay (2010). "Suprachiasmatic nucleus: cell autonomy and network properties". In: *Annual review of physiology* 72, pp. 551–577. DOI: 10.1146/annurev-physiol-021909-135919. URL: https://pubmed.ncbi.nlm.nih.gov/20148688.

Yagita, K and H Okamura (2000). "Forskolin induces circadian gene expression of rPer1, rPer2 and dbp in mammalian rat-1 fibroblasts." eng. In: *FEBS Lett* 465.1, pp. 79–82. ISSN: 0014-5793 (Print); 0014-5793 (Linking). DOI: 10.1016/s0014-5793(99)01724-x.

Yamazaki, Shin et al. (2000). "Resetting Central and Peripheral Circadian Oscillators in Transgenic Rats". In: *Science* 288.5466, pp. 682–685. ISSN: 0036-8075. DOI: 10.1126/science.288.5466.682. eprint: https://science.sciencemag.org/content/288/5466/682.full.pdf. URL: https://science.sciencemag.org/content/288/5466/682.

Yan, Jie and Albert Goldbeter (2019). "Robust synchronization of the cell cycle and the circadian clock through bidirectional coupling". In: *Journal of The Royal Society Interface* 16.158, p. 20190376. DOI: 10.1098/rsif.2019.0376. URL: https://doi.org/10.1098/rsif.2019.0376.

Ye, Rui et al. (Sept. 2014). "Dual modes of CLOCK:BMAL1 inhibition mediated by Cryptochrome and Period proteins in the mammalian circadian clock". In: *Genes*

& development 28.18, pp. 1989–1998. DOI: 10.1101/gad.249417.114. URL: https://www.ncbi.nlm.nih.gov/pubmed/25228643.

Zámborszky, Judit, Christian I Hong, and Attila Csikász Nagy (2007). "Computational analysis of mammalian cell division gated by a circadian clock: quantized cell cycles and cell size control." eng. In: *J Biol Rhythms* 22.6, pp. 542–553. ISSN: 0748-7304 (Print); 0748-7304 (Linking). DOI: 10.1177/0748730407307225.

Zhao, Xuan et al. (2016). "Circadian Amplitude Regulation via FBXW7-Targeted REV-ERBα Degradation". In: *Cell* 165.7, pp. 1644–1657. DOI: 10.1016/j.cell.2016.05.012. URL: https://doi.org/10.1016/j.cell.2016.05.012.